SUNMASTER

VPI/NASA/Senior Design Project 1990-91

An SEP Cargo Vehicle for Mars Missions

Aleasa Chiles
Jennifer Fraser
Andy Halsey
David Honeycutt
Michael Madden
Brian McGough
David Paulsen
Becky Spear
Lynne Tarkenton
Kevin Westley

Professor A. Jakubowski
VPI Aerospace Engineering Department

Davy A. Haynes
Space Exploration Initiative Office
NASA Langley Research Center

June 1991
Department of Aerospace and Ocean Engineering
Virginia Polytechnic Institute and State University
Blacksburg, Virginia 24061

Abstract

This study examines options for an unmanned solar powered electric propulsion cargo vehicle for Mars missions. The six primary areas of investigation include: trajectory, propulsion system, power system, supporting structure, control system and launch consideration.

Optimization of the low thrust trajectory resulted in a total round trip mission time just under 4 years. The argon-propelled electrostatic ion thruster system consists of seventeen 5 N engines and uses a specific impulse of 10,300 seconds. At Earth, the system uses 12 engines to produce 60 N of thrust; at Mars, five engines are used, producing 25 N thrust. The thrust of the craft is varied between 60 N at Earth to 24 N at Mars due to reduced solar power available.

Solar power is collected by a Fresnel lens concentrator system using a multi-stacked cell. This system provides 3.5 MW to the propulsion system after losses. Support for the concentrator systems is provided by a three ring, hexagonal shaped, precision truss system constructed of aluminum coated, graphite-epoxy, thin-walled struts. The center of the ship is supported by a three-cell, orthogonal, tetrahedral truss.

Control and positioning of the craft are provided by a system consisting of three double gimballed control moment gyros (CMG). Four shuttle "C" launches will be used to transport the unassembled vehicle in modular units to low Earth orbit where it will be assembled using the Mobile Transporter of the Space Station Freedom.

Acknowledgements

The design team would like to acknowledge the efforts of Julie Fraser, who, with her creative knowledge of software packages and graphic artistry and ability to work several days without sleep, helped in the compilation of the report.

Table of Contents

List of Figures

List of Tables

Introduction

As the United States looks forward to the challenges of space exploration in the twenty-first century, many objectives and missions will become feasible. None of these is more likely to inspire the nation and the world as landing men and women on the surface of another planet: Mars. Even with projected technology, such manned missions will be long and costly. To minimize the number of man-hours in space required for such an objective as well as reduce the cost, the possibility of having several unmanned cargo missions precede the manned expeditions becomes attractive. Costs could be minimized by having cargo vessels employ a high specific impulse electric propulsion system. This type of propulsion system allows for a much higher payload to total mass ratio than is attainable with conventional propulsion. Although electric propulsion results in relatively long trip times, this consideration is not as great a concern as it would be for a manned mission. With this philosophy in mind, this preliminary study was prepared in accordance with a number of design parameters specified by the Space Exploration Initiative Office of the NASA Langley Research Center.

To fulfill its Mars mission, the cargo ship must meet several design requirements and goals. First, the vehicle is an unmanned cargo vessel employing argon-propelled, ion thrusters. The electric propulsion system will be powered by solar arrays that will convert the sun's energy directly into electric current. Because of the very large size of this solar powered craft, it will have to be assembled in low Earth orbit near Space Station Freedom (SSF). After leaving low Earth orbit, the craft will deliver a 61 mT payload to a low Mars orbit and return to Earth, and it must be designed to survive three such missions without extensive overhaul. Several specific design requirements were also provided. The LEO orbit of SSF is taken to be a 400 km circular orbit at an angle of inclination of 28.5°. The destination orbit upon arrival at Mars is

specified as a 500 km circular orbit at an inclination of 70°. Finally, Earth-to-Orbit launches will be performed by the Shuttle-C. The payload specifics for Shuttle-C are 61 mT, 7.6 x 27 meter volume for cargo launches.

Several key areas of interest and analysis require special attention during this study. The first of these areas addressed is the analysis of the low thrust trajectories required by the mission. These trajectories must be optimized to require a minimum of propellant and thrusting time, as well as result in acceptable refit time, loiter at Mars, and overall mission durations.

Next, the selection and optimization of the propulsion system is considered in Section Two. Important parameters considered here are the optimized specific impulse, power level, and thrust level for the craft. In addition to the selection and optimization process, the problem of thruster degradation over the course of the mission is discussed. Also included in this discussion are the power processing system, propellant storage tank and propellant system, and the problem of rejecting the appropriate heat loss to space, as well as several other topics.

The propulsion system will be powered by a photovoltaic system that will convert sun light into electrical energy. Section Three begins with a discussion of various options for collecting this solar energy. The two primary options considered were a flat array of solar cells, and a Fresnel lens concentrator array. For the option selected, a discussion of heat transfer and wiring requirements is presented, as well as the general array specifications.

This large solar array must be supported by a truss structure able to withstand the anticipated loads. An analysis of this structure is presented in Section Four. This analysis includes the configuration, a discussion of the forces carried by the truss members, as well as the allowable freedom of movement of the overall structure.

Finally, the logistical problem of launching and assembling the components of the craft need to be considered. With the high cost involved in lifting heavy payloads to orbit, as well

as the difficulty and cost of assembly in orbit, it is very desirable to optimize both the launch and construction processes. The details of the solution of this obstacle can be found in Section 5.

Appendices 1 through 3 provided detailed calculations for the trajectory, the propulsion system, and the solar array assembly, respectively.

The attitude and direction of the craft are controlled and adjusted by a system of Control Moment Gyros (CMGs). This system is examined in Appendix 4, and includes a discussion of the control loop.

Appendix 5 discusses the navigation and communication systems of the spacecraft.

With this framework in mind, this preliminary study was organized into the areas of study outlined above.

SECTION 1

Orbital Analysis

Nomenclature

HTO	Heliocentric transfer orbit
IMLEO	Initial mass in low Earth orbit
Isp	Specific impulse
LEO	Low Earth orbit
mT	Metric tons
SSF	Space Station Freedom

1.1 Preliminary Delta-V and Propellent Mass Estimates

The most important calculation for any orbital transfer is the estimate for the total change in velocity (delta-V) required to complete the mission. This delta-V represents the total impulse that the propulsion system must provide, and is therefore critical in estimating the mass of propellant required.

This mission will require a number of orbital transfer maneuvers. In the vicinity of Earth, the craft must initiate a plane change to get from the orbital inclination of SSF to roughly that of the ecliptic, as well as escape from the Earth's gravity. Upon Earth escape, the craft must inject itself into some heliocentric transfer orbit (HTO) that will allow it to reach the orbital radius of Mars. Once there, the craft must allow itself to be captured, then execute another plane change to reach the destination orbit. This process would essentially be reversed for the return trip. Initial estimates of the delta-V's for the trajectory are given in Table 1.1. These values were estimated using computer models that assumed constant tangential thrust.

Table 1.1 Initial Delta-V Estimates

Maneuver	Delta-V (km/s)
Spiral Earth	6.5
HTO	6.0
Spiral Mars	3.0

With the delta-V break down, it is possible to roughly estimate the initial mass of propellant required for the entire mission for a given "dry mass" (no propellant or cargo) for the ship. This is done by using the delta-V for each maneuver and equation 1.1:

$$\Delta V = I_{sp} G \ln \frac{M_p}{M_o} \qquad (1.1)$$

to determine the mass ratio M_p/M_o for each maneuver, taking the total mass of the previous maneuver to be the payload mass of the next maneuver. Program PMEFDMAI.BAS (Propellant Mass Estimate From Dry Mass And Isp) cycles through various dry masses and specific impulses and estimates the mass of propellant required as a function of these parameters (Appendix 1).

1.2 Trajectory Optimization

1.2.1 Introduction

Allowing the thrust vector to change not only its magnitude, but its direction was the next logical step in our analysis. This optimization step required the use of a low-thrust, orbital calculation program published by NASA Ames in 1973. QUICKTOP, and its companion

program CHEB3, are both FORTRAN source codes that compute the optimum low-thrust interplanetary trajectories with variable thrust vector programs.

The QUICKTOP input file contains numerous variables that may be specified. Through proper use of this data file, it is possible to simulate a solar powered-electric propulsion departure from orbit to any given destination planet. The initial and destination orbits can be specified, as well as many other parameters and options. From this data, QUICKTOP generates a complete analysis of the trajectory. The program contains provisions to account for the loss of power available for propulsion due to increasing distance from the sun.

The output variables of primary importance in this study were propellant required (and thus, IMLEO), thruster firing time, loiter time at Mars, refit time at Earth, and overall mission times. Loiter and refit times were addressed using the TIMEOPT code which is described below (see Appendix 1 for details).

Based on propulsion system optimization, a specific impulse of 10,300 seconds was selected. This corresponded to a required power of 3.5 megawatts. These parameters were held constant throughout trajectory calculations.

Mission trajectories were generated by inputing a large variety of heliocentric travel times. The return trip from Mars to Earth and the outward trip from Earth to Mars were analyzed independently. The input data were manipulated so that the payload each way was zero and the IMLEO was estimated. The resulting negative value for payload represented a first estimate for the propellant required for that trajectory. After selecting an optimum trajectory, the solution was iterated until the output was consistent.

1.2.2 Propellant and Thrusting Considerations

For each of the input HTO travel times that converged, QUICKTOP produced the required

propellant, thrust time, as well as spiral escape and capture times. Twenty outward and twenty return trajectories were created and compared on this basis. The results are shown in Figures 1.1 through 1.4 which indicate propellant mass required and thrusting time as a function of travel time. Figures 1.1 and 1.2 refer to the outward trajectory, while Figures 1.3 and 1.4 refer to the return trip. Figure 1.1 presents the propellant mass required for the outward trajectory. As can be seen, propellant requirements tend to increase as HTO time decreases. Some peaks and valleys occur, indicating that there is no absolute relationship involved or single thrust program that will result in the optimum trajectory. Figure 1.4 shows the variation of the required thrusting time for the return trip and indicated a minimum of about 5500 hr. The results obtained allowed us to select the final trajectory and mission times. Shorter trip times result in generally increased propellant requirements. Lower trip times often did not converge to solutions at all.

1.2.3 Time Considerations

Having compared a wide range of trajectories on the basis of HTO travel time, propellant required, and thrusting time, the synodic considerations of meeting with the target planet were examined. The escape time, capture time, HTO travel time, and the change in orbital true anomaly resulting from the HTO transfer, generated by QUICKTOP, were input into TIMEOPT, a program that calculates the required phasing of the planets for successful rendezvous. In addition, TIMEOPT also computes the necessary loiter time at Mars and refit time at Earth to match these phasing ("launch window") requirements. This resulted in approximately 400 possible round trip trajectories. These round trip trajectories were then evaluated in terms of the following criteria:

1. **Total mission time.** The total time for three consecutive missions is not allowed to exceed 12+ years. This was the minimum time calculated for three missions; other possibilities were 18+ and 23+ years. These times were considered too long to support a reasonable mission.

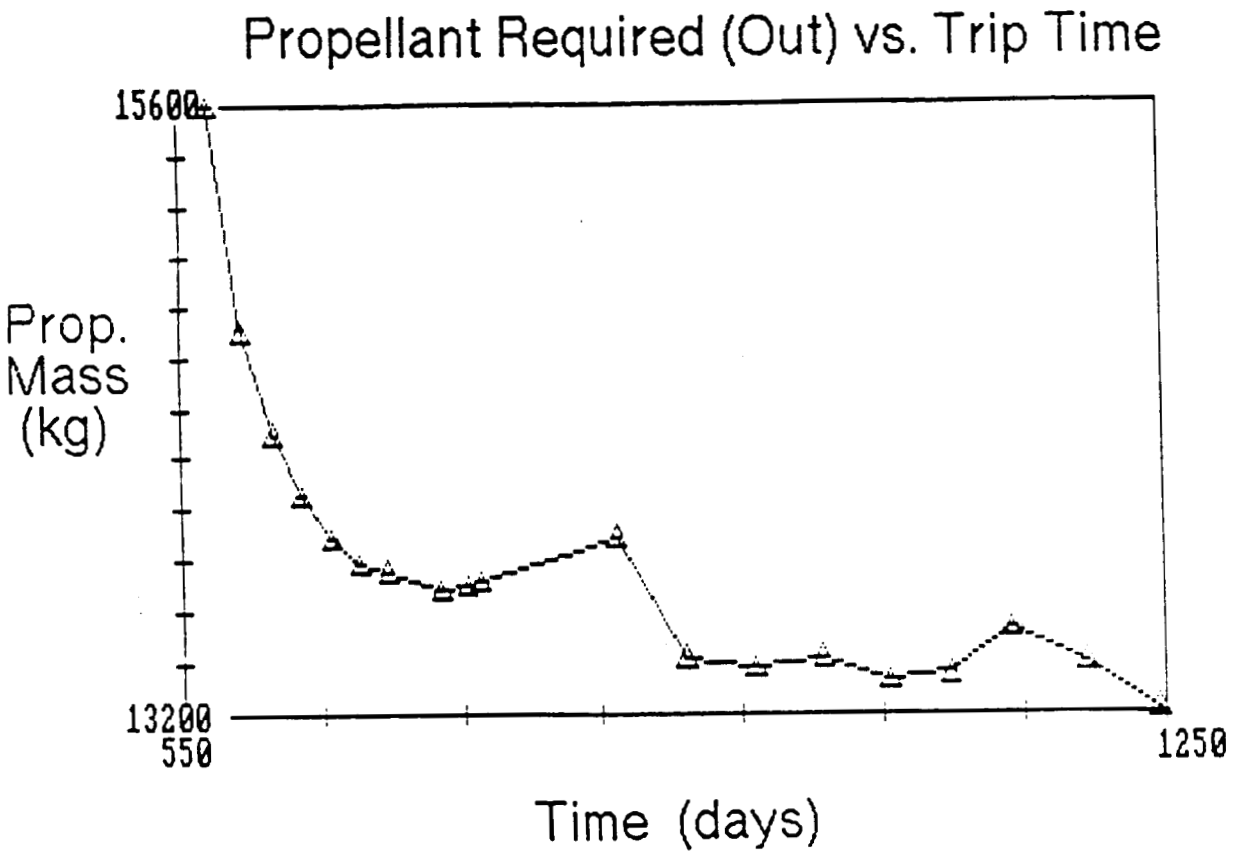

Figure 1.1: Propellant Required (Out) vs. Trip Time

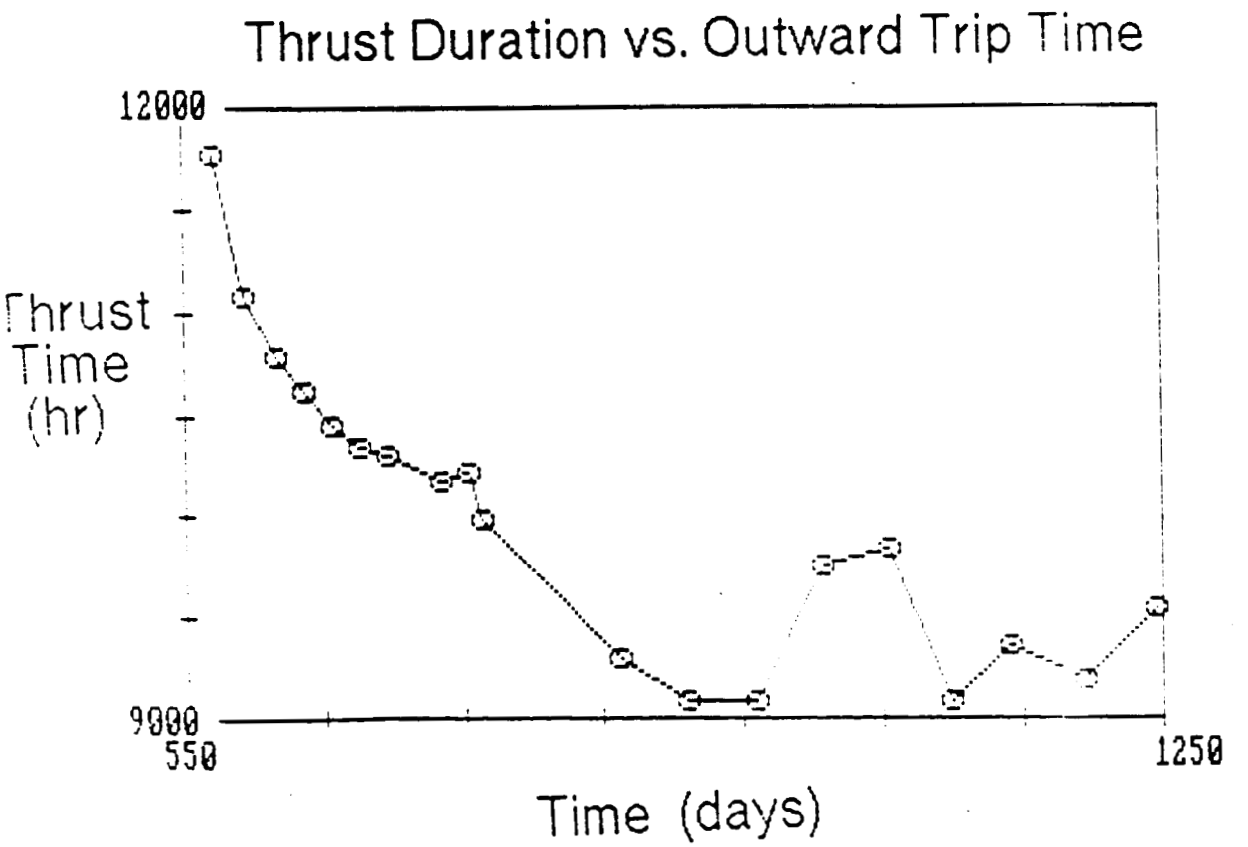

Figure 1.2: Thrust Duration vs. Outward Trip Time

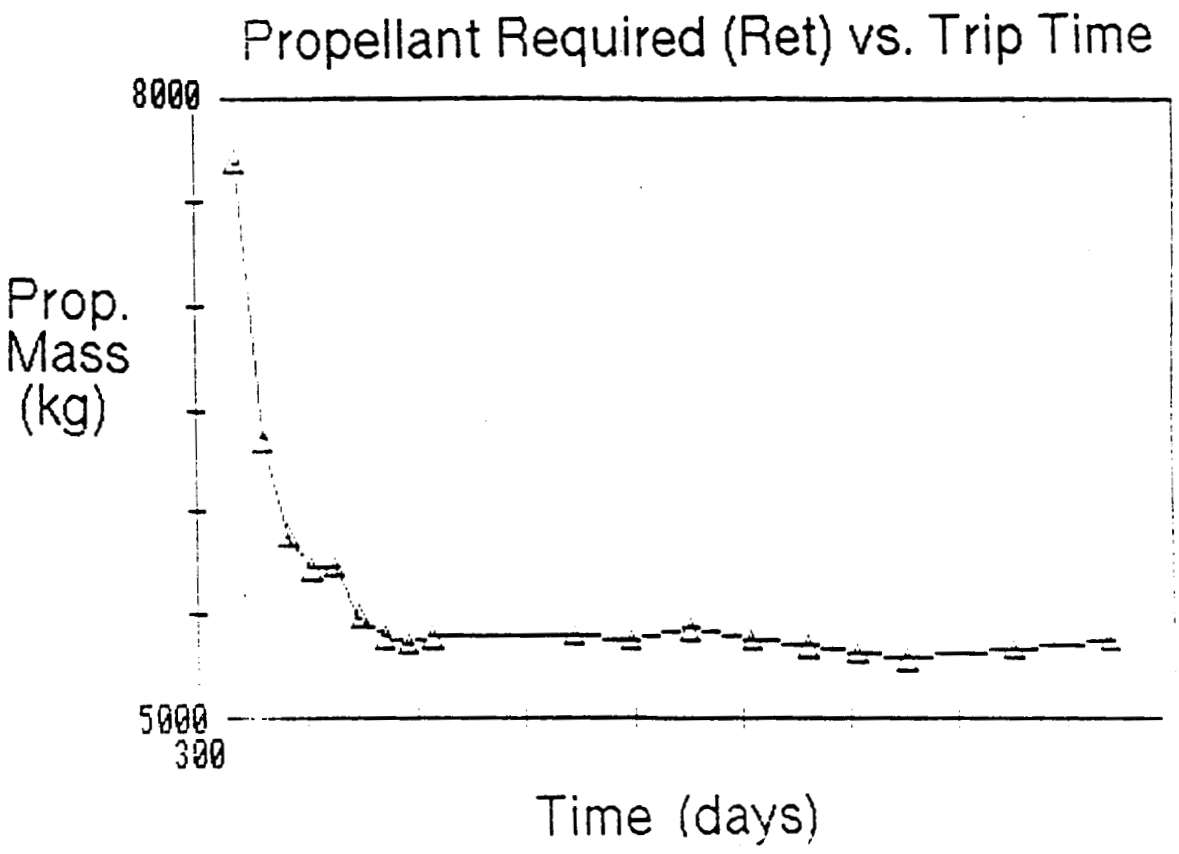

Figure 1.3: Propellant Required (Ret.) vs. Trip Time

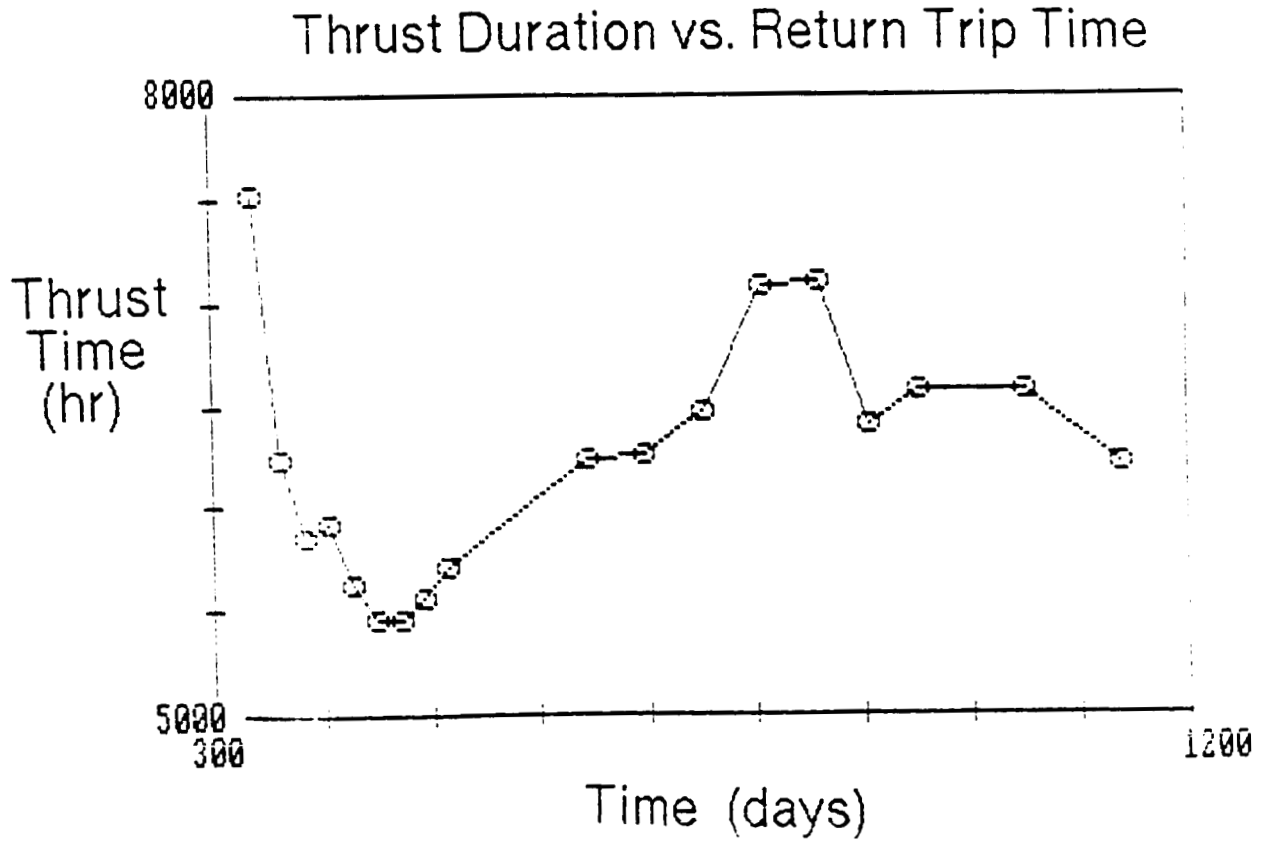

Figure 1.4: Thrust Duration vs. Inward Trip Time

2. **Loiter time at Mars.** This time was not to exceed 70 days or fall below 20 days. A minimum delay at Mars is desirable, since the craft cannot be serviced or overhauled realistically in Mars orbit. A delay of at least 20 days was specified to allow for unexpected delays in off-loading cargo or unanticipated trajectory changes. Shorter loiter times could result in the missing of a launch window should the craft be delayed. This would cause a very extended, costly stay at the red planet. These times were arbitrarily selected and could easily be changed in the optimization process.

3. **Refit time at Earth.** A maximum, or at least very long, time for refit at Earth was desired. This would obviously allow more time for loading of cargo and refit/repair operations. This would also maximize the fraction of time that the craft was in Earth orbit or Earth's vicinity, where unexpected problems or malfunctions are more easily corrected.

4. **Propellant and Thrusting Time Considerations.** Plots 1.1 through 1.4 were used to evaluate the propellant consumption and thrusting time required for each round trip trajectory. Minimums were sought in each of these parameters; low propellant mass translates into low IMLEO, and short thruster firing time results in reduced degradation of engines (and lower redundancy requirements) and less extensive (and costly) refit time to replace degraded thrusters. Some thruster refit will invariably be necessary, however. The result of this analysis was a matrix of data concerning the possible round trip trajectories. Many of the candidates were eliminated by the time requirements listed above. A few of the remaining trajectories could be eliminated because of extensive propellant or thrusting time requirements. This still left about a dozen or so trajectories of which there was no clear choice.

At this point, it was decided that, given relatively similar thrusting times and propellant requirements, the longest Earth refit time possible should be selected, within the bounds of the parameters listed above. The resulting trajectory is summarized in Table 1.2; and illustrated graphically in Figures 1.5 and 1.6.

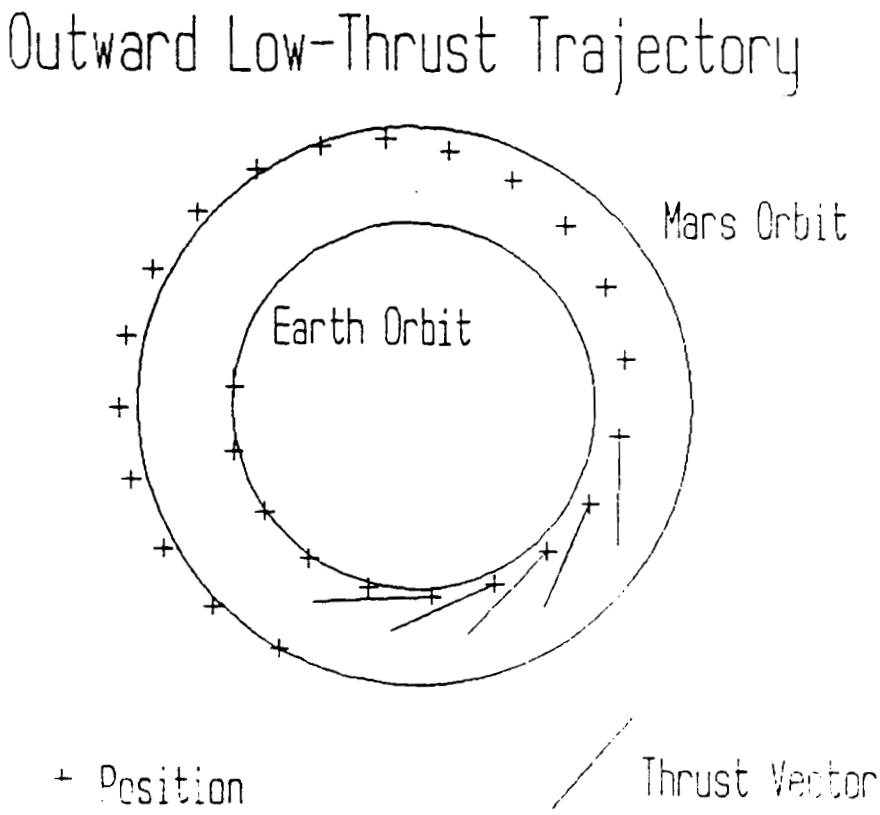

Figure 1.5: Outward Heliocentric Transfer Orbit Trajectory

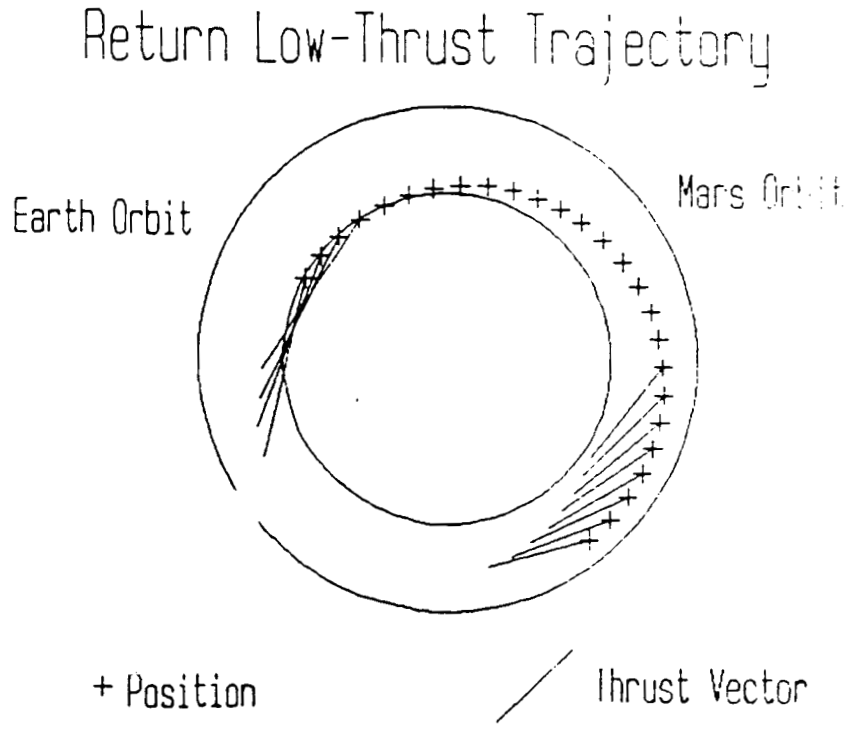

Figure 1.6: Return Heliocentric Transfer Orbit Trajectory

Table 1.2 Mission Architecture Summary

Phase	Phase Time (days)	Earth Position (rads)	Mars Position (rads)	Mission Time (days)
Start	0	-2.62	0.183	0
Earth escape	152	0.00	1.57	152
Out HTO	650	11.19	7.52	802
Mars capture	108	13.04	8.51	910
Loiter @ Mars	60	14.08	9.06	970
Mars escape	38	14.73	9.41	1008
Return HTO	260	19.21	11.79	1268
Earth Capture	84	20.65	12.55	1352

Planet positions defined from arbitrary reference position of Earth at escape defined as 0.00 radians.

Refit time until next launch window = 210 days = 7 months

Total mission duration (3 round trips) = 12.2 years

1.2.4 The Optimized Trajectory

The selected outward trajectory requires 910 days from the beginning of the Earth spiral to the completion of Mars capture. The propellant required for this trajectory is 13,258 kg (expressed as a negative payload in the optimization process). Thruster time for this trajectory is 8766 hrs. The IMLEO was taken to be roughly 130,000 kg. The Earth escape spiral time is 152 days, the heliocentric transfer time is 650 days and the Mars capture time is 108 days.

The position and orientation of the craft as a function of the time in the HTO for the outward trip is graphically represented in Figure 1.5. For this study, the z coordinate of motion (out of the ecliptic plane) was ignored because it was small relative to the x and y components. The data is given in radius-angle format. The angle (THETA) was very important, since the

change in this angle for the HTO trajectory was required to compute loiter and refit times.

For the outward trip, the craft coasts for about 100 days after Earth escape, then thrusts for about 80 days in a gradually rotating direction and decreasing magnitude. The craft then coasts outside of Mars' orbit, then rendezvous after crossing its HTO aphelion. Figure 1.5 indicates the magnitude and orientation of the thrust vector during the HTO trajectory.

Figure 1.6 describes the return trajectory. Interestingly, the return trajectory consists of an acceleration and a deceleration rather than a single coast-thrust-coast program. This probably is necessary because the return trip was a relatively short trajectory (relative to the other return trajectories), whereas the outward trajectory was one of the longer HTO times considered.

A few additional comments concerning Figures 1.5 and 1.6 are in order. These two plots represent the heliocentric phase of the outward and inward trajectories, respectively. In Figure 1.6, the time between each of the position data points is approximately 20.5 days. The maximum acceleration required in this HTO is about 3.6 AU/yr^2, or about 0.00054 m/sec^2.

In Figure 1.6 (return trajectory), the time interval between position data points in about 11.6 days. The maximum acceleration required in this HTO is about 5.6 AU/yr^2 or 0.00084 m/sec^2. Both of these accelerations are well within the capabilities of the electric propulsion system.

1.3 Conclusions

In conclusion, a general comment concerning the optimization of low-thrust trajectories is in order. For a wide range of trip times selected, propellant masses and thrusting times required did not vary significantly. Only several extreme trajectory cases could be eliminated because of excessive propellant or thrusting time requirements. Hence, the mission trajectory is driven primarily by the desired loiter, refit, and total mission time parameters.

This variation is possible because the nature of low thrust propulsion makes trajectory adjustments relatively easy compared to high thrust systems. Since the delta-V is applied gradually over a long thrusting arc, small corrections or changes can be made at relatively little cost in propellant. This characteristic of low thrust propulsion is very desirable; it enables the same system to be used for very different missions without a drastic increase in propellant mass. This gives a wide margin for error and unexpected delays in the mission execution. If a malfunction occurs or the craft is unexpectedly delayed, it is very likely that a suitable trajectory could be found that would fulfill the mission, or at least salvage the craft.

References

1. Bate, Rodger., Donald D. Mueller, and Jerry E. White. Fundamentals of Astrodynamics. Dover Publications, New York, NY 1971.

2. Battin, Richard H. An Introduction to the Mathematics and Methods of Astrodynamics. The American Institute of Aeronautics and Astronautics, New York, NY, 1987.

3. Brusch, Richard G. and Thomas L. Vincent. "Low-Thrust, Minimum-Fuel, Orbital Transfers" Astronautica Acta, Vol. 16, Pergamon Press, Great Britain, 1971. pp. 65-73.

4. Edelbaum, Theodore N. "Optimum Power-Limited Orbit Transfer in Strong Gravity Fields" AIAA Journal, Vol. 3, No. 5, May 1965. pp. 921-924.

5. Gobetz, Frank W. "Optimal Variable-Thrust Transfer of a Power Limited Rocket between Neighboring Circular Orbits" AIAA Journal, Vol. 2, No. 2, February 1964. pp. 339-343.

6. Mascy, Alfred C., Richard W. Schaupp, and Shirley A. Hayes. "QUICKTOP III - A Computer Program For Low-Thrust Trajectory and Mass Optimization." NASA TM-62,305. Ames Research Center, Moffett Field, CA. 1973.

7. Melbourne, W.G., and C.G. Sauer Jr., "Optimum Interplanetary Rendezvous With Power-Limited Vehicles" AIAA Journal, Vol 1, No. 1. pp. 54-59.

8. Stuhlinger, Ernst. "The Flight Path of an Electrically Propelled Space Ship" Jet Propulsion, April, 1957. pp. 410-414.

SECTION 2

Propulsion Systems

Nomenclature

A - area
C - exhaust velocity
D - diameter of screen grid
d - grid spacing
F,F' - variables in Isp optimization
J_b - beam current
J_n - neutralizer current
k - thermal conductivity
m_L - engine and propellant mass
m_O - total craft mass
m_o - mass of propellant atom
MW - molecular weight
P_b - beam power
P_n - neutralizer power
P_{tot} - total power
q_{vap} - heat of vaporization
S_{dp} - chamber specific loss level
T - thrust
V_b - beam voltage
η_i - ionization efficiency
η_e - electrical efficiency
η_p - propellant efficiency
η_{tot} - total efficiency
Γ''/Γ' - ratio double to single ions
δ - neutralizer voltage
γ - thrust correction factor
Δv - velocity increment
α - specific power

2.1 Introduction

The primary difference with this mission as opposed to many other space missions is the requirement of electric propulsion as the sole means of propulsion. The key justification for the electric propulsion is its high specific impulse and ability to provide very high payload to craft mass ratio. These factors may significantly reduce the transportation system mass and cost and make electric propulsion reasonable for long-term interplanetary missions.

2.2 Preliminary Concepts

There are three general types of electric thrusters: electrothermal, electromagnetic, and electrostatic. Resistojets and arcjets are two types of electrothermal thrusters. Each of these engines electrically heats the propellant and expands it through a nozzle to produce thrust. These engines are characterized by a relatively low (less than 1,500 sec.) specific impulse. Electromagnetic engines use an electromagnetic field to accelerate particles and produce thrust. The electrostatic engine accelerates ions through a voltage difference to produce thrust [5].

The electrostatic ion thruster was chosen for two critical reasons. First, it can reach very high specific impulses. Then, the ion thruster has the most fully characterized technology. Much research has been done on ion thrusters, and it is the most likely candidate for use in a deep space mission in the post 2010 time frame. An important feature of these thrusters is that they are scaleable, which means that they may be increased in size and power from smaller thrusters which presently exist. This may allow a significant reduction of lab research and experimentation.

Once the ion thruster is chosen; the task of deciding on a propellant still remains. As specified in NASA's criteria, the recommended choice of propellant is argon; however, to be complete, analysis of this recommendation is necessary. From recent evaluations, the only two

propellants under serious consideration for such a long term mission are argon and xenon, but, to be complete, mercury will also be included. One case study gave estimates of the benefits and drawbacks of each propellant for a specific system (Figure 2.1). Because of the higher specific impulse that can be provided by an argon thruster compared to a xenon thruster the argon will consume more power, per unit thrust, than a xenon (or mercury) engine. This, as one might assume, leads to a larger dry system mass for argon due to the increased power requirement. However, higher specific impulse has an opposite effect on the propellant mass, causing that the latter decreases with an increase in specific impulse, which gives preference to argon. The propellant mass saved by using argon more than compensates for that needed by the increased power supply and therefore may give better total system performance.[1]

An evaluation was made for the characteristics of our system with both argon and xenon, and because of the length of the mission, it can be assumed that the relatively large propellant masses are the main contributing factor in choosing the propellant. In this case argon gives lower propellant mass and therefore a lower overall mass. Xenon is unable to achieve the same low propellant masses at the higher range of specific impulses because the beam voltages at high specific impulse may be beyond the technology of cathode construction. For example, for xenon to run at an specific impulse of 10,300 seconds it would require a beam voltage of just over 6000 V. Xenon also has the additional burden of being very expensive due to its limited supply. Because this mission would require large propellant mass, this cost must play an important role in the selection process. In contrast to xenon, argon is inexpensive, abundant, and easy to handle. Based on these characteristics the original choice of argon seems justified.

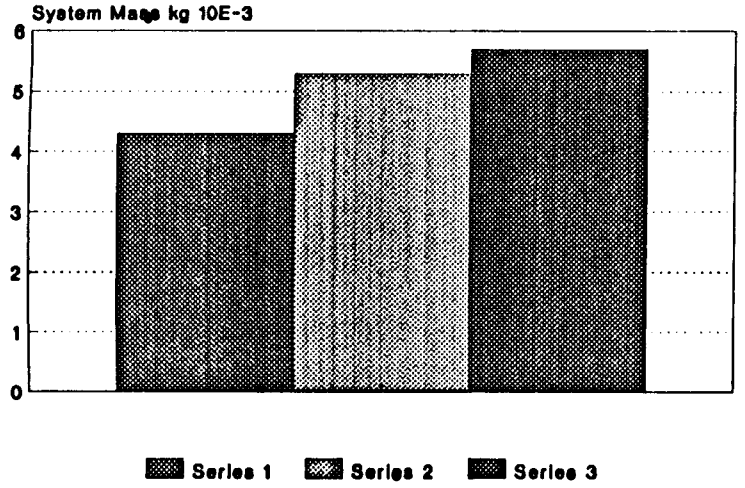

Figure 2.1a

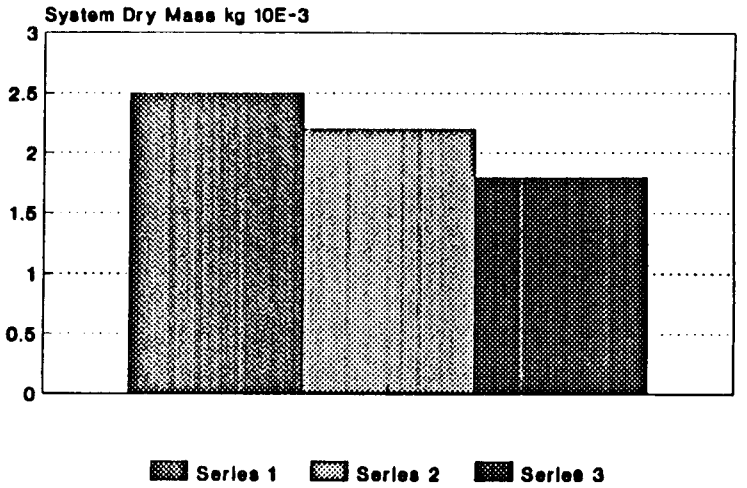

Figure 2.1b

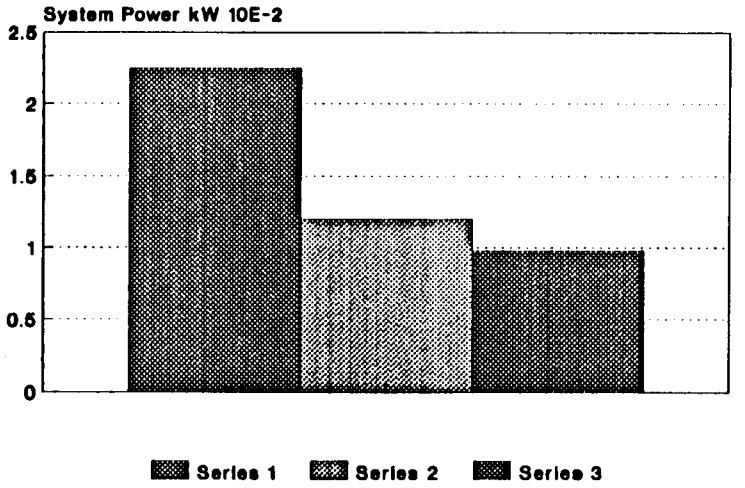

Figure 2.1c

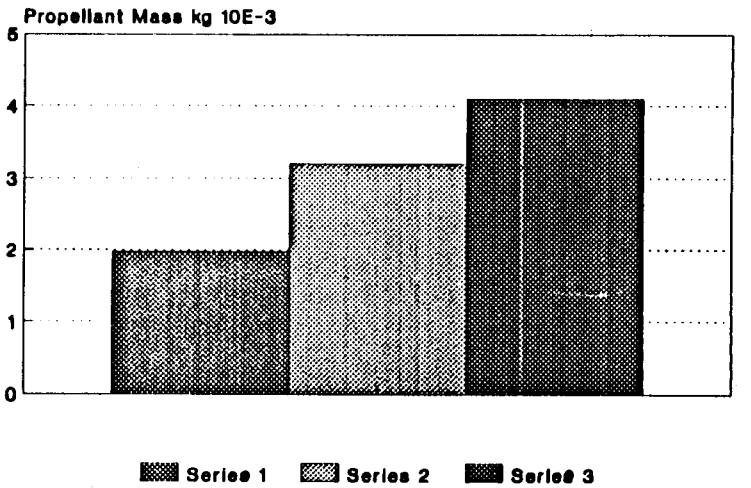

Figure 2.1d

Figure 2.1: Propellant Comparison

2.3 Thruster Optimization and Configuration

From information received from trajectory analysis it was decided that an initial total thrust of 60 Newtons is reasonable to allow an adequate trip time. The power decrease that will occur on the trip to Mars is estimated by Figure 2.2, which shows that the power at Mars will be approximately 40% of the original power at Earth. This will cut the thrust at Mars to nearly 25 Newtons. This thrust decrease during the trip to Mars has been taken into account when estimating trip time.

A 5 Newton thruster was selected as a suitable thruster size. When comparing thrusters of various sizes while keeping the total thrust constant, the craft characteristics (e.g. mass, power) remained essentially unchanged. Therefore, the choice of the 5 Newton thruster was based on a compromise between flexibility and unnecessary complication. This selection would give 12 operating thrusters at Earth and 5 at Mars. Obviously, if more thrusters were used, each with a smaller individual thrust, then the flexibility or throttling capabilities would increase. However, a large number of thrusters in operation may over-complicate the power processing and distribution systems to such an extent that the extra mass needed would become cumbersome. Therefore, twelve engines were chosen for the initial configuration to allow for enough flexibility without over-complication of the power processing systems. For the case of engine malfunction a redundancy of 5 engines is assumed, bringing the total number of thrusters to 17. This, obviously, does not increase the power requirements but only adds engine mass to the ship. The 17 thrusters also allow for a flexible thruster firing configuration which allows thrusters to be cut off one at a time, thereby saving on throttling demands.

Specific impulse optimization of the 5 Newton thruster was accomplished through the use of two methods. The first method made use of the trajectory program which we wrote, through

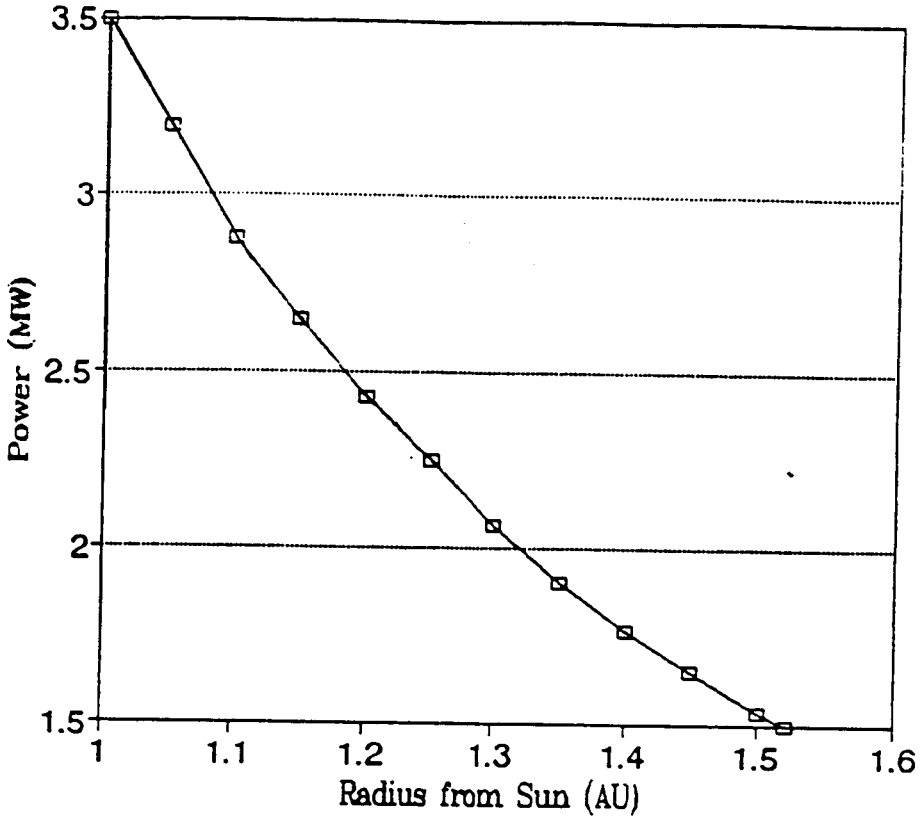

Figure 2.2: Power Provided

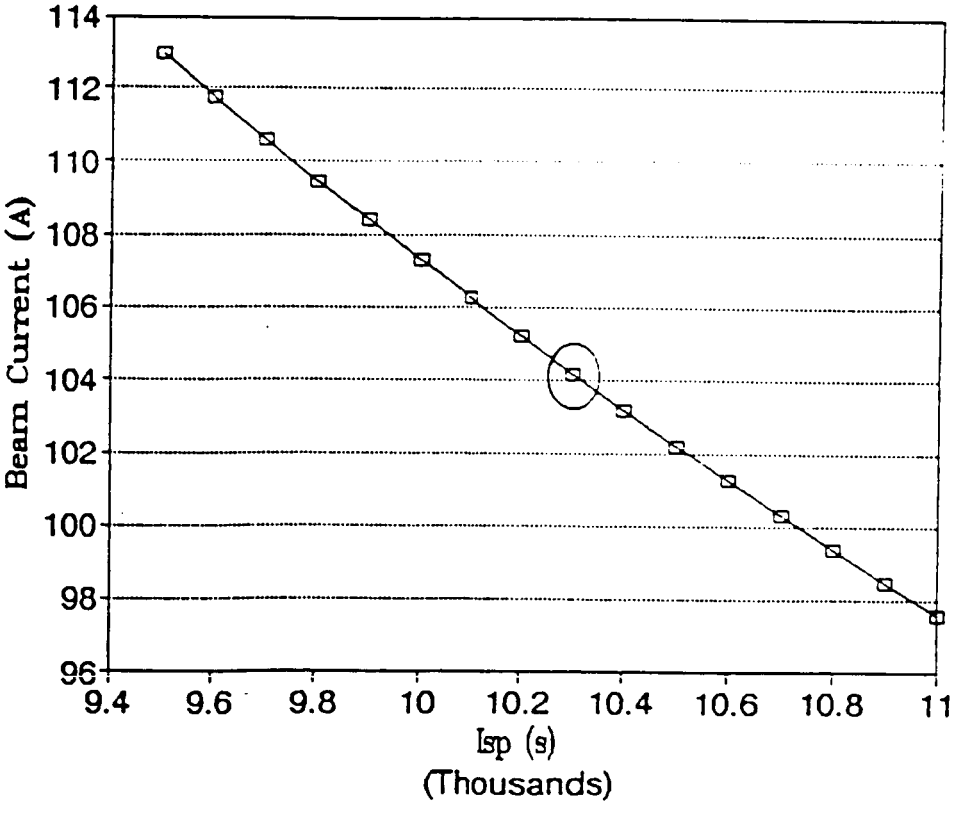

Figure 2.3: Beam Current vs. Isp
T=5N

which a range of specific impulses was run in an attempt to find the lowest initial craft mass, while still insuring a reasonable spiral out escape time. The lowest initial craft mass was found to be about 143 metric tons which corresponded to an optimum specific impulse of 10300 seconds. The second method also optimized by minimizing initial craft mass (m_o), but accomplished it through a process of solving equations for optimum specific impulse by a Newtonian iterative process [8].

$$F = 1 - \alpha/2 - e^{-\alpha} - m_L/m_O(e^{\alpha} - 1 - \alpha/2)$$

$$F' = -0.5 + e^{-\alpha} - m_L/m_O(e^{\alpha} - 0.5)$$

$$\alpha^{j+1} = (\alpha - F/F')^j$$

$$C = \Delta v/\alpha$$

$$I_{opt} = C/9.807$$

The algorithm was iterated through by updating the initial guess for the alpha value($\alpha_0=1-m_L/m_O$) until the desired accuracy of Isp was obtained. This algorithm gives an optimum Isp of 10,289 seconds, which so closely matched our first method that the number is assumed correct. Later investigations through the use of a more complex trajectory analysis proved to show a decrease in total mass to 131 mT (for the assumed performance of the power supply), however, an Isp optimization proved to be too time consuming, therefore the previously calculated Isp was kept. Once the Isp was chosen the parameters of the thruster could be found as shown in Appendix 2.1 [13]. Thruster beam current, beam voltage, total power required and efficiency were analyzed for a range of Isp and are shown in Figures 2.3 through 2.6. Total power required by the engines is 3.3 MWe at Earth and 1.32 MWe at Mars.

To estimate thruster mass, a linear scaling based on thrust to mass ratio for smaller engines was done to achieve a mass of approximately 86 kilograms (Figure 2.7). Inspection of most

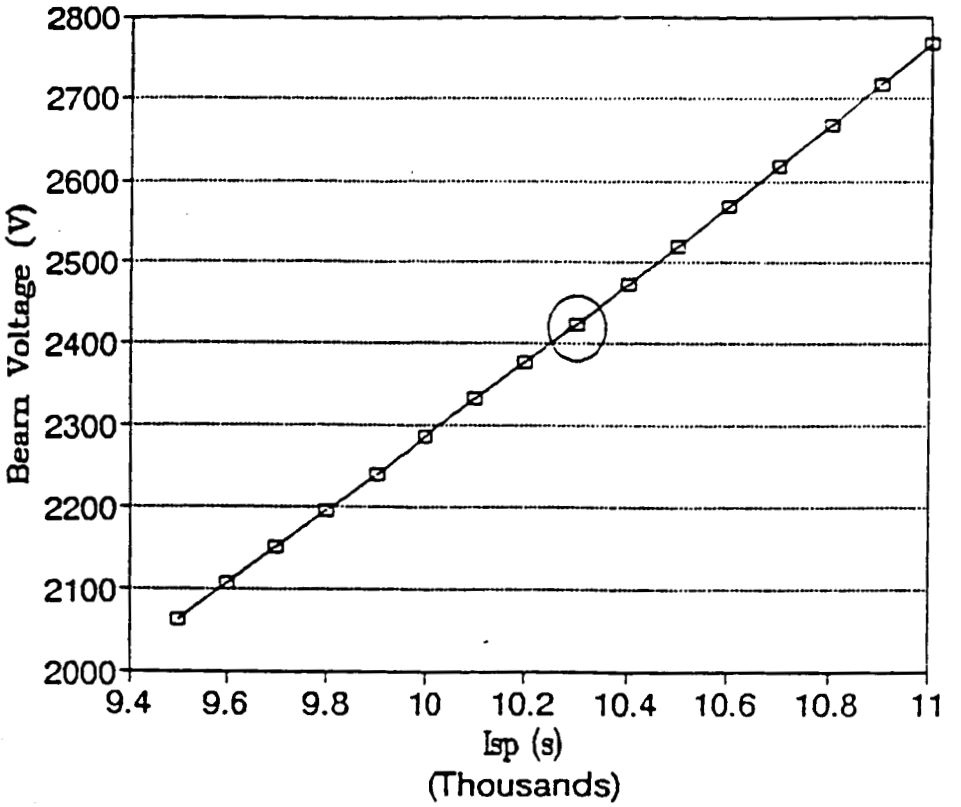

Figure 2.4: Beam Voltage vs. Isp
T=5N

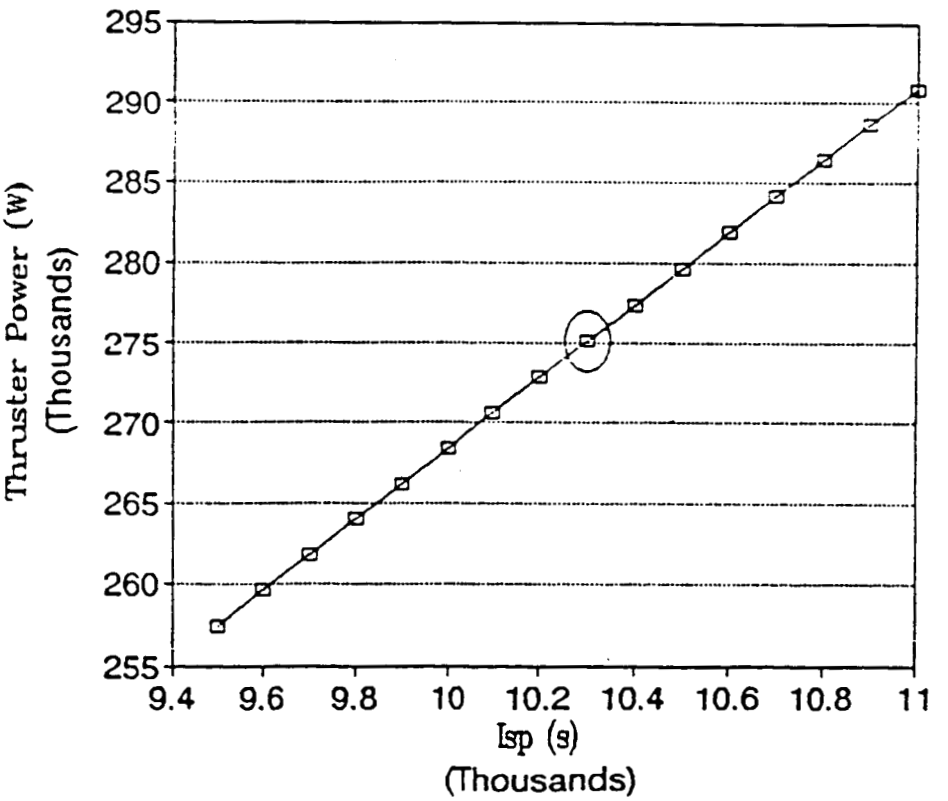

Figure 2.5: Thruster Power vs. Isp
T=5N

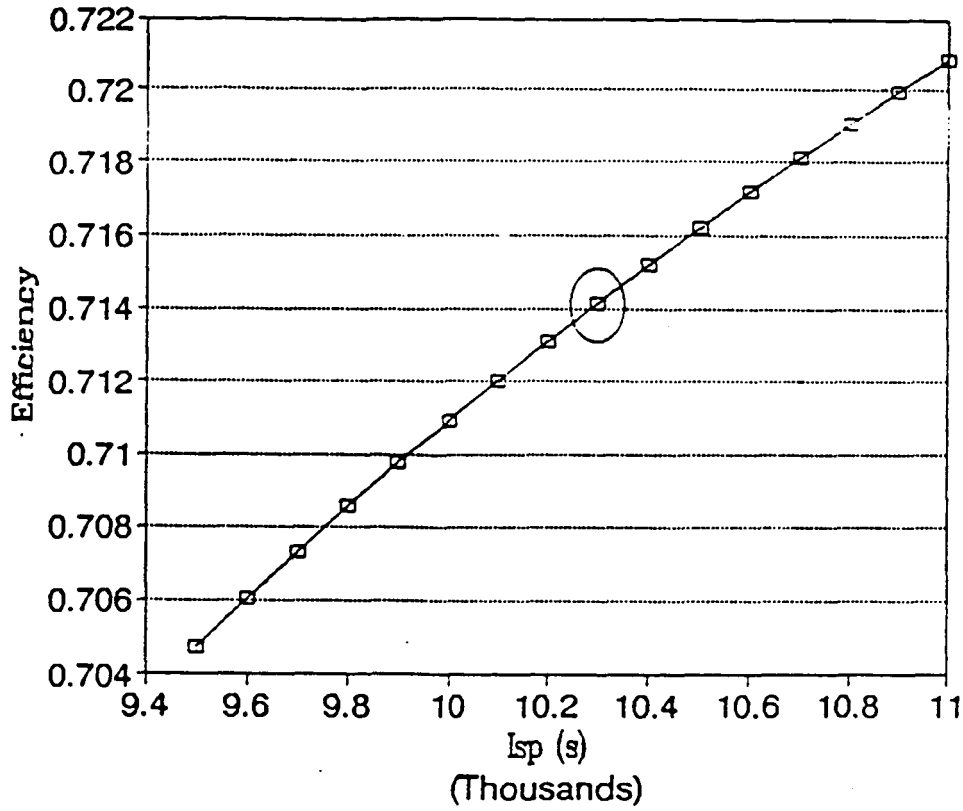

Figure 2.6: Total Efficiency vs. Isp

T=5N

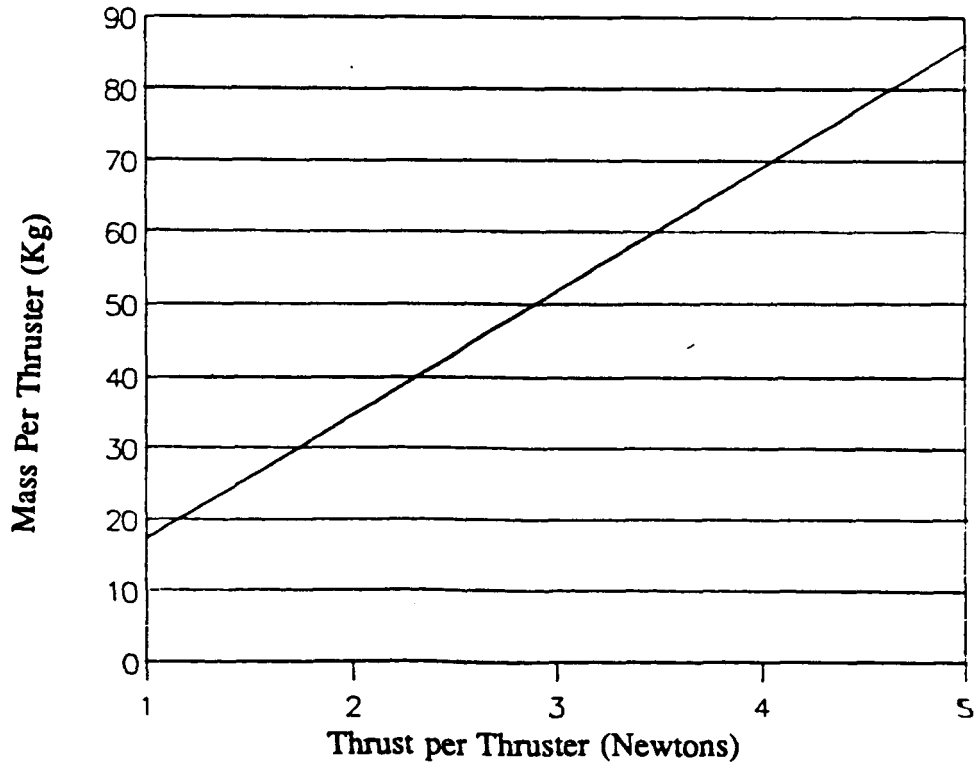

Figure 2.7: Thruster Mass Scaling

recent information from NASA led us to a final estimate of 75 kg. The diameter was found using an equation for the thrust to area ratio:

$$T/A = 2/9\varepsilon_o g^4 (m/e/d)^2 Isp^4$$

where:

$\varepsilon_o = 8.85 \times 10_{-12}$ F/m and

$D = 2(A/pi)^{0.5}$

The parameter d is the grid spacing which was taken as 0.01 meters. This value was chosen because it gives an acceptable beam current density for a long thruster lifetime. For a 5N engine, a beam diameter of 130.6 cm was obtained. The diameter including thruster casing is about 150 cm. Overall thruster dimensions are given in Figure 2.8a and the propulsion module configuration can be seen in Figure 2.8b. The main characteristics of the thruster are presented in Table 2.1.

Table 2.1 Thruster Characteristics

Thrust	5 N
Specific Impulse	10,300 sec
Propellant mass flow rate	4.9 X 10^{-5} kg/s
Beam voltage	2424 V
Beam current	104.2 A
Beam power	252.6 A
Discharge power	20.84 kw
Neutralizer power	1.69 kw
Total power	275 kw
Electrical efficiency	0.9185
Propellant efficiency	0.8619
Total efficiency	0.714
Thruster mass	75 kg

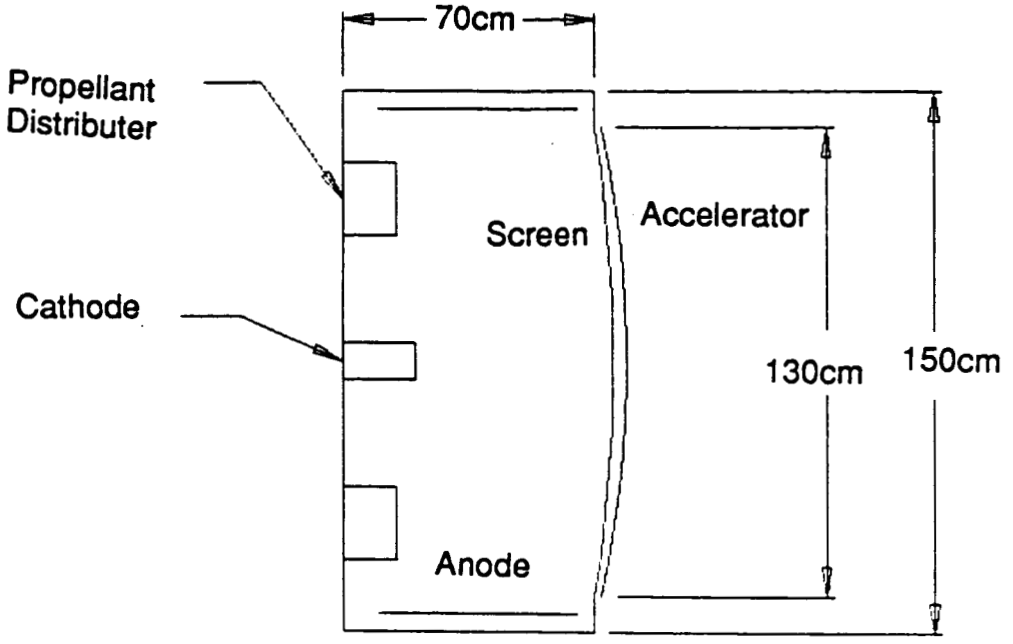

Figure 2.8 a: Electrostatic Thruster

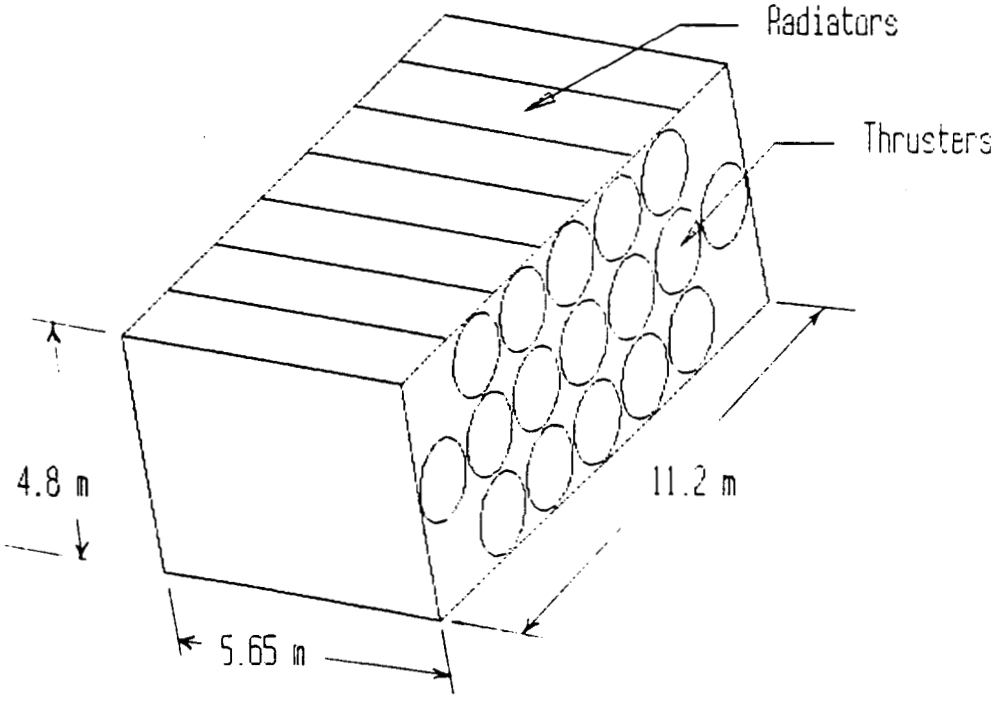

Figure 2.8 b: Propulsion Module

2.4 Thruster Degradation and Lifetime

The lifetime of an ion thruster is limited by sputtering which occurs when surface ions are emitted by collision of incident ions. This causes erosion of discharge chamber components. The lifetime is limited specifically by the erosion of the screen grid. Lifetime may be defined as the time necessary for the screen to erode to half-thickness [4].

The erosion rate is highest at the center of the grid because of the high plasma density and the high ratio of doubly to singly charged ions near the centerline, but this problem may be alleviated by the use of the ring-cusp magnetic configuration, which lowers the concentration of double charged ions at the centerline [12]. An apparent solution to the wearing of the screen grid would be to just thicken it, but this causes unacceptable decreases in thruster efficiency. Some experiments have been done with adding small amounts of nitrogen to the discharge chamber when using xenon propellant. This has increased projected lifetimes from two to four times over what was achieved without using nitrogen [10]. The effect of adding nitrogen or some other life increasing agent to argon remains to be seen. As beam current density increases the lifetime of the thruster decreases. A xenon engine with a 0.00232 A/cm^2 beam current density was shown to have a lifetime in excess of 25,000 hours. When the density was increases 3.5 times the lifetime decreased to 14,000 hours [4]. This was without the introduction of nitrogen. For the 5N thruster, beam current density of 0.00617 A/cm^2 is an acceptable value. If the nitrogen can increase the lifetime of a thruster by a factor of two, then a projected lifetime of 25,000 hours may easily be achieved. Since it is estimated from the amount of propellant needed for the round trip and the mass flow rate of the thrusters that the lifetime of the thrusters (without redundancy) must be about 14,500 hours, a lifetime of 25,000 hours would give several thousand hours above the necessary thrust time.

2.5 Propellant Tank

The propellant tank chosen is of cylindrical design with spherical ends (Figure 2.9). The tank has two shells. The outer is a vapor cooled, thin aluminum shield, while the inner serves as a pressure vessel. Trajectory estimates give a minimum propellant mass of 21,040 kg. A 15% contingency and reserve for auxiliary propulsion is added to this mass giving a final propellant mass of 24,200 kg. The argon propellant is to be stored cryogenically at a pressure of 1 atm and a temperature of 87K. From these parameters the fluid density is found to be 1420 kg/m^3 which gives a tank volume of 17.04 cubic meters. An extra 0.46 cubic meters is added to allow for fluid expansion upon vaporization, giving a total volume of 17.5 m^3.

The tank pressure vessel is composed of pre-approved cryogenic alloy, Ti-5 Al-2.5 Sn. The tank wall thickness calculated as a function of pressure, tank radius and allowable stress (0.15mm) is near or below the thickness that can be reliably manufactured. The tanks will be fabricated so that the thickness will vary from a nominal 0.4 mm to about 3 mm at the attachment points of the external supporting straps and at the locations of internal heaters and vapor acquisition devices. The tanks will be designed for space environment and will be filled in orbit. Because of the long propellant storage time in both near Earth and interplanetary space, the tank requires an adequate meteoroid/debris protection as well as thermal insulation. The latter is required to reduce boil-off during long waiting (no thrust) periods. The protective and insulating shield will consist of a surface coated polyamide face sheet, low density foam spacer with intermediate Kevlar reinforcement and multi-layer insulation (MLI) made of aluminized Mylar radiation films separated by Dacron net spacers. Assuming MLI thermal conductivity (k)

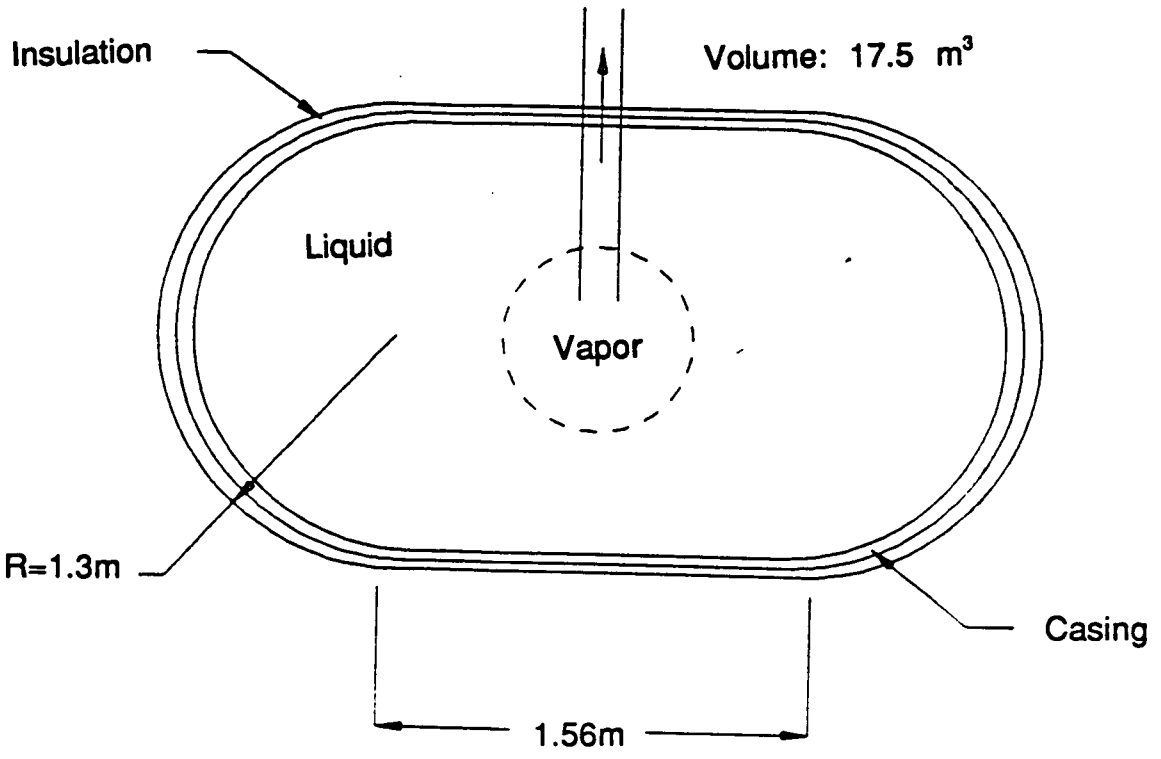

Figure 2.9: Cryogenic Propellant Tank

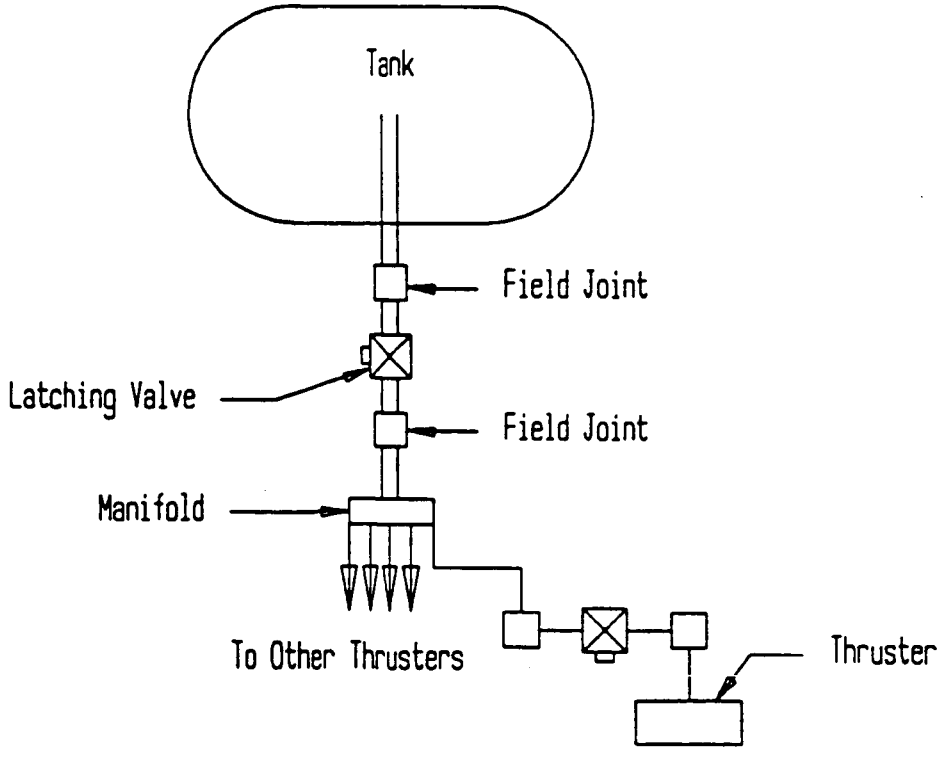

Figure 2.10 Propellant Distribution

of 0.0175 mW/m-K and 8 cm thick (d) insulation, the heat penetrating the MLI will be:

$$Q = (kA/d)(T_{ts} - T_v)$$

where
A = tank surface
T_{ts} = tank surface temperature
T_v = vapor temp

Near LEO, T_{ts} will have a value of around 330 K, and Q is 1.8 W. Assuming that additional heat conducted through the straps supporting the tank, propellant lines and electrical lines is less than 2 W, the total thermal energy reaching propellant is less than 4 W. When the thrusters are not in operation, the vaporized argon will be re-liquified by a Stirling refrigerator.

When all 12 engines are thrusting near Earth, the propellant mass flow rate is 5.88×10^{-4} kg/s and the heat required to vaporize the liquid argon is

$$Q = m\, q_{vap} = 5.88 \times 10^{-4} \times 160 \times 10^{3} = 94 \text{ W}$$

This heat, only slightly reduced by the amount penetrating insulation, must be provided by the heating coils inside the internal tank shell. A very simplified diagram of propellant distribution is shown in Figure 2.10. The mass summary of the tank system is given in Table 2.2.

Table 2.2 Mass Summary

Tank	230 kg
Meteoroid/Debris Shield/Insulation	210
Electrical heaters, sensors, controls	90
Refrigeration unit	130
Propellant lines, valves	160
	-----
	820 kg

2.6 Power Processing

The power processing is an important part of the total SEP system. This system is responsible for conditioning the power generated by the solar arrays and distributing it among the craft systems. The thrusters require the majority of the power and therefore have a separate power distribution center contained within the engine system itself. The distribution center consists of one beam and discharge power filter for each thruster. These filters are used to modify any current fluctuations that might cause inefficiencies in thruster operation leading to engine degradation [9]. These filters are grouped together in sets of three in the thruster modularization scheme; the exception being the two end thrusters which are modularized separately. All processing units are located near the center of mass of the ship in order to keep transmission line length to a minimum. The propulsion power processing system consists of the low voltage discharge and neutralizer power supplies and of DC-DC converter units for the grid power supply which requires the majority of the power input. It is assumed that the power processing unit has an overall efficiency of 95 percent and operates at 600 K. After power processing, the voltage and current supplied to individual thrusters are 2424 volts and 130 Amp.

The remaining generated power is designated to all other on-board systems. Since this power is to be conditioned for the ships operating systems it must conditioned between the standard voltages of 100 to 200 V. The systems include navigation, guidance, control, and communication. A small amount of power must be rerouted to the thruster control mechanisms and then be used when needed for thruster shutdown or control in the event of a malfunction [9]. A block diagram of the power breakdown can be seen in Figure 2.11.

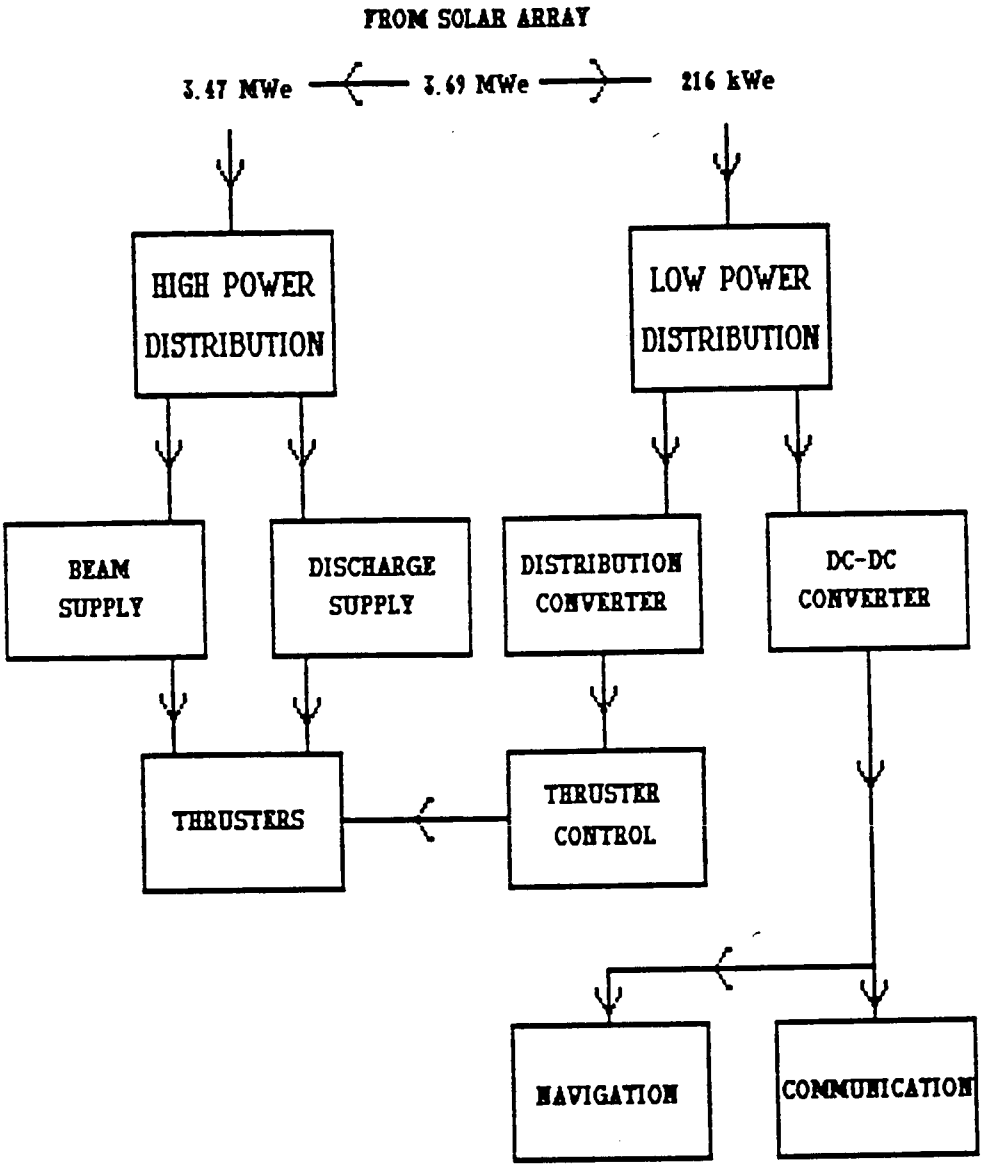

Figure 2.11: Power Distribution Diagram

2.7 Thermal Control

The heat generated by the engines and power processing units must be dissipated to space by a radiator. The latter is sized so as to be able to reject up to 11 percent of the input power, or about 370 kW. A radiator/heat pipe system was chosen as the simplest and yet most effective way of removing this heat into space. The heat pipe system will operate at a temperature of about 600 K and use stainless steel (or nickel) for pipe vessel and wicking material and potassium as a working fluid. The main design parameters of the radiators are the area and materials. Since a large amount of heat must be radiated, the main concern of the radiator design is to keep the mass down while maintaining high emissivity and conductance. The radiator will be constructed of titanium alloy providing good high temperature operation (see Appendix 2.2 for calculation). Two modularized radiator panels, each sized at 40 m^2, will be mounted on the two opposite sides of the thruster module, facing directions perpendicular to the rotation axis of the solar arrays. Radiator modularization can be accomplished alongside the thruster modularization into one large component. In this way the radiator array can be broken down in such a way that there should be no problem fitting aboard the shuttle cargo bay. The main characteristics of the thermal control system are given in Table 2.3.

Table 2.3: Characteristics of the Thermal Control System

Heat rate capacity	370 kW
Heat pipe fluid	potassium
Radiator temperature	600 K
Total radiator area	80 m^2
Total mass	1200 kg

2.8 Propulsion Module Structure

The propellant module is 11.2 meters wide by 4.8 meters tall by 5.65 meters deep. The system is modularized in groups of three thrusters, except for the two outside modules, which only have one thruster. Each module also has the power processing unit, one seventh of the radiator, and its own structure. An overall schematic diagram of the configuration may be seen in Figure 2.8b. All systems will fit as is or equipped with a modular ability, such as the engine modules, within the cargo bay of the Shuttle C. The mass breakdown of the propulsion system is given in Table 2.4.

Table 2.4: Propulsion System Overall Specifications and Mass Breakdown

Number of engines (no redundancy)	12
Number of engines (including redundancy)	17
Engine beam diameter	130 cm
Specific impulse	10,300 sec
Engine thrust	5 N
Engine input power	275 KW
Power processing efficiency	0.95
Propulsion system efficiency	0.714
Engine mass	75 kg
Gimbal mass	15
Power processing unit, per engine	330
Thermal control system	1200
Interface module and housing structure, lines, controls	800
Propulsion system mass	**9140 kg**

References

1. Byers, David C., "Characteristics of Primary Electric Propulsion Systems," NASA TM-79255, 1979.

2. Dunn, P. and D.A. Reay, Heat Pipes, Pergamon Press, Oxford, England, 1982.

3. Gilland, J.H., and Myers, R. M., "Multimegawatt Electric Propulsion System Design Considerations," AIAA Paper 90-2552, July 1990.

4. Hardy, T.L., and Rawlin, V. K., "Electric Propulsion Options for the SP-100 Reference Mission," NASA TM-88918, 1987.

5. Haselden, C.G., Cryogenic Fundamentals, Academic Press, New York, 1980.

6. Jahn, R.G., Physics of Electric Propulsion, McGraw Hill, New York, 1968.

7. Kreith, Frank and William Z. Black, Basic Heat Transfer, Harper and Row Publishers, New York, 1980.

8. Oates, G.C., Aerodynamics of Gas Turbine and Rocket Propulsion, AIAA, New York, 1984.

9. Poeshel et al., "Extended Performance Solar Electric Propulsion Thrust System Study," Hughes Research Labs, 1977.

10. Rawlin, V.K., "Internal Erosion Rates of a 10-kW Xenon Ion Thruster," NASA TM-100954, 1988.

11. Siegel, Robert and John R. Howell, Thermal Radiation Heat Transfer, Hemisphere Publishing Corp., New York, 1981.

12. Sovey, J.S., "Improved Ion Containment Using a Ring-Cusp Ion Thruster," Journal of Spacecraft and Rockets, Vol. 21, Sept.-Oct. 1984, pp. 488-495.

13. Jakubowski, A. K., notes.

SECTION 3

Solar Power

Nomenclature

AMO	Air mass zero
GaAs	Gallium Arsenide
GaAsP	Gallium Arsenic Phosphide
GaP	Gallium Phosphide
InAsP	Indium Arsenic Phosphide
InP	Indium Phosphide
Si	Silicon

3.1 Introduction

In researching standard photovoltaic cells, it was discovered that predictions for new technology and advancements in these materials are very encouraging. Efficiencies which have previously been in the 10 to 15 percent range have skyrocketed to above 30 percent. Assuming technology remains on its current course of advancement, photovoltaic cell will reach outputs of over 300 W/kg. Solar cell material tends to degrade when left exposed to the space environment without any protection and thus efficiencies decrease. Concentrator arrangements provide this protection of the raw cell material from the hostile space environment, particularly in the Van Allen radiation belts.

Indium phosphide is a leading candidate for cell materials used in space applications due to its high efficiency and radiation resistivity. Although only achieving 19% efficiency in the laboratory, there is great reason to expect AMO efficiencies above 20% based on experience with gallium arsenide and silicon [1]. With respect to exposure to electron and proton fluence, InP out-performs GaAs and ultra thin Si [8], although both of these latter materials are considered to be good radiation resistant materials with slightly higher specific powers and efficiencies than

InP [1,9]. Another impressive property of InP is its ability to essentially completely recover after exposure to a fluence of 10^{17} electrons by heating the cell at 115•C [4]. InP, therefore, possesses the ability for supplying significantly more end of life array output power than Si of GaAs in high radiation environments [8].

3.2 Solar Power Options

Flat array and concentrator systems were two photovoltaic options considered for the solar power supply. Both options utilize a InP cell material due to the properties and abilities mentioned above. The cell was also assumed to operate at 115•C in order to take advantage of indium phosphide's ability to completely anneal at this temperature. The cell for the concentrator system, however, will be a multi-stacked cell using InP as only one of the cell layers since the structure will help to protect the cell.

3.2.1 Concentrator Array

The concentrator option was prepared using Fresnel lens concentrators, selected for its superior projected optical efficiency of 96% [1]. This efficiency compares well with other concentrator systems that are based on mirrors or internal reflection. The mirror concentrators of the TRW Cassegrainian system, for example, projected lower future efficiencies in the 80% range.

3.2.1.1 Array Parameters

Taking an operating temperature of 115•C into consideration, the module efficiency at AMO was assumed to be 27.7%. The module has the dimensions 6 cm x 6 cm and a specific mass ratio of 1 kg/m^2. As seen in the calculations appearing in Appendix 3.1, the specific power of the module was found to be 320.8 W/m^2. This specific power lead to the total array area of

10,910 m and to the similar array mass of 10,910 kg. This mass value includes the mass of the radiators required to keep the module temperature at a constant value. The dimensions of the hexagonal panels are given in Appendix 3.1, as well.

3.2.1.2 Wiring Configuration

The following wiring configuration for the concentrator system was limited by a maximum voltage of 200 V, a maximum current of 20 Amps and an open current cell voltage of 945 mV. The maximum number of cells connected in series was calculated as 211 (Appendix 3.2). From this value, the length of each series, 12 meters, and the resistance through each series wire of Aluminum gage #7, 0.032 Ω, was determined. Along with the calculated current of 1.155 A, the power loss per series was found to be 0.0429 W, resulting in a total power loss of 80.2 kW. The total length and mass of the series and parallel Al gauge #7 wires were estimated to be 286.5 m and 8,225 kg, respectively.

3.2.2 Flat Panel Array

Next, a flat solar array option was developed. Since this array must survive three long round trip missions without large power losses, Indium Phosphide was chosen as the material for the solar cells for reasons mentioned earlier in the discussion on cell materials.

3.2.3 Array Specifications at Earth

An achievable cell efficiency of 21.7% was assumed from a consensus of participants of the 1987 work-shop on InP at the NASA SPRAT conference [7]. Using this efficiency, the specific power (assumed at 25•C) was calculated as 255 W/m^2. Assuming a steady state operating temperature of 115•C, the specific power and efficiency dropped to 198.5 W/m^2 and 17.6%, respectively. These values along with the total array power needed (3.5 MW) lead to a total

array area of 17,632 m^2 and total weight of the array (not including supporting structure) of 14,987 kg. The flat panel calculations and dimensions are listed in Appendix 3.3.

3.2.4 Array Heat Transfer

The steady state temperature used for the calculated values stated above was chosen for continuous annealing at the orbit around Earth. The annealing will help prevent long term power losses from the radiation encountered within the Earth orbits. Assuming a constant temperature and radiation heat transfers out into free space, heat transfer calculations (Appendix 3.4) were performed for two different scenarios. The first scenario assumed continuous annealing for the entire mission and the second scenario assumed continuous annealing only for near Earth trajectories. The assumption of continuous annealing over the entire mission was found to require a high temperature of 206•C at Earth. A better solution was found by assuming 115•C near Earth, leading to about 42•C at Mars. This will allow for annealing in the radiation belts encountered while spiraling out of Earth's influence. Although this does not allow for annealing at Mars, the lower operating temperature will give better cell efficiency and specific power at Mars.

3.2.5 Array Wiring Connections

To obtain the high cell efficiency of 21.7%, the cell voltage was assumed to equal 945 mV. For a 2 x 2 cm cell, the power per cell, 0.120 W, lead to the power of each series wire equalling 25.3 W and to the current found in each series connection equalling 0.126 Amps. Using a similar wiring scheme to the one formulated for the concentrator system and an Aluminum gauge #7 wire, the total wire mass was estimated to equal 11,100 kg, bringing the mass of array and wiring to 26,087 kg. Calculations are given in Appendix 3.5.

3.3 Selection of Solar Power System

Initially, the concentrator system was chosen for several reasons including the higher specific power achievable and the added radiation protection which the lens provided for the solar cell. Through comparison of the concentrator system and the flat array option, justification for the use of concentrator systems over flat arrays can be seen.

Table 3.1 compares some assumed and calculated values for these two solar power options. The specific power at 115•C for the concentrator is about 62% greater than that achieved by the flat plate; therefore, the area of the concentrator array is 62% less than the flat plate area. The mass of the concentrator array is also much lower than that of the flat plate array. Supporting structure considerations also lean in favor of the concentrators which themselves provide a great deal more rigidity. For the supporting structure, the enlarged area of the flat system will increase the array support mass. Linearly scaling for characteristic length of array, a mass increase of about 17% for array support was found. Comparing the value of the flat panel and wiring mass to that of the concentrator and wiring mass, the flat array combined mass was found to be 6,952 kg more than the concentrator system value. Finally, the power losses calculated for the flat array are over 2.5 times greater than concentrator system losses.

Table 3.1 Comparison of Flat Array and Concentrator System

Attribute	Flat Array	Concentrator
Specific Power at 115°	198.5 W/m^2	320.8 W/m^2
Area of Array	17,632 m^2	10,910 m^2
Characteristic Length (d)	93.0 m	79.4 m
Masses: Array Wiring	14,987 kg 11,100 kg	10,910 kg 8,225 kg
Power Loss of Wiring	297,850 W	80,170 W

While the comparison above is preliminary and based on highly simplified assumptions, it does indicate that a concentrator system used in multi-megawatt applications may greatly outweigh the performance of a flat array power system.

3.4 Selected Solar Power System Design

3.4.1 Solar Cell Configuration

Combining the materials mentioned in the Introduction and stacking them in a configuration provides added efficiencies to the top cell. Lower cells absorb a different bandgap (wavelength) of light which adds efficiency numbers to the top cell. Cells stacked in this configuration have efficiencies much higher than 30 percent with efficiencies under concentration predicted above 40 percent. Figure 3.1 shows the three solar cell stack selected for our array [5]. This cell will use a six-terminal wiring configuration to minimize current mismatch losses which may be caused by different degrees of radiation damage to the three solar cells. The GaAsP on GaP top cell which determines the performance of the triple stack is the most advanced wide bandgap cell currently under development. The state-of-the-art GaAs cell will serve as the middle cell. The InAsP bottom cell is the best developed, and, even when "immature" can only improve the total conversion efficiency by scavenging the low energy photons from the top two solar cells. A theoretical efficiency limit of this triple solar cell stack is 42.8% at AMO, and a practical system efficiency of 35.9% is predicted by Barnett, Trumble, et al [3]. In application to this mission, an efficiency of 27% is chosen to account for the high operating temperature of about 150•C and the radiation damage occurring during the three Mars missions.

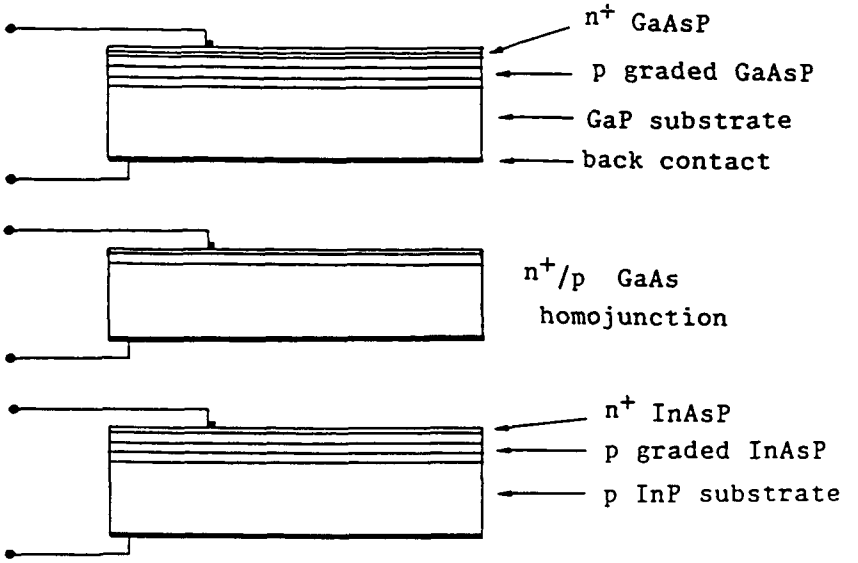

Figure 3.1: Triple Stacked Solar Cell
(Barnett and Trumble)

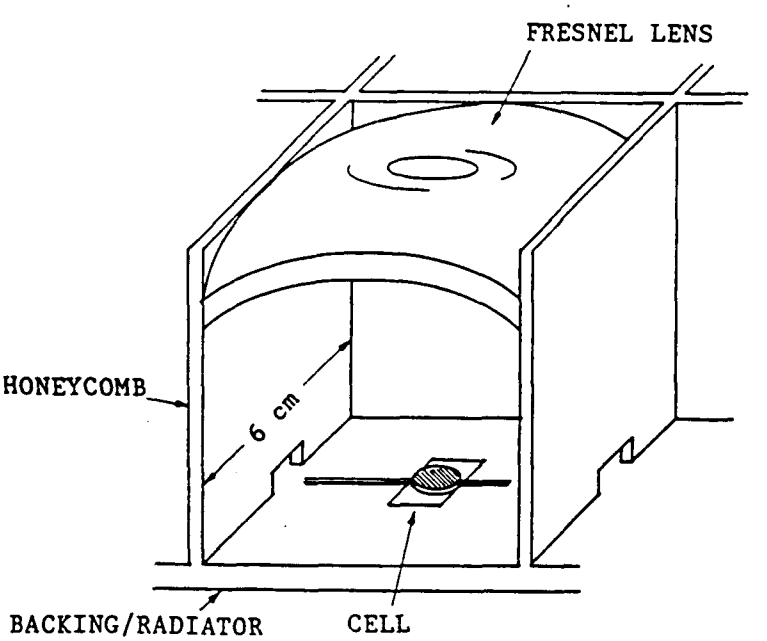

Figure 3.2: Fresnel Lens Module

3.4.2 Fresnel Lens Concentrator Array

The solar array is made up of many small modules. Each small module consists of a Fresnel lens dome that concentrates the incident sunlight on the solar cell, a honeycomb supporting structure, a multistacked cell, and a back radiator surface to dissipate excess heat produced by the cell.

The Fresnel lens dome consists of annular prisms made of silicone that use refraction to concentrate light on the cell. Optical efficiencies of 92% have been achieved and with the addition of anti-reflective coating to the lens, the already mentioned projected optical efficiency of 96% can be obtained [1]. This dome system can take up to one degree tracking error and, if necessary, can be modified to allow for a tracking error of up to four degrees [1].

The honeycomb structure will be made of graphite-epoxy with a protective coating. This structure provides a simple way to create a rigid array with less weight penalty than other systems. A thin aluminum sheet covers the rear of the panel in order to radiate excess heat from the power producing cell. The mass estimate of the radiator is based on a 150•C cell operating temperature (thickness = 0.0025 cm). A detailed mass breakdown of the array is given in Appendix 3.9.

3.4.3 Selection of Array Parameters

The selection of array area parameters was determined from the power requirements of the propulsion system combined with the efficiency of the Fresnel lens system in converting sunlight into electric power. The thickness of the array was determined from strength parameters. The array was designed so as to allow a maximum of 2 degrees deflection between any point on the array and the central point of attachment to the ship's truss.

The honeycomb structure (Figure 3.2) provides essentially all of the array's resistance to

bending. The two parameters that can be varied are the thickness and the height of the honeycomb walls. Increasing the height of the walls will increase the thickness of the array and, therefore, increase the volume of the array, which means the array will increase in both strength and mass. These parameters were chosen so as to minimize mass while keeping a reasonably small array volume while also maintaining a maximum array angle of deflection of 2 degrees.

The array optimization program (see Appendix 3.6) plotted wall thickness against array mass. At each height value, wall thickness was chosen so as to maintain a deflection of 2 degrees at point A, as seen in Figure 3.3.

The plot generated by the optimization program was the basis for the choice of honeycomb substructure parameters. Looking at Figure 3.4 and realizing that increasing the height of the cell compromises the number of units which can be launched in the space shuttle, a wall height of 6.48 cm was chosen as a compromise, corresponding to a 6 cm x 6 cm x 6.48 cm module size. The honeycomb wall will be .015 cm thick, and using these parameters for the array, we have a maximum deflection at point A of 1.89 degrees and at point B of 1.69 degrees (Figure 3.3).

The total array area of both hexagons will cover 11,957.76 m^2 and have a total mass of 6,792 kg with an added 15% contingency of 1,019 kg for a total mass of 7,811 kg estimated. The solar cells have the capability to provide 3,836,133 Watts of power before transmission.

3.4.4 Array Wiring

The 3,321,600 Fresnel Lens concentrator modules are arranged into two hexagonally shaped arrays. The objective was to deliver the power produced by the cells to the power processing units aboard the ship. The following criteria were established in wiring of the solar cells. A maximum voltage of 200 Volts was established to prevent arcing in the array. The wires going through the array should not carry more than 20-25 Amperes in order to reduce high power

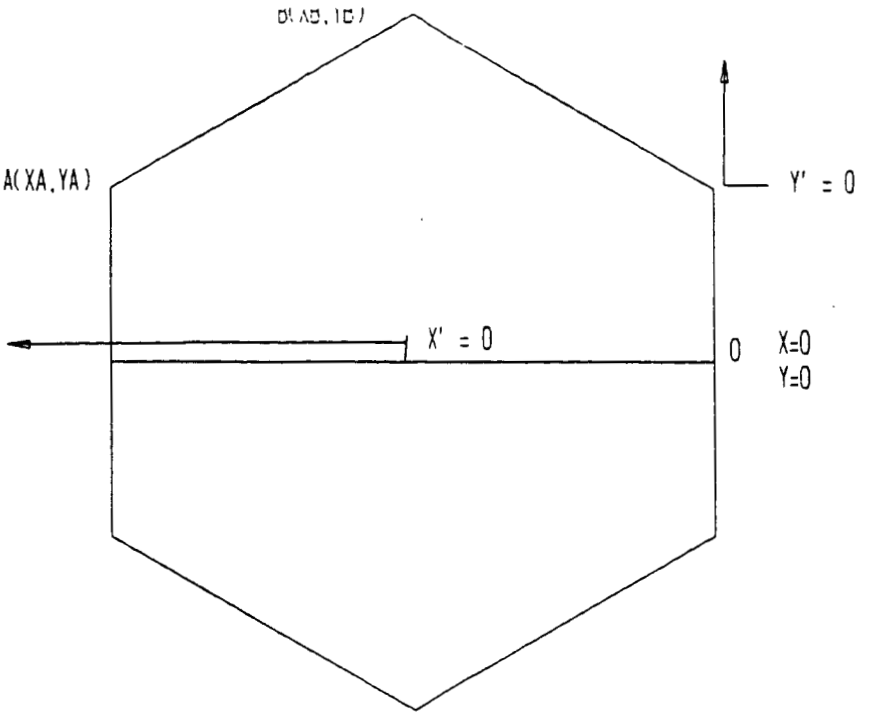

Figure 3.3: Diagram for Sizing Program

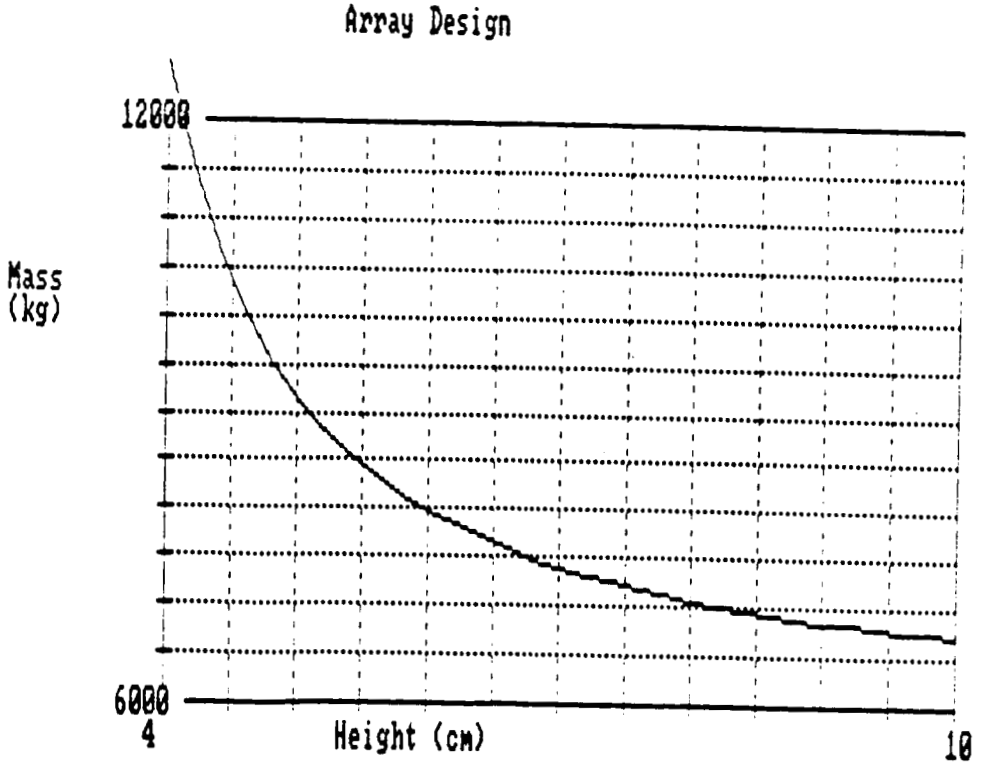

Figure 3.4: Box Sizing

losses and to prevent the creation of large magnetic fields within the panel. The wiring scheme was established systematically to ensure easier assembly of the solar arrays as the design evolves. To prevent high power losses and prohibitive wiring weights, the lengths of the high carrying wires was reduced as much as possible. The total length of wire was also kept to a minimum. Final wire design calculations appear in the Appendix 3.8.

Each of the two arrays is divided into three equal parallelograms, as seen in Figure 3.5. Each parallelogram is divided into 173 segments that deliver their power to an electrical load carrying cable that runs beneath the array and along a side of the parallelogram. Each segment is made of 16 series in a line. See Figures 3.6 and 3.7 for the design of these segments and series. The series contain 4 rows and 50 columns of modules that are linked together by one wire. This wire connects itself to wires running along both sides of its segment.

Table 3.2 shows the wires selected in order to minimize power losses and wiring mass. Standard sizes of copper and aluminum wire were considered. The selection was broken up into: wiring of modules into series, wiring of series into segments, wiring of segments to deliver power to the center of the arrays, and the wiring of the array to the engines' power processing units. The wiring program is set up such that 50 Watts of power loss is equivalent to 1 kg of wire mass and the wire that minimized this combination was chosen for each different wire current (see Appendix 3.7). Using this wiring system, transmission power losses equal 140,327.7 Watts and the wiring mass equals 1,696 kg. With a 15% contingency of 254 kg, the wiring mass is estimated at 1,950 kg. The total power delivered to the ship's power processing units, then, becomes 3,695,805 W.

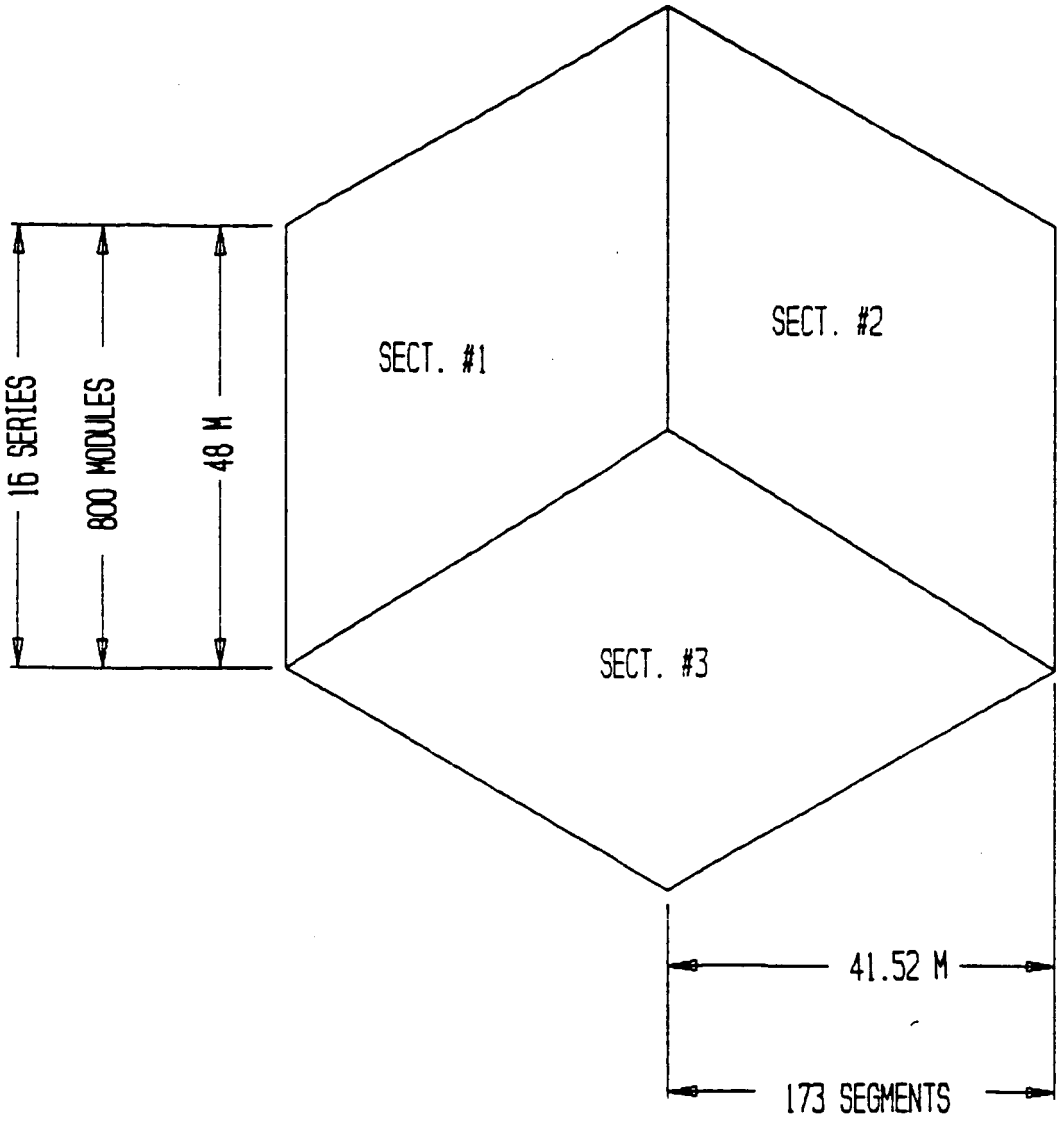

EACH MODULE: 0.06 M X 0.06 M

EACH SERIES: 5 ROWS X 50 COLUMNS

EACH SEGMENT: 16 SERIES LONG

EACH SECTION: 173 SEGMENTS

Figure 3.5: Concentrator Wiring Breakdown

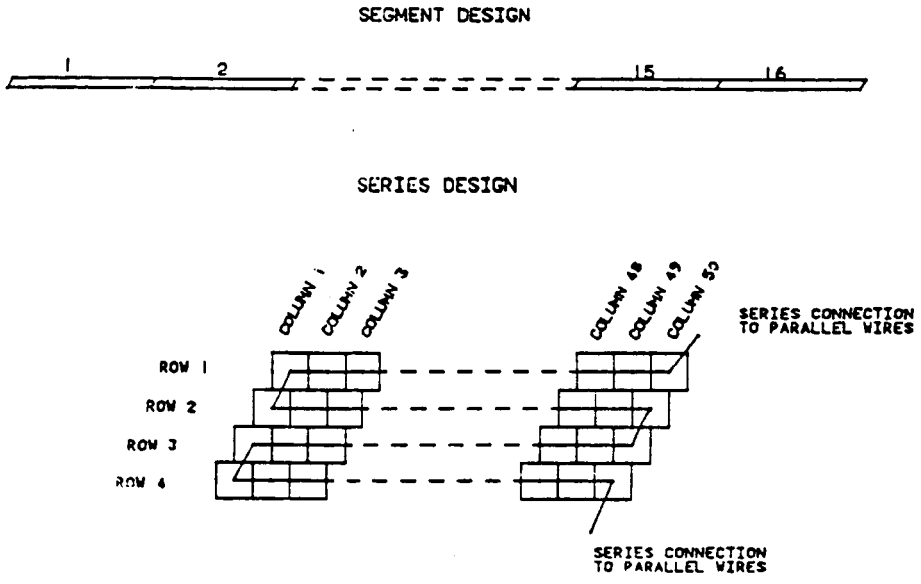

Figure 3.6: Wiring Divisions of Sections #1 and #2

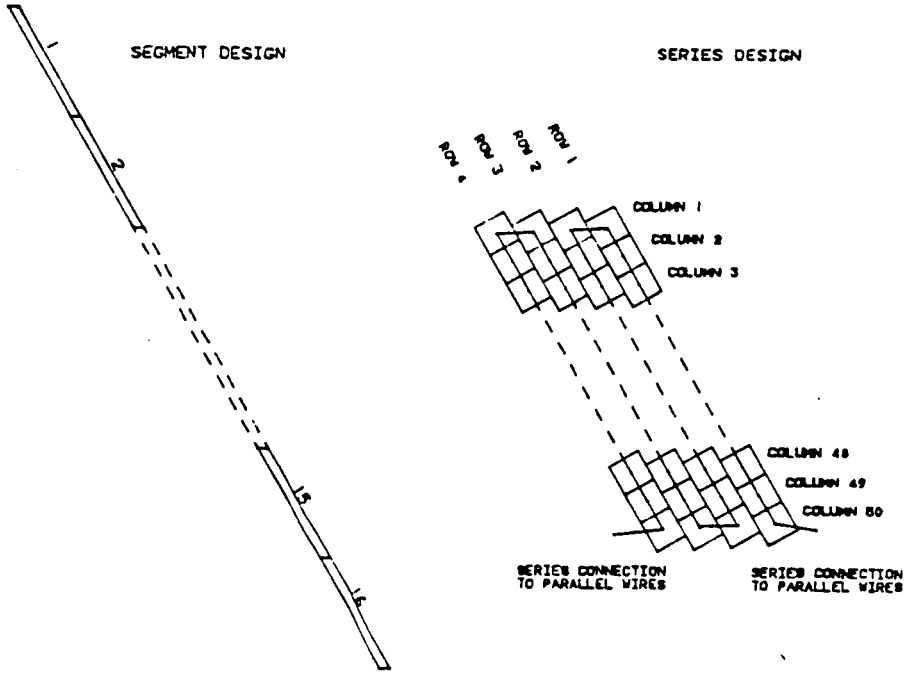

Figure 3.7: Wiring Divisions of Section #3

Table 3.2: Specific Wire Selection

Current (A)	Length (km)	Material Gauge #	Power Loss (W)	Mass (kg)
Modules Wired Into Series				
1.2286	216.0915	Al 20	17810.12	302.53
Series Wired Into Segments				
2.4572	6.5500	Al 17	1079.69	18.34
3.6859	6.5500	Al 15	1521.66	29.21
4.9145	6.5500	Al 14	2151.48	36.81
6.1431	6.5500	Al 13	2669.57	46.37
7.3717	6.5500	Al 12	3043.31	58.49
8.6004	6.5500	Al 11	3284.76	74.02
9.8290	6.5500	Al 11	4290.30	74.02
11.0576	6.5500	Al 10	4308.69	93.01
12.2862	6.5500	Al 10	5319.37	93.01
13.5148	6.5500	Al 9	5096.51	117.25
14.7435	6.5500	Al 9	6065.27	117.25
15.9721	6.5500	Al 9	7118.27	117.25
17.2007	6.5500	Al 8	6550.14	148.03
184293	6.5500	Al 8	7519.30	148.03
		Subtotal:	77,828.52	1473.62
Segments wired to center of hexagon				
19.658	.0033255	Al 8	4.34	.07516
2x 19.658	.0033255	Al 5	8.69	.15065
3x 19.658	.0033255	Al 3	12.26	.23944
4x 19.658	.0033255	Al 2	17.29	.30196
5x 19.658	.0033255	Al 1	21.43	.37911
6x 19.658	.0033255	Al 0	24.47	.47888
7x 19.658	.0033255	Al 0000	1.66	.96108

Current (A)	Length (km)	Material Gauge #	Power Loss (W)	Mass (kg)
8x 19.658	.0033255	Al 0000	2.17	.96108
.	.	.	.	.
.	.	.	.	.
173x 19.3658	.0033255	Al 0000	.	.96108
		Subtotal	59,148.32	162.12
Hexagon to power processing units on ship				
784.8 (at 2444 V)	.20608	Al 0000	3350.87	59.56

Total Transmission Power Loss = 140,327.71 W
Total wire mass = 1,695.53 kg
+ 15% contingency = 1,950 kg

References

1. Mark O'Neill and Michael Piszczor. "An Advanced Space Photovoltaic Concentrator Array Using Fresnel Lenses.", Twentieth IEEE Photovoltaic Specialists Conference, 1988, Volume II, pp. 1007-1012.

2. Mark O'Neill and Michael Piszczor. "Development of Fresnel Lens Concentrator for Space Application." N87-26427, NASA Lewis Research Center and Entech, Inc.

3. Barnett, Trumble, et al. "Three Solar Cell Mechanically Stacked, Multijunction System with Energy Conversion Efficiency Greater than 30% AMO." Twenty second IECEC Conference.

4. F.H. Valade. "Space Station Solar Concentrator Development." Harris Corporation, Government Aerospace Systems Division, Melbourne, Florida.

5. Weinberg and Brinker. "Indium Phosphide - Status and Prospects for Use in Space." NASA Lewis Research Center.

6. Goradia, Ghalla-Goradia, and Curtis. "Optimal Design of GaAs - Based Space Solar Cells for 100x AMO, 80•C Operation." NASA Lewis Research Center and Cleveland State University.

7. T. J. Coutts. "InP Materials/Cell Fabrication." Solar Energy Research Institute, Golden, Colorado, 1987.

8. Flood, Dennis J. and Brandhorst, Henry. "Chapter 3: Space Solar Cells." from "Current Topics in Photovoltaics", Volume 2. (Academic Press, Inc.), London, 1987.

9. Hirano, et. al. "Ultrathin Silicon Solar Cell for Space Application." Proceedings of 3rd Photovoltaic Science and Engineering Conference in Japan, 1982. Japanese Journal of Applied Physics, Vol. 21 (1982) Supplement 21-22, 23-26.

SECTION 4

Structures

Nomenclature

a_1	acceleration of point 1
a_{ship}	linear ship acceleration
A	cross sectional area
A_{panel}	fractional area of panel
A_{strut}	equivalent strut area
D	plate stiffness
D_{max}	maximum diameter
E	Young's Modulus
f	natural frequency
H	support truss depth
I	area moment of inertia
I_o	initial I of the strut
L	strut length
L'	strut half-length
m_{ij}	consistent mass matrix entry i,j
$m_{inertial}$	mass of inertial load at pt 1
m_{lp}	mass of fraction of solar panel
m_{node}	node mass
m_{strut}	strut mass
N_i, N_j	shape functions
P_{cr}	critical load
r_1	distance from c.o.m. to point 1
t	strut wall thickness
t_{face}	solar panel flat plate thickness
U	strain energy
w	mass fraction
α	moment of inertia exponent
ν	Poisson's ratio
ρ	density
ϖ	vibration rate

4.1 Truss Systems

The supporting structures of the craft are crucial to the overall system. Since we are dealing with a very large solar array system, the main concern is that the supporting structure be lightweight, yet sturdy and controllable. Choices for such truss systems must be both adaptable and functional.

Supporting truss structure for space applications has become an area of extensive study. Most of the research done on space applied truss structures and the construction scenarios for these systems has been directed for use by the Space Station Freedom (SSF). Much of it is extremely well suited for our purposes.

4.1.1 Strut Elements

A tetrahedral truss system made up of individual strut members and nodes, is widely studied for use on large, low mass structures, such as in the support of large reflector panels and for use on the Space Station Freedom [8]. A strut formed from two conical half-struts joined at their larger ends as seen in Figure 4.1 is suggested for space applications. The columns, end joints, and unions are designed for low-weight, high packing efficiency, single-assembly space truss applications [2]. The non-uniform cross sectional area allows for making the struts hollow, i.e. lighter, while not compromising the strut's strength and actually increasing its resistance to buckling.

This particular design aids in the prevention of buckling of individual members by tapering their cross sections. By increasing the thickness at the center of the half-conical strut to about 10 cm and tapering it to about 5 cm on the end, the resulting strut is sturdier [1]. Using strain energy principles, the critical buckling loads can be compared for a tapered and a uniform beam. Consider a uniform cross sectional beam that has an area moment of inertia, I, equal to

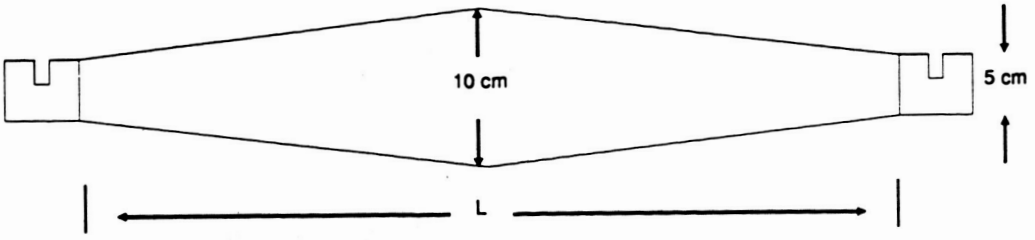

Figure 4.1: Strut Configuration

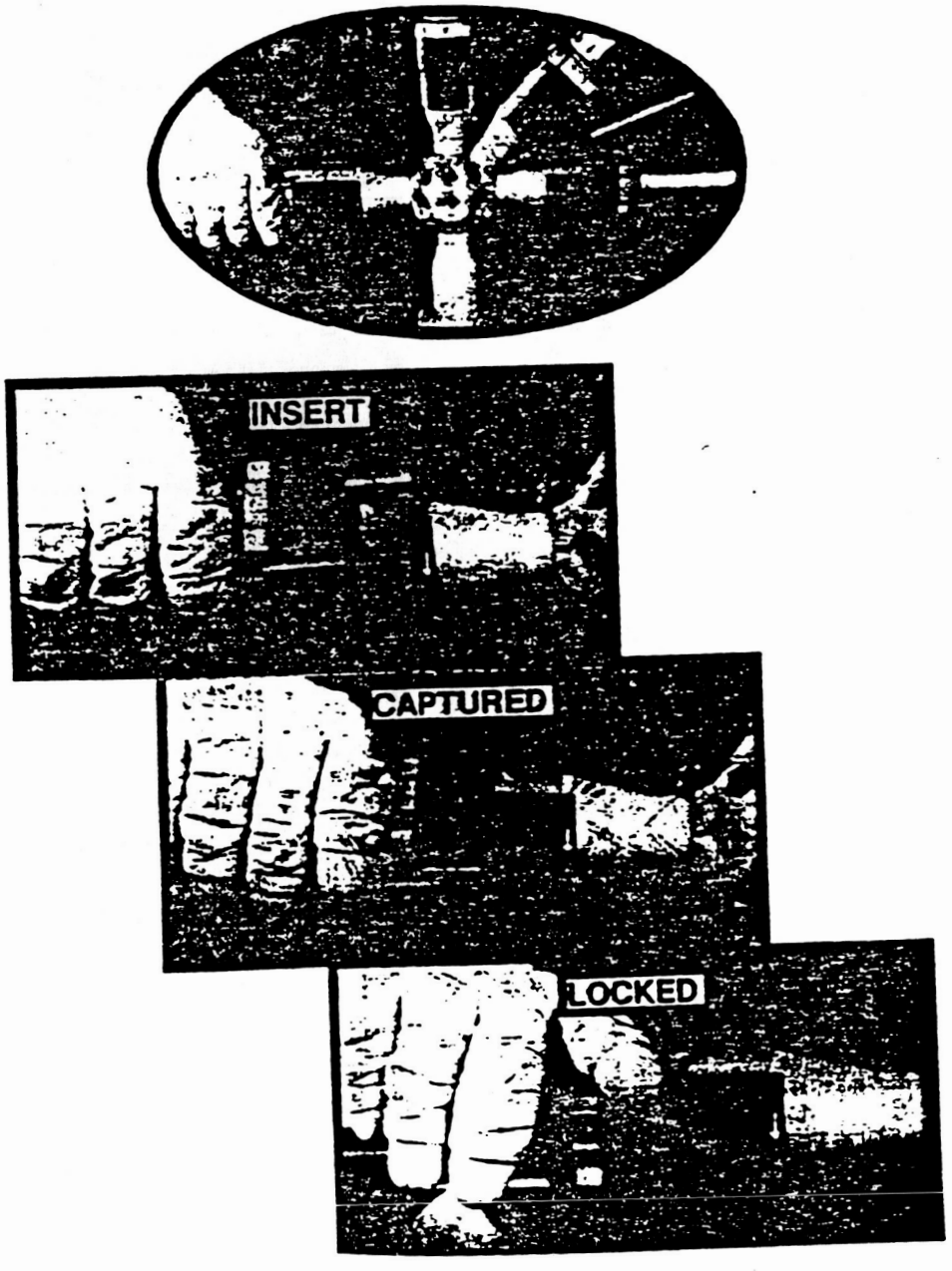

Figure 4.2: Node Attachment Illustration

the average of the tapered beam. The resulting critical buckling load for the tapered beam is 1.3 times higher than for the non-tapered beam. Thus, a typical strut member like that in Figure 4.1 can carry a higher load per unit mass than a uniform cross sectional beam.

4.1.2 Strut Assembly

Each half strut is connected by interlocking spring latches that are tapered to aid in alignment of the joint halves. The smaller end of the strut is threaded to receive one half of an internal spring loaded latching pawl that is designed for both quick attachment and quick release. One end of this joint is permanently attached to a nodal cluster similar to Figure 4.2, whereas the other half is attached to the strut itself [4]. Attachment of the strut to the node is also outlined on Figure 4.2. The strut end must be inserted into the node element and is then rotated to capture. It is then locked into place by rotating a locking collar 45 degrees [11]. The painted code, i.e. the black squares that line up when the strut is locked, was developed to ensure a quality connection and was suggested by astronauts while doing assembly tests at the Marshall Space Flight Center in their Neutral Buoyancy Simulator [5]. Assembly times of truss members, materials and masses will be discussed later in this section.

4.2 Solar Array Support

For the support of the solar arrays, we are faced with a number of specific criteria that will help determine the supporting structure. The power requirements of the ship establish the total area of solar panels that must be supported. Also, the solar cell system has a margin of sunlight detection error that dictates the maximum amount of out of plane deformation the structure can tolerate. In essence, this must be a near precision system with a maximum deflection of less than two degrees on its outer edge. For a large structure such as this, it is desirable to make it as stiff as possible [3]. That is, it must be resistant to vibration as well as

having the ability to support sufficient loads.

Several methods were considered for the support of the solar panels. Solar blankets were first considered for the flat solar arrays since this method was easy to deploy and had a very small mass per unit area. However, as the parameters of the ship, such as power required and choice of the solar cell evolved, this method became inadequate. The Fresnel lens system could not be "rolled up," as in a blanket, due to its rigid structure. Also, the required area was too large to be adequately supported against vibrations and deflections with the blanket method. Thus, the solar blanket was completely inadequate and not stable enough to justify its simplicity. Another method considered was to just wrap the solar cell membrane around a hexagonal frame. This also proved to be insufficient due to the nature of the Fresnel lens system. The Fresnel lens system cannot be wrapped around a frame which added very little support to the solar system against vibrations out of plane.

An alternate method of support was needed with better stability for a large surface area. Current research in precision reflector systems seemed well suited for our purposes. The underlying principle lies in that a hexagonal support structure made up of tetrahedral elements, as shown in Figure 4.3, is extremely stable. A hexagonal truss system has the tetrahedral, a 3-dimensional triangle, as its primitive. A type of pyramid, the tetrahedral is the most basic 3-dimensional, non-collapsible unit [7]. Thus, large arrays of tetrahedral elements, which can be easily arranged in the form of a hexagon, are currently being studied for large space structure applications [2].

The total solar panel area is assumed to be 11,600 m^2. Each support structure must cover an area of 5,800 m^2 which corresponds to a hexagon that is 48 m on a side. A hexagonal truss made up of tetrahedral elements is usually characterized by the number of "rings" it incorporates. The number of nodes, struts, and strut length size for a fixed area of 5,800 m^2 for a number of

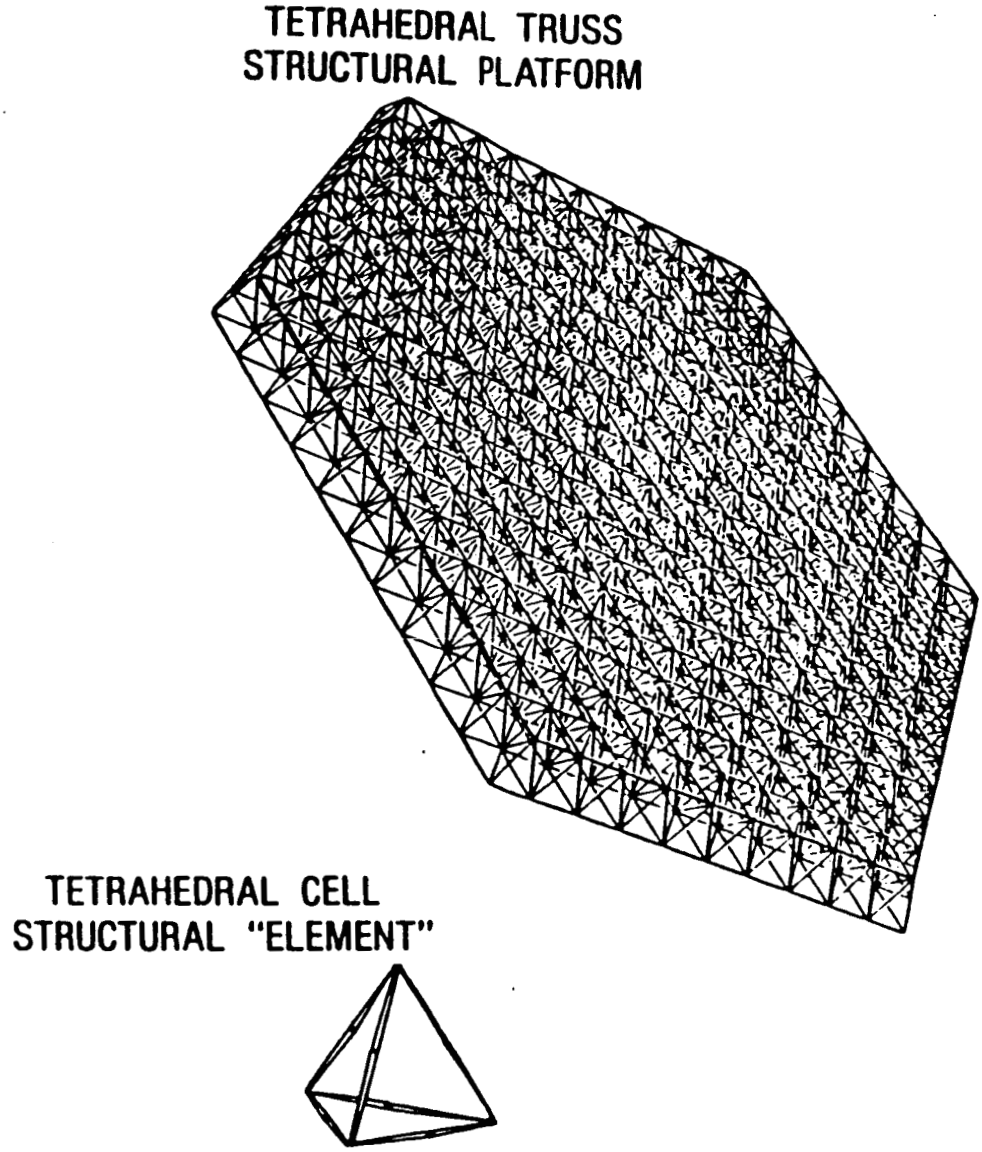

Figure 4.3: Hexagonal Truss

"rings" is given in Table 4.1. These numbers were found by a systematic counting system developed with the aid of a computer program that found the number and placement of the nodes for a given number of "rings" where a "ring" consists of a concentric array truss structure shells increasing the truss diameter. This was done in preparation for the structural analysis of several different numbers of rings. As seen in Table 4.1, the number of struts starts increasing dramatically as the number of rings increases. More importantly, with the exact number of nodes and struts known, supporting truss system masses have been determined for the solar panels using different numbers of rings (Table 4.1).

Table 4.1
Hexagonal Support Truss Parameters

Rings	Nodes	Struts	Strut Length
3	64	243	16
4	109	420	12
5	166	660	9.6
6	235	954	8
7	316	1302	6.9
8	409	1704	6

4.3 Structural Analysis

The structural analysis of this design consists of several parts. The stresses in individual members of all truss structure are of great importance, since we do not want to exceed the maximum allowable stress for the material. With the use of the finite element code, STAP, the box truss and the Solar Panel support structure were analyzed. STAP stands for Static Analysis Program and is a computer program that carries out a static linear elastic finite element analysis.

4.3.1 Strut Analysis

The half conical hollow strut members need to be modeled as a uniform truss element of uniform material and area. An equivalent area may be determined using the principle of conservation of strain energy. Taking advantage of the symmetry of the strut, we only have to model half of the strut. The equivalent area can be expressed as:

$$U=\int\frac{EA}{2}(\frac{\partial u}{\partial x})^2dx=\int\frac{EA_{eq}}{2}(\frac{\partial u}{\partial x})^2dx$$

Knowing that, for beam elements, du/dx is a constant and the material Young's modulus is also constant, this relation becomes:

$$A_{eq}=\frac{1}{L'}\int A(x)dx$$

Hence, the equivalent area is simply an average over the half strut length, L'. It is now necessary to find the initial cross sectional area as a function of x. Assuming that the wall thickness is constant and specifying a maximum strut diameter of 10 cm with a minimum diameter of 5 cm, this function becomes:

$$A(x)=\pi(\frac{0.05t}{L'}x+0.05t-t^2)$$

Integrating from 0 to L', this reduces to:

$$A_{eq}=\pi(0.075t-t^2)$$

which is only a function of the wall thickness. Therefore, finding an equivalent area, using this method of energy conservation, becomes a simple task of setting the wall thickness. With the wall thickness and the strut length as parameters, the final strut element to be used can be

determined by examining the results of the STAP program.

Based on overall performance of the support structure for a number of rings, i.e. a number of strut lengths, the final sizes of the individual parts of the truss system were determined. The stress criteria, critical buckling loads, deflections, as well as overall mass, are the deciding factors in sizing. Although dynamic thermal loads will be the most crucial source of loads and deflections for this design, they are difficult to analyze with the resources available.

Inertial loads due to the ship's acceleration and rotation were evaluated in the STAP program. These loads are highest when the ship is spiraling out or in to Earth. Given a forward acceleration, a_{ship}, due to thrusting, of 5×10^{-4} m/s^2, and an angular rotation rate, ϖ, of 1.13×10^{-8} rad/sec, the local acceleration at any point along the ship is:

$$a_1 = a_{ship} + \omega^2 r_1$$

The radial distance, r_1, to a point on the ship is measured from the center of mass of the ship. The center of mass is 0.78 m offset toward the cargo pod from the center of the box truss connected to it. The resulting inertial forces are simply the mass of the component times the local acceleration given by the above equation and are applied as point forces.

The strain energy of a tapered element is given by:

$$U = \frac{E}{2} \int I(x) \left(\frac{\partial^2 v}{\partial x^2} \right)^2 dx$$

where I(x) is the area moment of inertia. This is given as:

$$I(x) = I_o \left[1 + r \left(\frac{x}{L'} \right)^a \right]$$

where I_o is moment of inertia at the tip. I_o is 3.742×10^{-8} m^4 for a strut wall thickness of 0.0008

m. The factors r and α are 7.1967 and 1.5663 respectively if symmetry is used and L' is half the strut length. The stiffness matrix is found by invoking Castigliano's theorem and the buckling load, P_{cr}, may be found by solving the eigenvalue problem that results from work principles [13]. The geometric stiffness matrix, $[k_g]$, is the same as for a straight beam, thus giving the eigenvalue problem,

$$|[k]-\lambda[k_g]|=0$$

where λ is a function of P_{cr}. This calculation for a strut 16 m in length (L'=8m) with E equal to 1.723×10^{11} N/m^2 yields a critical buckling load of 112.2 N. This method was also used to justify a tapered strut earlier.

4.3.2 Hexagonal Tetrahedral Truss Analysis

An exact analysis of the solar array support structure would incorporate plate elements as well as truss elements. Plate elements are needed to accurately model the added stiffness due to the solar panels. The STAP program considers only truss elements. Therefore, in order to account for the solar panel stiffness, mass as well as cross sectional area of the top truss elements are increased in the following manner.

An equivalent flat plate representing the solar panels has a thickness of 0.00566 m consisting of graphite epoxy. The cross sectional area of the top truss elements is then increased by $(w*t_{face})$ or $2(w*t_{face})$, where t_{face} is the plate thickness of 0.00566 m and w is a fraction of the strut length less than 1/3 the length. For example, a top strut, not on the edge, has an equivalent cross sectional area of:

$$A_{eq}=A_{strut}+2*w*t_{face}$$

Several values of w were tested with STAP to show that in the worst case of a small w

(corresponding to the highest stresses), the stresses were considerably smaller than critical and displacements were on the order of 10^{-6} m maximum.

The inertial forces were adjusted by equally distributing the plate mass on the top truss nodes. This assumes that the panel will be attached to the truss at all top nodes. For example, consider a center top node. There are 9 struts attached to the node. Therefore, the mass for the inertial load at that node is:

$$m_{inertial}=m_{node}+9(\frac{1}{2})m_{strut}+6(\frac{m_{ip}}{3})$$

where m_{ip} is the mass of the solar panel divided by the number of equilateral triangles of the strut length that form the solar array hexagon. The masses for the inertial loads of the top nodes are calculated in a similar manner where the mass depends on the number of struts attached to the node and how many of them are top truss elements.

The results from the STAP program for the solar support truss with 3 rings are shown in Figures 4.4 and 4.5. The out of plane displacements of the nodes were no greater than 0.439×10^{-6} m for the inertial loadings. The maximum stress is 0.854×10^{3} N/m^2 and the maximum axial force is 0.0753 N. Both of these values fall well below their critical values. It may be expected that any additional loads due to thermal variations should not cause any problems with solar array panel deformation or buckling of the truss members.

The resulting length of the individual struts is quite long (16 m). Therefore, the vibration of the truss structure must be examined. It is expected that the individual strut elements will vibrate at a lower frequency than the overall structure. Therefore, this is looked at first.

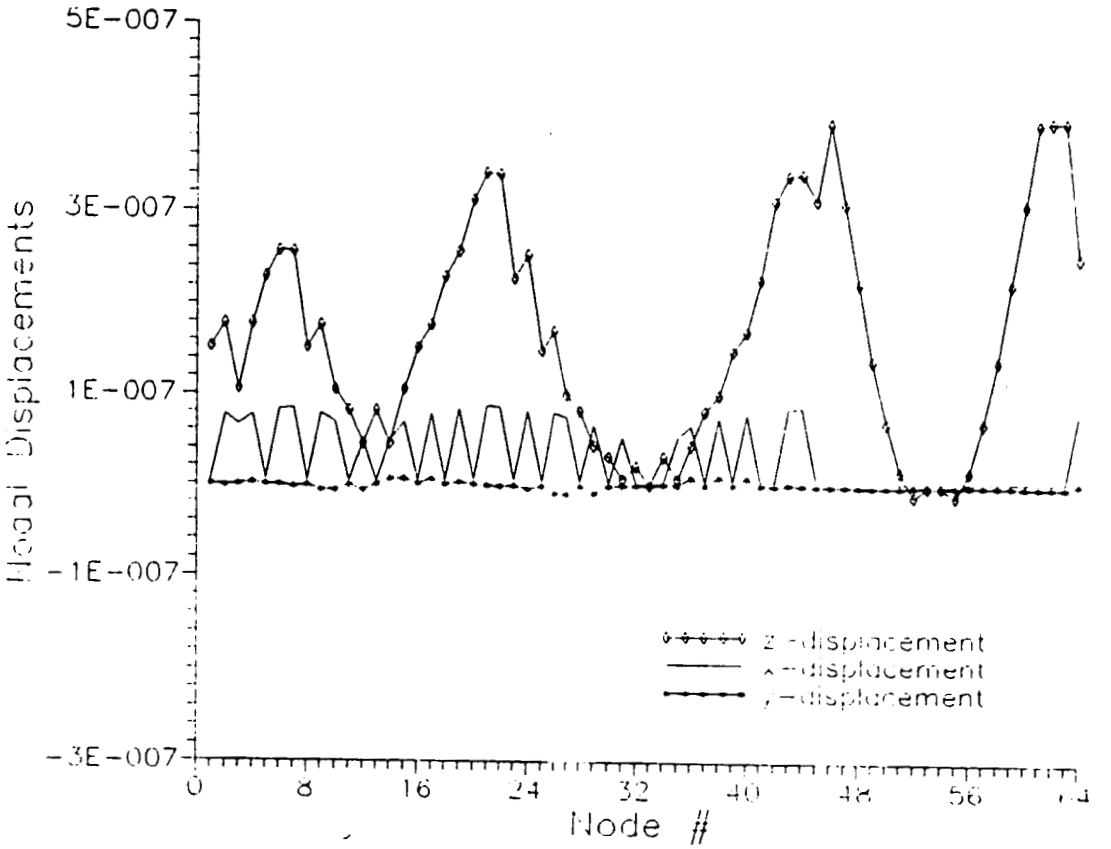

Figure 4.4: Nodal Displacements for the Hexagonal Truss

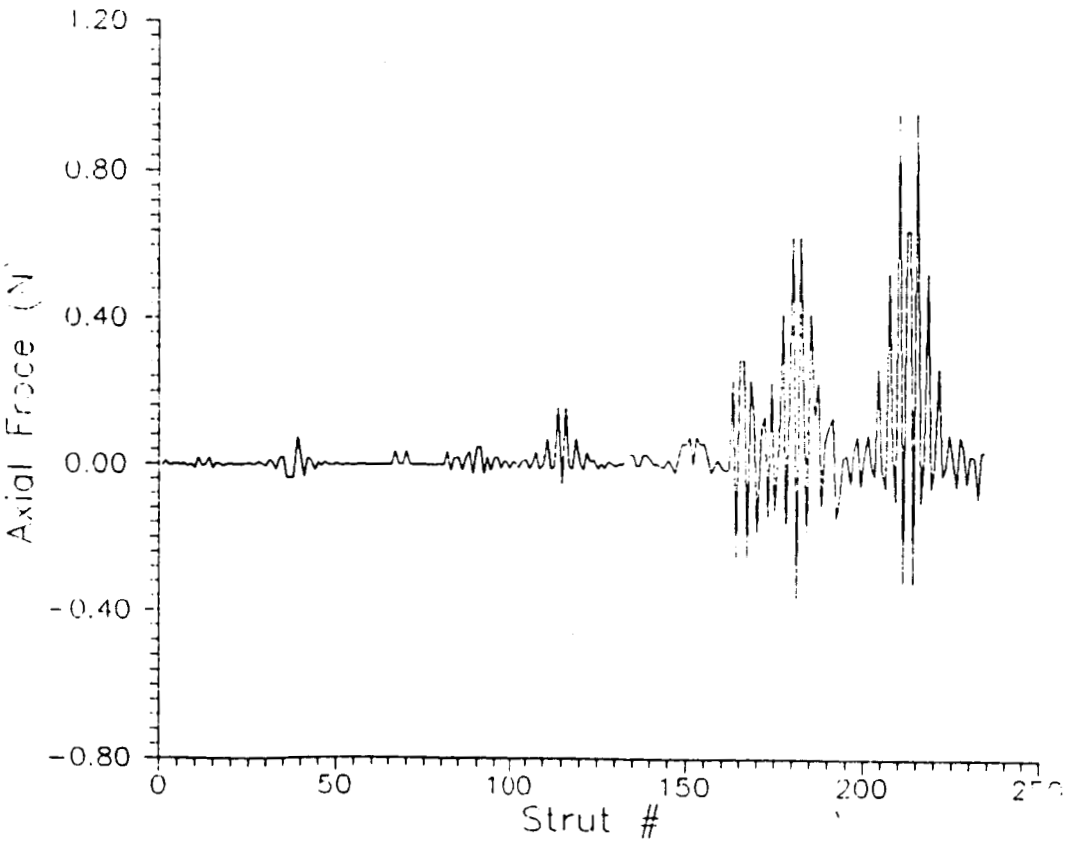

Figure 4.5: Hexagonal Truss Axial Forces

4.3.3 Vibrational Analysis

The tapered element will vibrate at rates given by the eigenvalue problem:

$$|[k]-\omega^2[m]|=0$$

where [k] is the same stiffness matrix defined in the critical buckling load analysis and [m] is the consistent mass matrix. The consistent mass matrix is found by

$$m_{ij}=\rho\int A(x)N_i(x)N_j(x)dx$$

where N(x) are the shape functions of a beam and A(x) is the cross sectional area as a function of x. If symmetry is used then half of the beam length can be used with the boundary conditions that the beam is pinned at one end and has zero slope at the other. This analysis results in ϖ equal to 12.1 rad/s, which corresponds to a frequency of 1.9 Hz. A non-tapered beam with the average radius of the tapered beam results in a frequency of:

$$f=(\frac{\pi}{L})^2\sqrt{\frac{IE}{\rho A}}\frac{1}{2\pi}=(\frac{\pi}{16})^2\sqrt{\frac{(1.325e-7)(1.72e11)}{0.29}}\frac{1}{2\pi}$$

which equals 2.46 Hz. This last rough calculation was done as a check for the frequency analysis. Since the two numbers are of the same order of magnitude the frequency analysis using energy methods is accurate.

The natural frequency of the entire hexagonal truss structure may be approximated by a circular sandwich plate. The truss/panel system is considered dynamically as an equivalent flat circular sandwich plate [8]. This is a fairly good assumption for thin trusses and will be only an approximation for the 3 ring truss system [6].

Plate bending stiffness is defined as:

$$D=\frac{E_{face}t_{face}H^2}{2(1-\nu^2)}$$

where,

$$H=\sqrt{\frac{2}{3}}L_{strut}$$

Truss Mass/Area may then be defined to be:

$$\frac{M}{A}=\frac{(struts)(M_{strut})+(nodes)(M_{node})}{A}$$

The resulting plate frequency is then calculated by:

$$f=\frac{3.343}{(D_{max})^2}\sqrt{\frac{D}{M/A_{truss}+M/A_{panel}}}$$

where D_{max} is the diameter of a circle having the same area as the solar panel surface [8]. That is,

$$D_{max}=\sqrt{\frac{5800*4}{\pi}}=85.9m^2$$

The parameters used for these equations are as follows:

E_{face} = 1.73 x 10^{11} (N/m^2) (graphite epoxy)

t_{face} = 5.66 x 10^{-3} (m)

ν = 0.3 (Poisson's ratio)

The resulting frequency for a 3 ring truss system is 42 Hz. As expected, this is higher than the natural frequency of the individual truss elements.

4.3.4 Central Truss Analysis

The orthogonal tetrahedral truss pictured in Figure 4.6 is analyzed in a very similar manner. The STAP program is quite accurate for this truss system. In an effort to keep the center of mass of the ship near the geometric center the propellant tank is placed in the center cell of the 3 cell truss. Since we want to minimize the distance to the solar panels from the center of mass of the ship, the strut length is 5.4 m. This is adequate for placing the propellant tank, with a length of 5.3 m, within a cell of the truss.

The critical loads for the orthogonal tetrahedral truss elements are found in the same manner as before. Using strain energy methods, we analyze the 5.4 m and 7.6 m strut elements. Once again, we assume a wall thickness of 0.0008 m, a maximum diameter of 10 cm and a minimum diameter of 5 cm. This analysis results in a critical buckling load of 984.13 N for the 5.4 m strut and 497.16 N for the 7.6 m strut. With these values known, we can examine the resulting axial forces to make sure no elements buckle. Once again, inertial forces due to the engine thrust are studied with STAP. The boundary conditions for this box truss include fixing the nodes that attach to the engine casing from displacement. This allows the STAP analysis to have a fixed reference, otherwise the applied forces would result in rigid body motion only. The propellant tank does not contribute inertial forces since it is attached to the four fixed nodes. An inertial force of $(61\times10^{3}\text{kg})(5\times10^{-4}\text{m/s}^{-4})$, which equals 30.5 N, is distributed equally on the 4 nodes where the cargo attaches to the truss. This assumes that the initial acceleration is 5×10^{-4} m/s^2. We then transfer the moment and shear force created by the solar panels to the four nodes at each end of the truss. Given that the mass of a solar panel with support truss and wiring equals 5750 kg, the resulting inertial force equals 2.875 N. This force is translated and equally distributed to the four connecting end nodes. Finally the moment caused by this inertial force

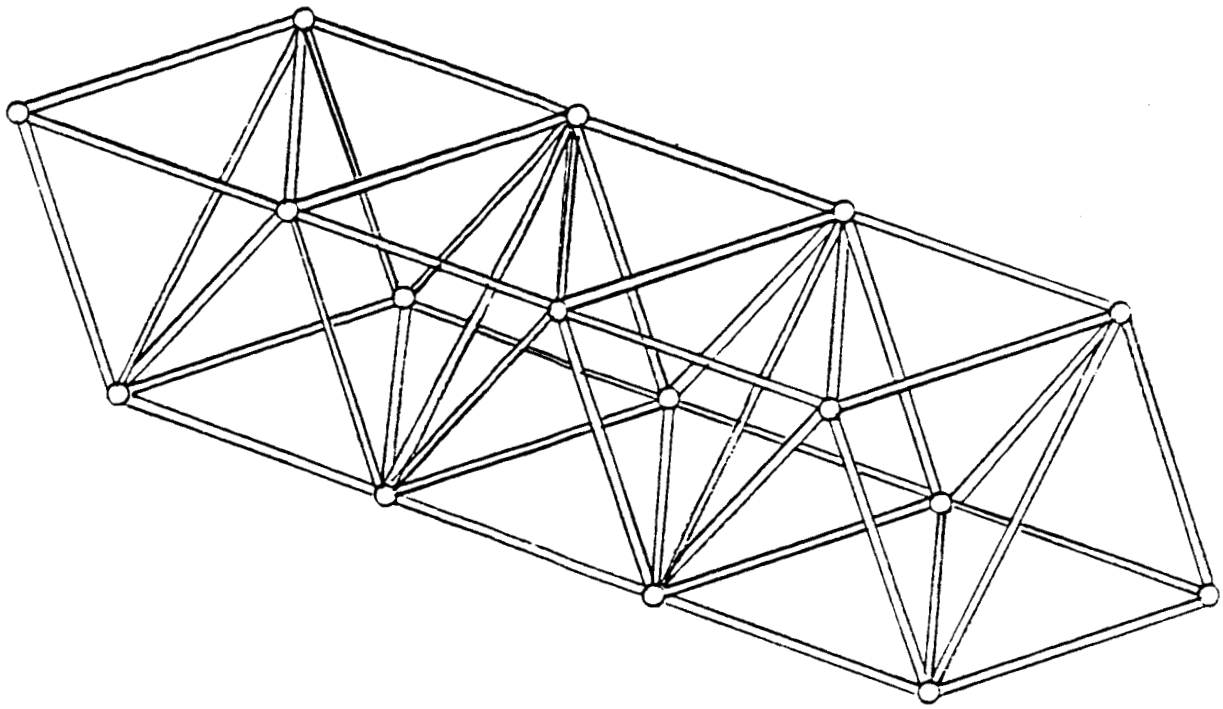

Figure 4.6: Orthogonal Tetrahedral Truss Configuration

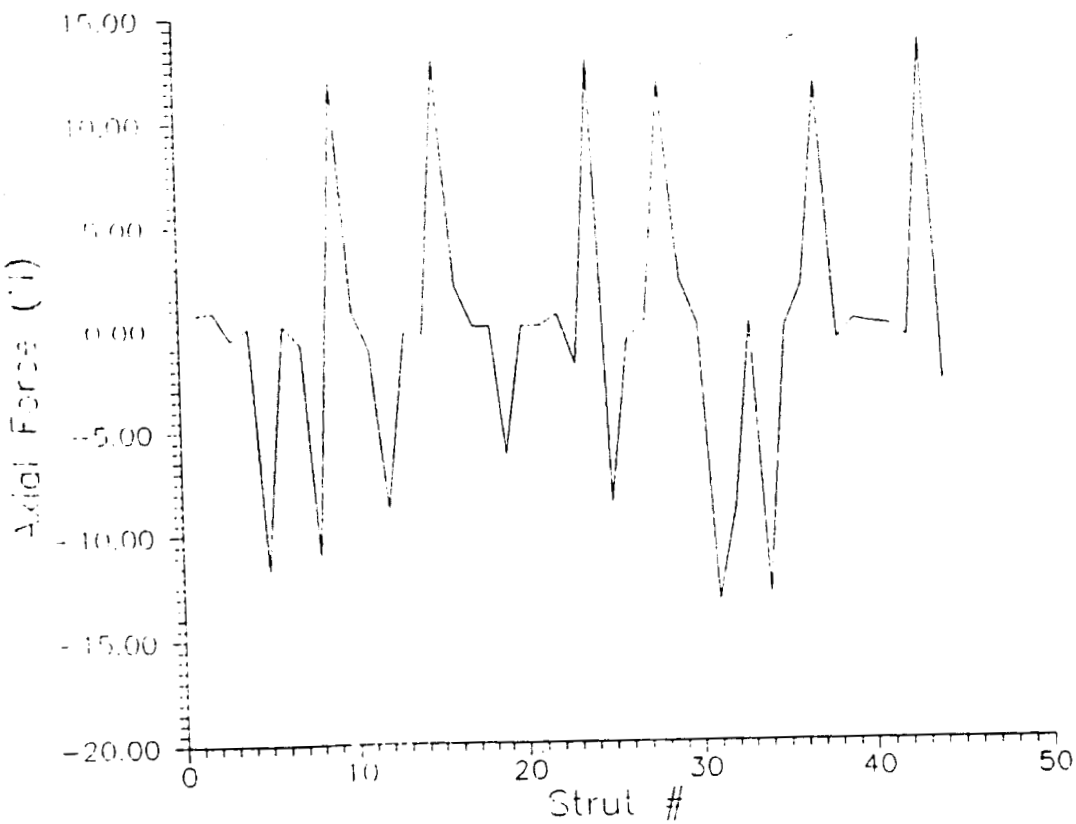

Figure 4.7: Box Truss Axial Forces

acting at the center of mass of the solar panel structure is transferred to the end nodes. This moment equals the inertial force, 2.875 N, times the moment arm of 51.5 m, giving a moment of 148.06 Nm. Coupled forces are applied to the four end nodes that are separated by 5.4 m. Therefore, a force of 13.7 N is applied to each of the four nodes.

The results from the STAP code are represented graphically in Figure 4.7 and 4.8. The maximum displacements do not exceed 0.305×10^{-5} m. The maximum stresses and axial forces do not exceed 0.736×10^{5} N/m^2 and 0.1375×10^{2} N, respectively. Given that the yield stress is on the order of 50×10^{6} N/m^2, these values are well below the critical buckling load and yield stress for the struts used. Once again a large margin of safety is available. This gap is necessary in order to insure a stable system under thermal and other loads not accounted for. Therefore, the truss is not decreased in strength even though this analysis shows that it more than meets the requirements.

4.4 Assembly Scenario and Time Estimates

A complex assembly such as this may be broken down into basic steps for the purpose of studying parameters such as assembly rates and tasks. These studies are being done at the NASA Langley Research Center where tetrahedral truss assembly is simulated in the Weightless Environment Training Facility [11]. In actual space studies, such as with the ACCESS shuttle mission, truss assembly studies were completed in space by astronauts with the aid of the Remote Manipulator System (RMS) [5].

The large structure of the spacecraft will require a significant amount of lead time so that the ship can be built in time for the launch window of our mission. From the NASA studies it was estimated that average in-space assembly rates of approximately 38 seconds per strut can be expected [5]. Therefore, a truss of consisting of 44 struts will require approximately 28 minutes

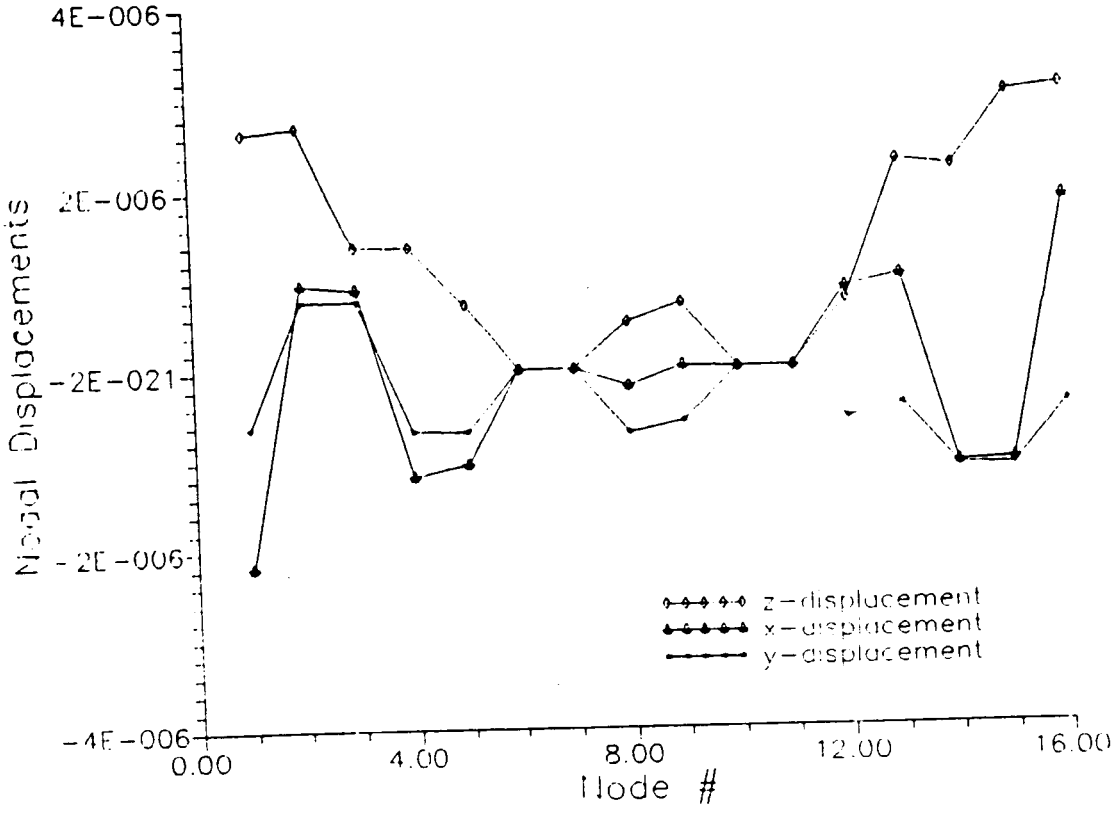

Figure 4.8: Nodal Displacements for the Box Truss

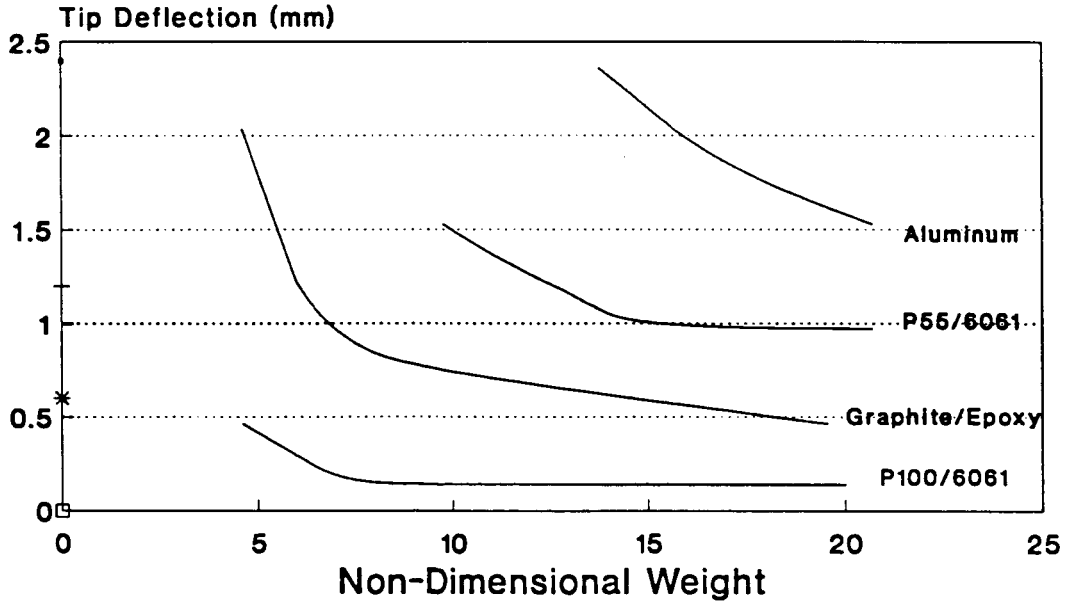

Figure 4.9: Thermally Induced Tip Distortion

to assemble in space. According to predictions made by NASA as a result of the ACCESS shuttle experiment, a hexagonal truss system consisting of 789 struts would require approximately 6 hours to assemble with the aid of the Mobile Transporter system [12]. The Mobile Transporter is a mobile work station concept currently being developed by NASA. It is assumed that this technology will be well developed by our launch time. Current projections lead to an assembly time for a hexagonal shaped truss system of 3 rings, such as the one considered for our ship, of approximately 3 hours if completed with the aid of the Mobile Transporter [4]. The total predicted time for assembly of the central box truss and both solar array support trusses is a more conservative 36 hours. This estimate is higher than NASA predictions due to the length of the elements and the overall size of our structure.

4.5 Materials Selection

An obviously important step is to specify the materials to be used in this design, why they were chosen, and what the resulting masses are. The criteria for material selection results from an analysis of what the ship will have to withstand. A low coefficient of thermal expansion is desired due to the dynamic nature of the thermal loadings. These loads will vary considerably during spiral out and in to Earth. Also desired is low density with high strength to minimize the ship mass safely. Finally the material must be stable in the space environment, i.e. not subject to breaking down in radiation and able to withstand collisions with micro-meteorites. Degradation caused by radiation, thermal distortion, and minute particle bombardment is a major concern when dealing with polymer-based composites. However, recent studies of aluminum reinforced graphite-epoxy have shown that this material has better thermal conductivity and lower susceptibility to space environmental effects. In other words, aluminum reinforced graphite epoxy has the advantage of a lightweight epoxy without the disadvantage of high thermal

distortion. However, due to the uncertainty of the effects of atomic oxygen on this material, aluminum coated graphite epoxy would be a better material choice. This material is the prime candidate for use on the SSF. Figure 4.9 and Table 4.2 display the comparisons of graphite epoxy, and two forms of graphite reinforced aluminum, P100/6061, and P55/6061. The data clearly shows that P100/6061 has the least thermally induced tip distortion per unit weight. Also, this material has a significantly larger thermal conductivity and modulus of elasticity. It is assumed that the aluminum coating on the graphite epoxy will not change the stiffness characteristics of graphite epoxy since the coating is thin. Thermal properties will most likely be similar to the aluminum reinforced graphite epoxy.

Table 4.2
Material Properties Comparison

Property	Graphite/Epoxy	P100/6061	P55/6061
A(11) 10^{-5}/K	-0.080	0.086	0.307
A(22) 10^{-5}/K	3.67	2.30	2.40
K(11) W/m K	54.0	240.0	98.0
K(22) W/m K	0.7	193.0	98.0
NU(12)	0.21	0.4	0.27
NU(21)	0.010	0.031	0.041
E(11) 10^{6} psi	24.97	51.0	30.8
E(22) 10^{6} psi	1.17	4.0	4.7
E(12) 10^{6} psi	0.62	2.0	1.9

A11 = Coefficient of Thermal Expansion (fiber direction)
A22 = Coefficient of Thermal Expansion (transverse direction)
K11 = Thermal Conductivity (fiber direction)
K22 = Thermal Conductivity (transverse direction)
NU12 = Poisson's Ratio
NU12 = Poisson's Ratio
E11 = Modulus of Elasticity (fiber direction)
E22 = Modulus of Elasticity (transverse direction)
E12 = Shear Modulus

Titanium and its alloys are rapidly becoming a leading space application material. In our situation they are considered for the fabrication of the nodal clusters. Pure titanium is as strong as steel, but 45% lighter. Although it is 60% heavier that aluminum, it is twice as strong [10]. A titanium alloy such as Ti-6A1-4 V, which is a titanium-aluminum alloy, has a lower density than pure titanium, slightly higher coefficient of thermal expansion, a slightly lower thermal conductivity, but a higher Young's modulus. For property values and comparison to other titanium alloys, see Table 4.3 [9].

Table 4.3
Material Properties of Titanium

Property	Titanium (99%)	Ti-6Al-4 V	Ti-5Al-2.5 Sn
Density lb/in^3	0.163	0.160	0.161
TEC 10^{-6} in/in F	4.7	5.0	5.2
TC Btu/ft^2 hr F ft	9.1-11.5	4.2	4.5
E 10^6 psi	15	16.5	16.0

TEC = Thermal Expansion Coefficient
TC = Thermal Conductivity
E = Young's Modulus

The resulting masses of the struts and nodes can now be determined. A hollow node, approximately 5 cm in diameter, can be estimated to be spherical with a thickness of about 1 cm. This gives a conservative nodal mass of 5.2 kg.

The mass of the struts is a function of their wall thickness. Specifying that the struts have a maximum diameter of 10 cm with a minimum diameter of 5 cm, their mass is given by:

$$M_{strut}=\frac{2}{3}\rho\pi L(0.075t-\frac{t^2}{2})$$

A half conical strut that is a total of 5.4 m long, made of aluminum coated graphite epoxy, with

a wall thickness of 0.8 mm, can be estimated to have a mass of 1.56 kg. Using the above formula, the strut mass may be determined for a number of cases as shown in Table 4.4. (Table 4.4 was calculated for a wall thickness of 0.8 mm.)

Table 4.4
Solar Support Structure Parameters

Rings	Strut Length m	Strut Mass kg	Truss Mass kg	Mass/Area kg/m^2
3	16	4.60	1450.6	0.2501
4	12	3.48	2027.1	0.3495
5	9.6	2.78	2698.0	0.4652
6	8	2.32	3433.3	0.5919
7	6.9	1.99	4245.9	0.7321
8	6	1.74	5088.4	0.8773

It is apparent that the configuration and resulting mass of such a large hexagonal array is of great importance. Given that a aluminum coated graphite epoxy strut, 5.4 m in length, has a mass of approximately 1.56 kg and that a node has a mass of approximately 5.2 kg, the support structure mass is found and displayed in Table 4.4. The mass of the truss structure supporting the arrays is estimated at 2,901 kg with a 10% contingency of 290 kg to give a mass of 3,191 kg.

4.6 Notes on the Configuration

The development of a ship configuration is a trial and error process where ideas are brought up and either expanded to be incorporated into the configuration or discarded as inadequate. A crucial component of the vehicle was the solar array system and the supporting

structure.

Among the first choices for solar cell systems was a dynamic concentrator concept. This system would have required precise direction control and would have required the assembly of many individual cell packages. This lead to the first hexagonal shaped truss support. The hexagonal shape allowed for best packing efficiency and a very stable structure.

At the same time, flat solar cells such as silicon cells were considered. These solar arrays could be rectangular, but the area needed to produce the initial power requirements of about 3.5 MW was very large.

Once it was determined that the solar panel rotation only needed to be about one axis, the approximate points of rotation were determined. At this point, in an effort to keep the moments of inertia of the ship as small as possible for control purposes, these nodes were placed as close to the center of mass of the ship as possible.

The resulting layout is divided into four parts: the solar panel with its supporting structure, the connecting truss, the cargo hold and the engine support bay (Figures 4.10 a-b and 4.11 a-c).

A 5,800 m^2 solar array panel is located on two sides of the ship. The 48 m on a side hexagonal shaped arrays need to be attached in such a way that, when the ship is maneuvering, they can be rotated to an optimum position for gathering sunlight. Their need to be adjustable is why they are attached to the main body of the ship by rotational nodes. These rotational joints will carry the necessary moments and forces to rotate the panels.

The propellant tank was placed inside the inner most cell of the box truss. Since the tank has a maximum dimension of 5 m in length, a 5.4 m truss element is used so that it can be fitted in this way. This is done in an effort to keep the center of mass of the ship as close as possible to the geometric center.

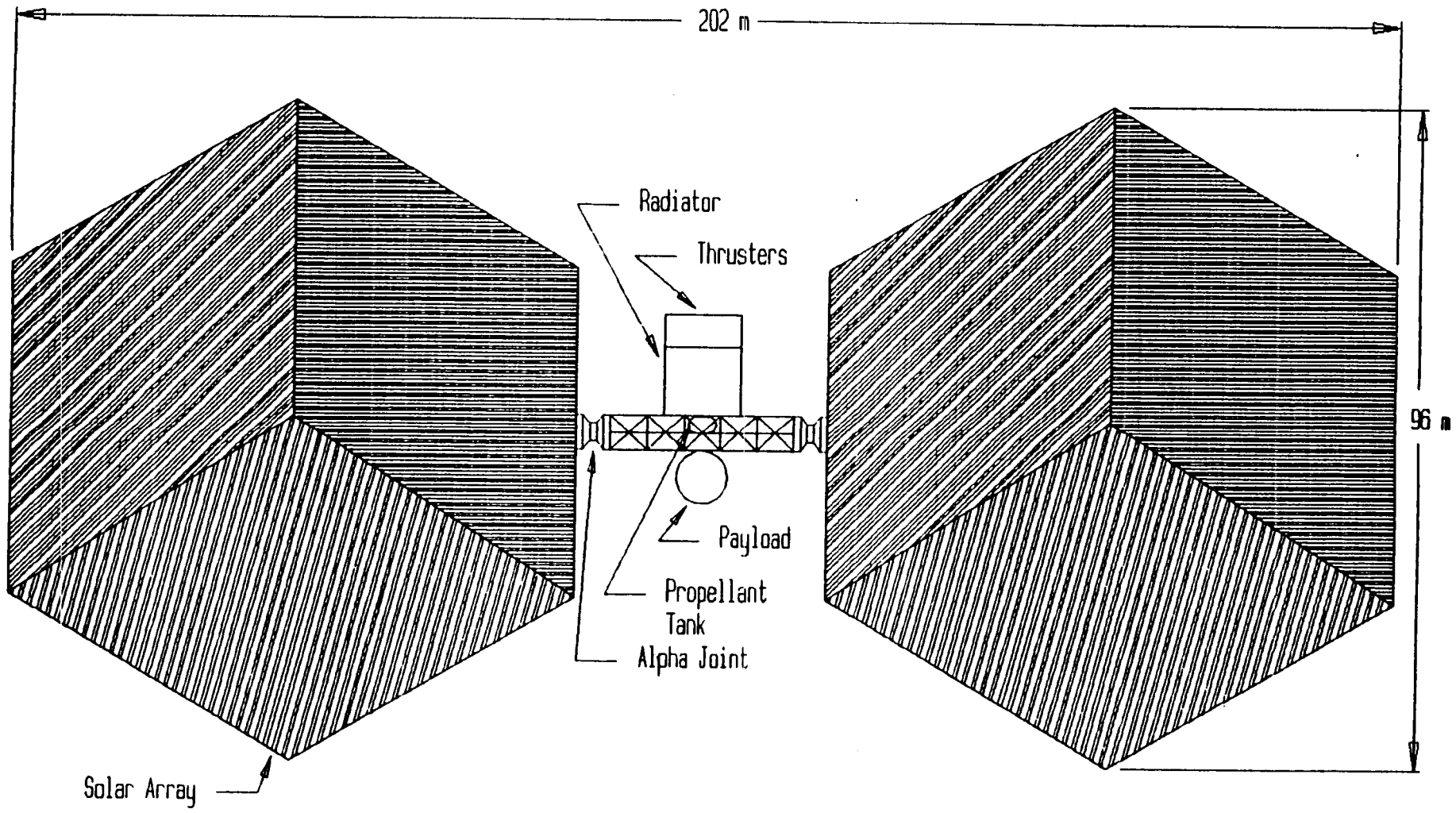

Figure 4.10a: **Configuration**

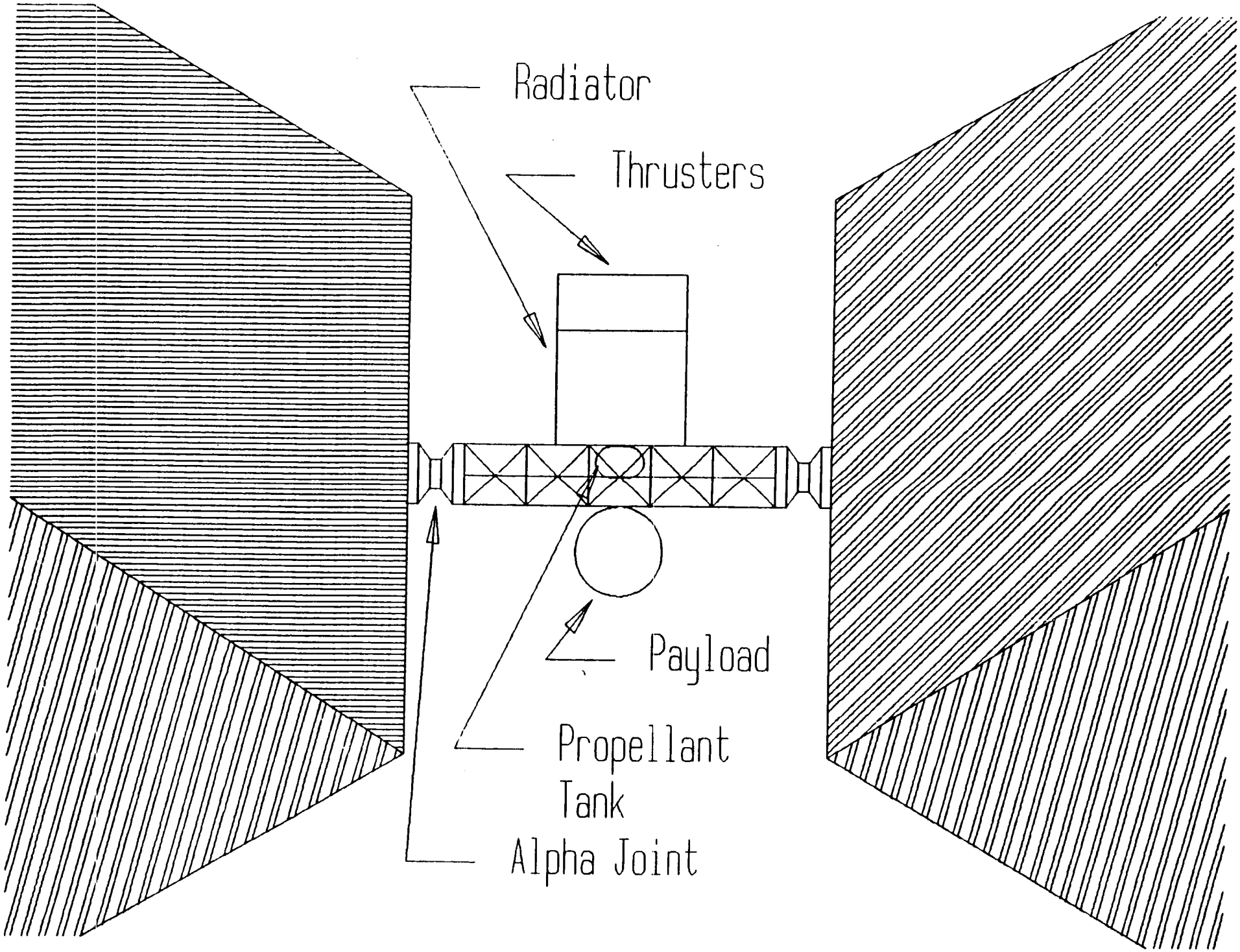

Figure 4.10b: Main Body Configuration

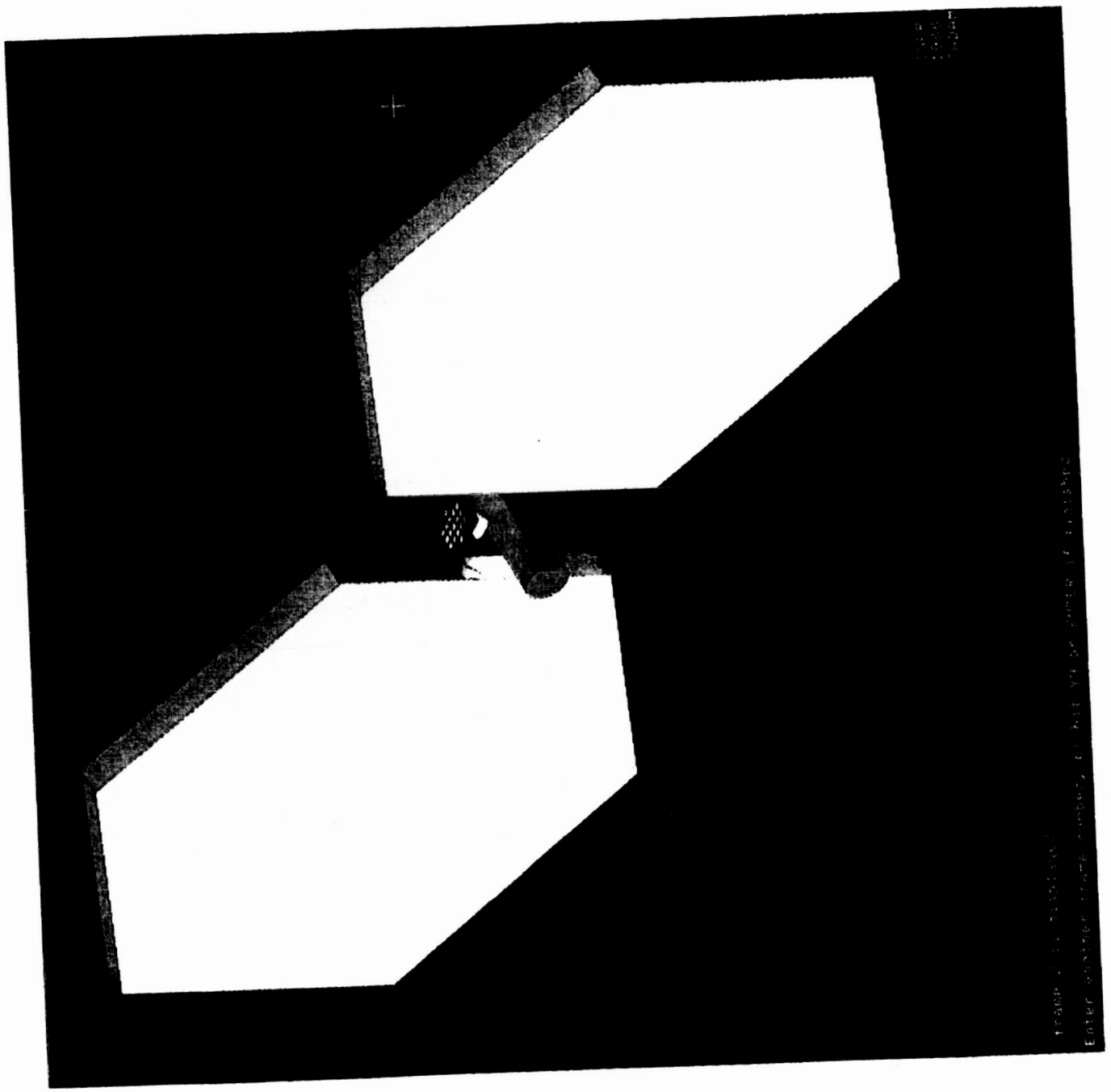

Figure 4.11a: Configuration

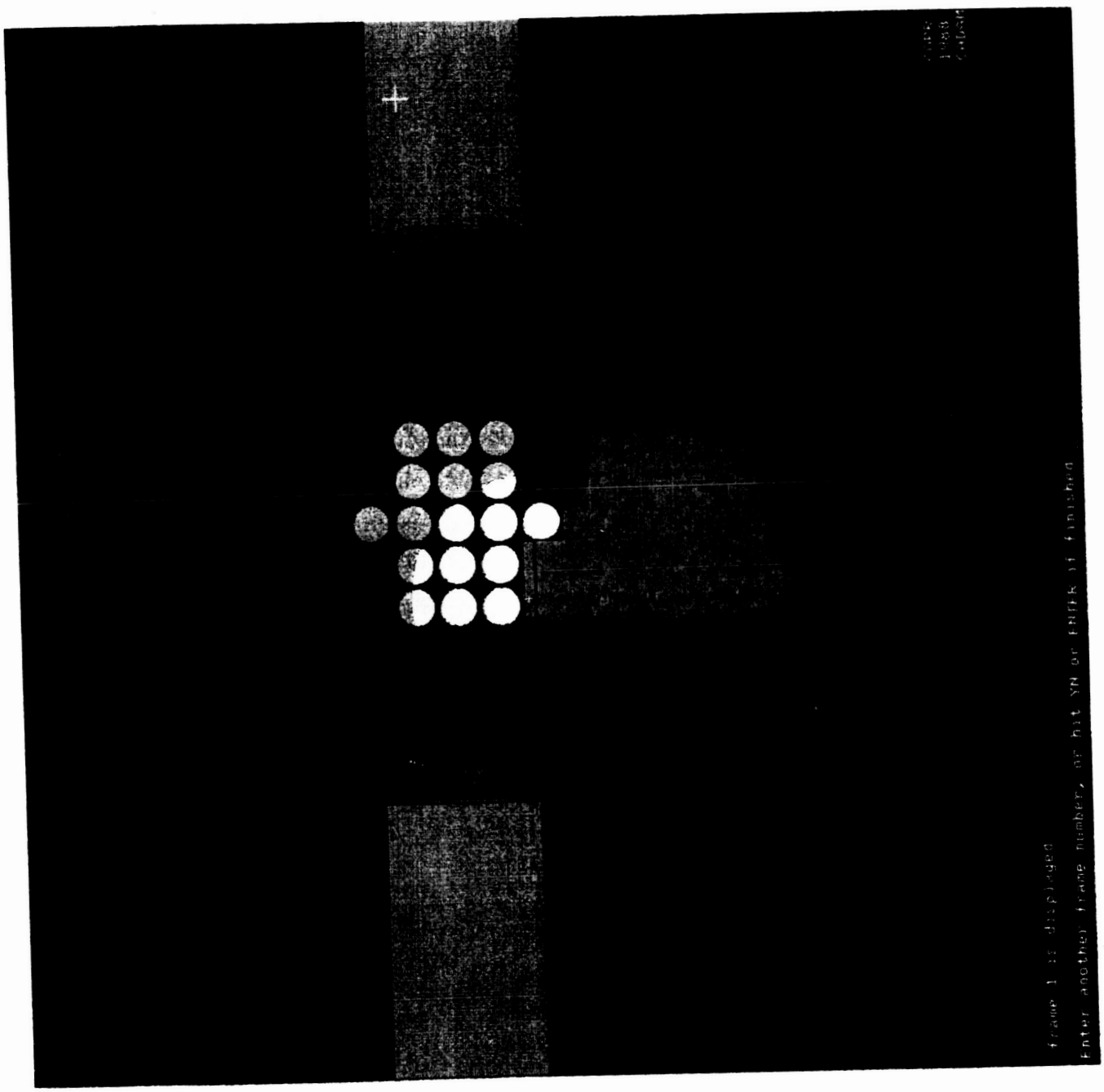

ORIGINAL PAGE
COLOR PHOTOGRAPH

Figure 4.11b: Main Body Configuration

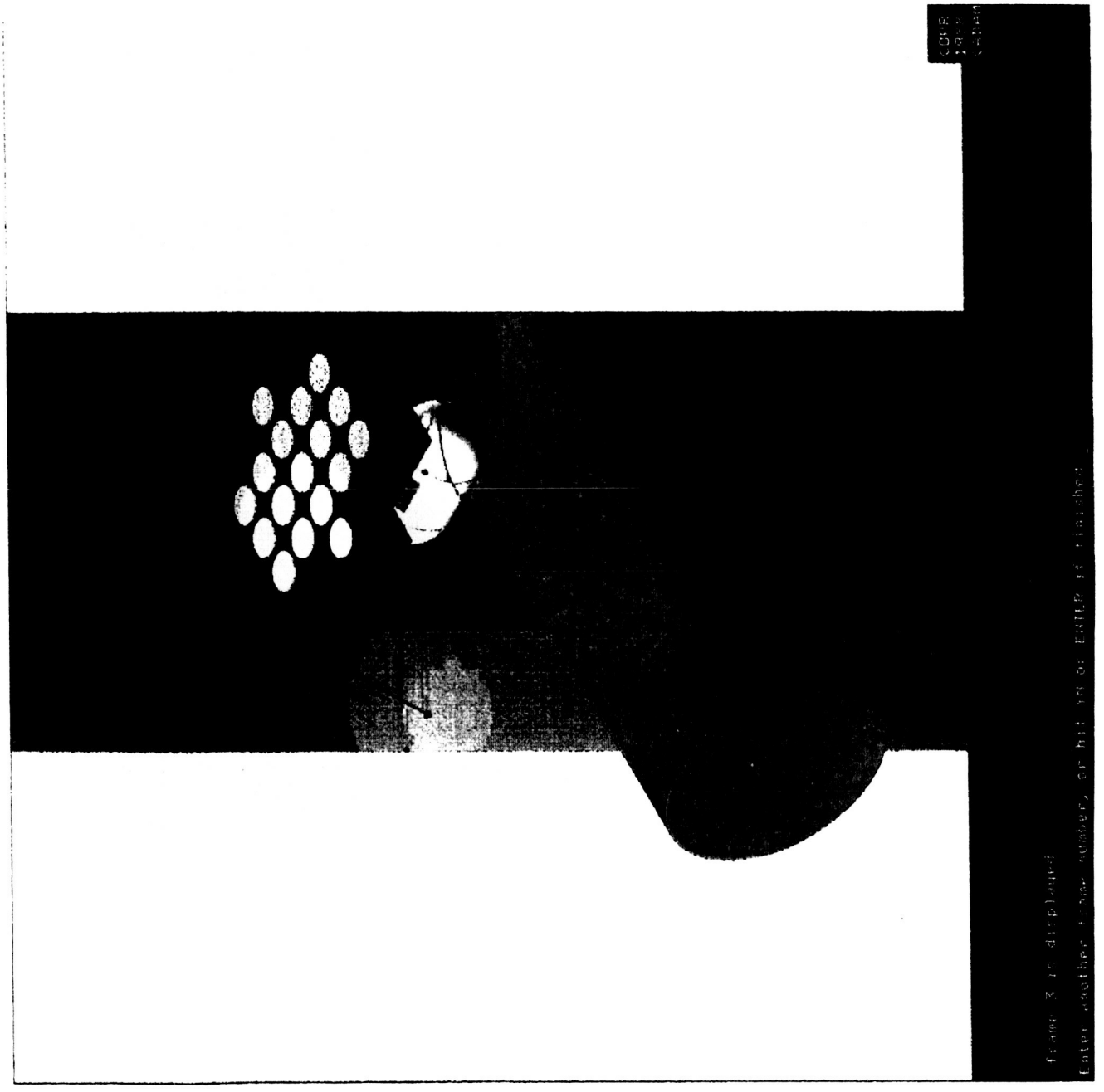

ORIGINAL PAGE
COLOR PHOTOGRAPH

Figure 4.11c: Main Body Configuration

The cargo pod contains the 61 mT payload and is oriented so that a minimum center truss length can be achieved while at the same time making it accessible for loading and unloading. The cylindrical hold is 27 m long and 7.8 m in diameter, as specified by the Shuttle 'C' cargo hold.

The engine pod consists of 17 engines that were placed on the aft end of the ship in such a manner that it will "push" the ship to its destination.

The main body of the ship is mostly symmetric for easier control. The distance from the center of the ship to the rotational nodes must be minimized in order to minimize the forces at that node as well as the moment of inertial of the ship. The ship has developed into its current configuration due mostly to power requirements, solar cell choice, and ship control. It is an adaptable design that can be adjusted to meet a variety of mission requirement changes.

The general specifications and mass summary of the ship are given in Table 4.5. In addition, a craft mass distribution is displayed in Figure 4.12.

Table 4.5 Ship Specifications and Mass Summary

Cargo mass	61,000 kg
Solar array type	Fresnel lens concentrator/ multi-stacked cell
Array area	10,800 m^2
Array output power	3.465 MW
Thruster specific impulse	10,300 sec
Number of engines	17 (including 5 redundant units)
Engine input power	275 kW
Engine thrust	5 N
Propulsion system efficiency	0.714
LEO to LMO trip duration	960 days
Return trip duration	382 days
Round trip (LEO-LMO-LEO) duration	3.8 years

	Masses, kg
Cargo	61,000
Propellant	24,200
Tankage	820
Propulsion system	9,140
Solar arrays	7,811
Wiring	1,950
Truss structure supporting arrays	3,191
Main body (trusswork, engine mounts, cargo bay, rotational α-joints)	3,600
Power distribution and auxilliary power systems	1,000
Attitude control system, CMG	2,000
Guidance/Navigation/Communications/ Data Systems	800
Total Mass	**115,510 kg**

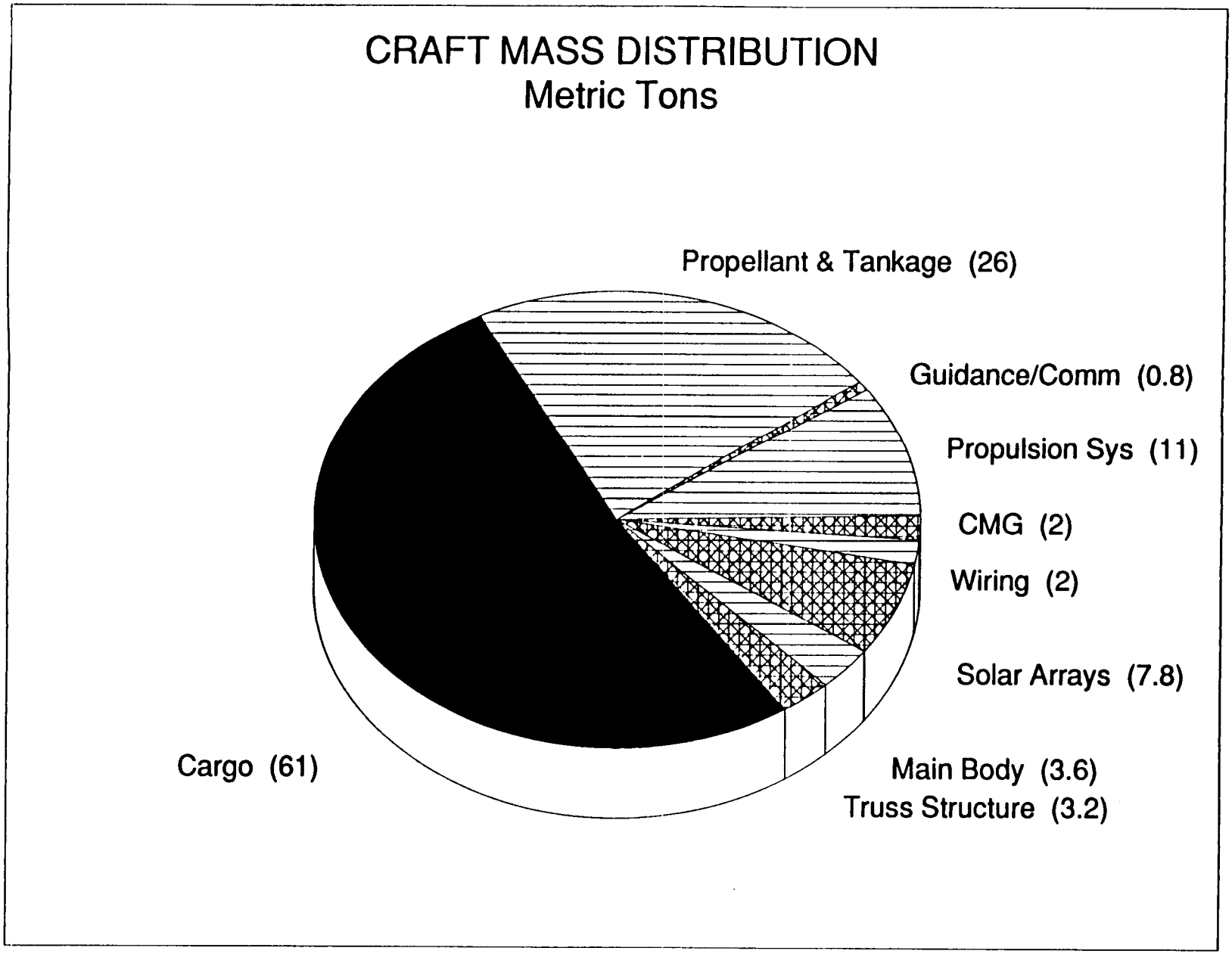

Figure 4.12: Craft Mass Distribution

References

1. Beer, Ferdinand P.; and Johnston, E. Russell Jr.: Mechanics of Materials. McGraw-Hill Book Company. New York, NY, 1981.

2. Bement, L. J.; Bush, H. G.; Heard, W. L.; Stokes, J. W.: "EVA Assembly of Large Space Structure Elements." NASA TP-1972, 1981.

3. Collins, T. J.; Fichter, W. B.: "Support Trusses for Large Precision Segmented Reflectors: Preliminary Design and Analysis." NASA TM-101560, 1989.

4. Heard, W. L.; Bush, H. G.; Wallsom, R. E.; and Jenson, J. K.: "A Mobile Work Station Concept for Mechanically Aided Astronaut Assembly of Large Space Trusses." NASA TP-2108, 1983.

5. Heard, W. L.; Bush, H. G.; and Watson, J. J.: "Astronaut/EVA Construction of Space Station." AIAA Paper No. 88-2454, 1988.

6. Hedgepeth, J. M.; and Adams, L. R.: "Design Concepts for Large Reflector Antenna Structures." NASA Contractor Report 3663, Contract NAS1-16134, 1983.

7. Meriam, J. L. and Kraige, L. G.: Engineering Mechanics - Statics. John Wiley and Sons, New York, NY, 1986.

8. Mikulas, M. M.; Collings, J. J.; Hedgepeth, J. M.: "Preliminary Design Considerations for 10 to 40 Meter Diameter Precision Truss Reflectors." AIAA Paper No. 90-1000, 1990.

9. Moses, A. J.: The Practical Scientist's Handbook. Van Nostrand Reinhold Company, New York, NY, 1978.

10. Ross, R. B.: Metallic Materials Specification Handbook. E and F. N. Spon, New York, NY, 1980.

11. Watson, J. J.; Heard, W. L.; Bush, H. G.; Lake, M. S.: "Results of EVA/Mobile Transporter Space Station Truss Assembly Tests." NASA TM-100661, 1988.

12. Watson, J. J.; Bush, H. G.; Heard, W. L.; Lake, M. S.; Jensen, J. K.; Wallsom, R. E.; and Phelps, J. E.: "A Mobile Transporter Concept for EVA Assembly of Future Spacecraft." AIAA Preprint No. 90-1049, 1990.

13. Yang, T. Y.: Finite Element Structural Analysis. Prentice-Hall, Inc. Englewood Cliffs, NJ, 1986.

SECTION 5

SEP Vehicle Launch to LEO

Nomenclature

LEO	Low Earth Orbit
SSF	Space Station Freedom
CMG	Control Moment Gyro

5.1 General Considerations

The transportation of the vehicle components and the cargo to LEO will be performed using four Shuttle C missions (Table 5.1). The Shuttle C will have a cargo launch capability of 7.6 m diameter by 27 m length with a mass of 61 metric tons. Its tanker launch capability is 4.6 m diameter by 25 m length with a mass limit of 71 metric tons (Figure 5.1).

Critical components in planning the launch to LEO are a) the economical packaging of the components for assembly in LEO and b) packaging of the components in such a way that their resultant center of mass will fall inside the prescribed envelope of the Shuttle C cargo bay. One goal of the process of planning the launch scenario is to minimize the number of shuttle launches to the Space Station. Another consideration is the minimization of assembly work (both mechanical and human) at SSF. Most of the system will be assembled on the ground leaving only some mechanical assembly to be performed in LEO.

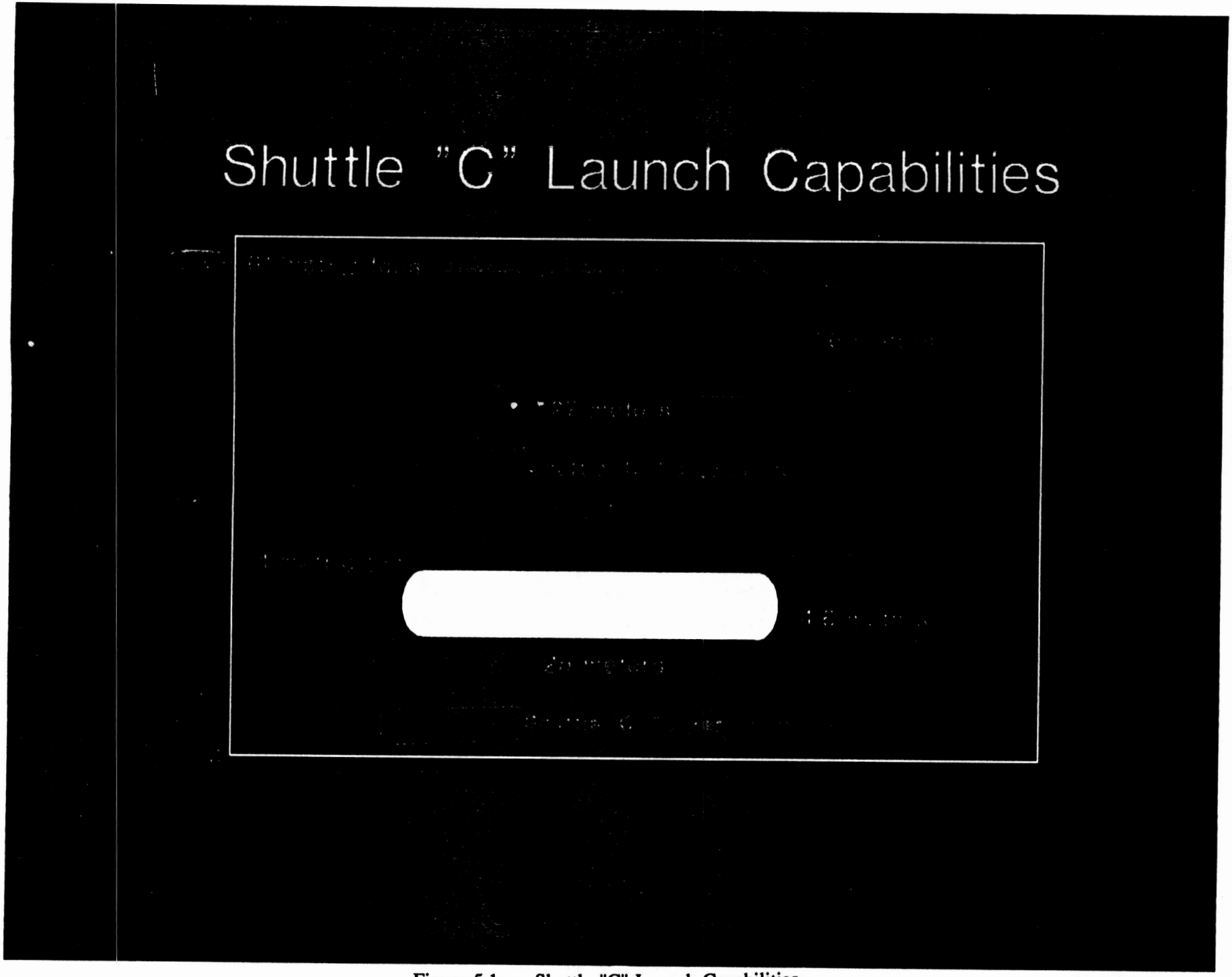

Figure 5.1: Shuttle "C" Launch Capabilities

5.2 Manifest

The manifest of components to be launched to LEO is as follows:

- Solar Array
- Supporting Truss Structure, Nodes, and Alpha Joints
- Propellant Tank
- Wiring for Solar Array
- Engines
- Control Systems
- Communications
- Power Conditioning Systems (for solar array and engines)
- Cargo

The order of the launches will be determined by the priority for assembly in space. The more complicated systems will be sent up first; the pre-assembled systems will be last.

5.3 Launch One

The first launch of the shuttle will contain the most complex components of the vehicle with regards to assembly in orbit: the support structure members and nodes. These members will be shipped unassembled and will be assembled in orbit at SSF using the mobile transporter. The remaining space in the first shuttle launch will be used to launch the solar array wiring from the arrays to the engines, which needs to be in place on the support structure before the solar array is attached, and some of the solar array. In addition, the control moment gyros will be launched at this time. Figure 5.2a shows a breakdown of launch one.

The individual strut members (Figure 5.3) will be arranged in a honeycomb box (Figure 5.4) pattern which will maximize packing efficiency. The struts for the support structure are in three different lengths: 16 m (4.6 kg), 7.6 m (2 kg), and 5.4 m (1.565 kg). The four-hundred-eighty 16 m struts which will be packaged in a box 3 m by 1 m by 24 m. The eighteen 7.6 m struts will be assembled in a container 0.475 m by 0.01 m by 26.6 m. The container for the twenty-eight 5.4 m struts will be 0.625 m by 0.01 m by 21.6 m. These smaller bundles will be

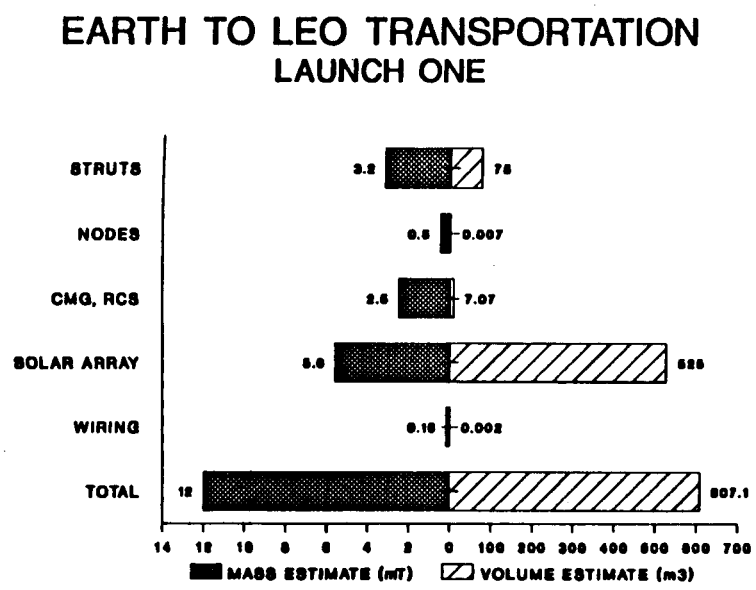

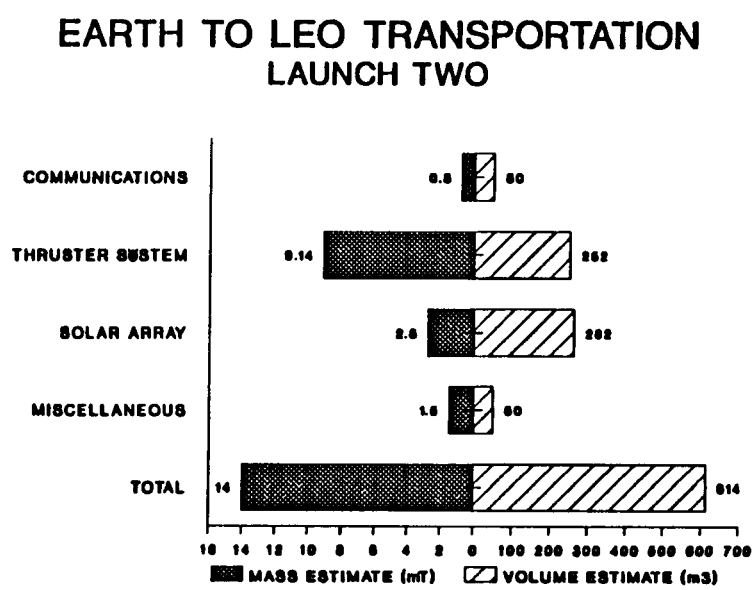

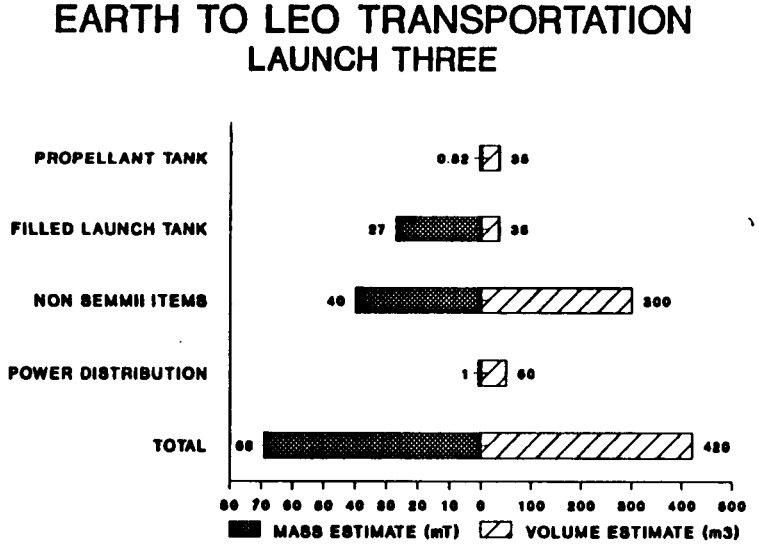

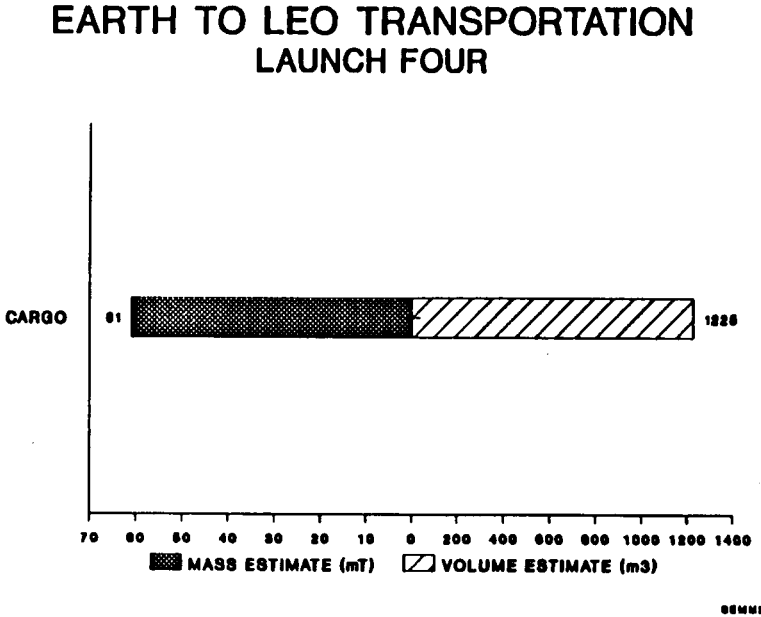

Figure 5.2: Earth to LEO Transportation Launch Scenario

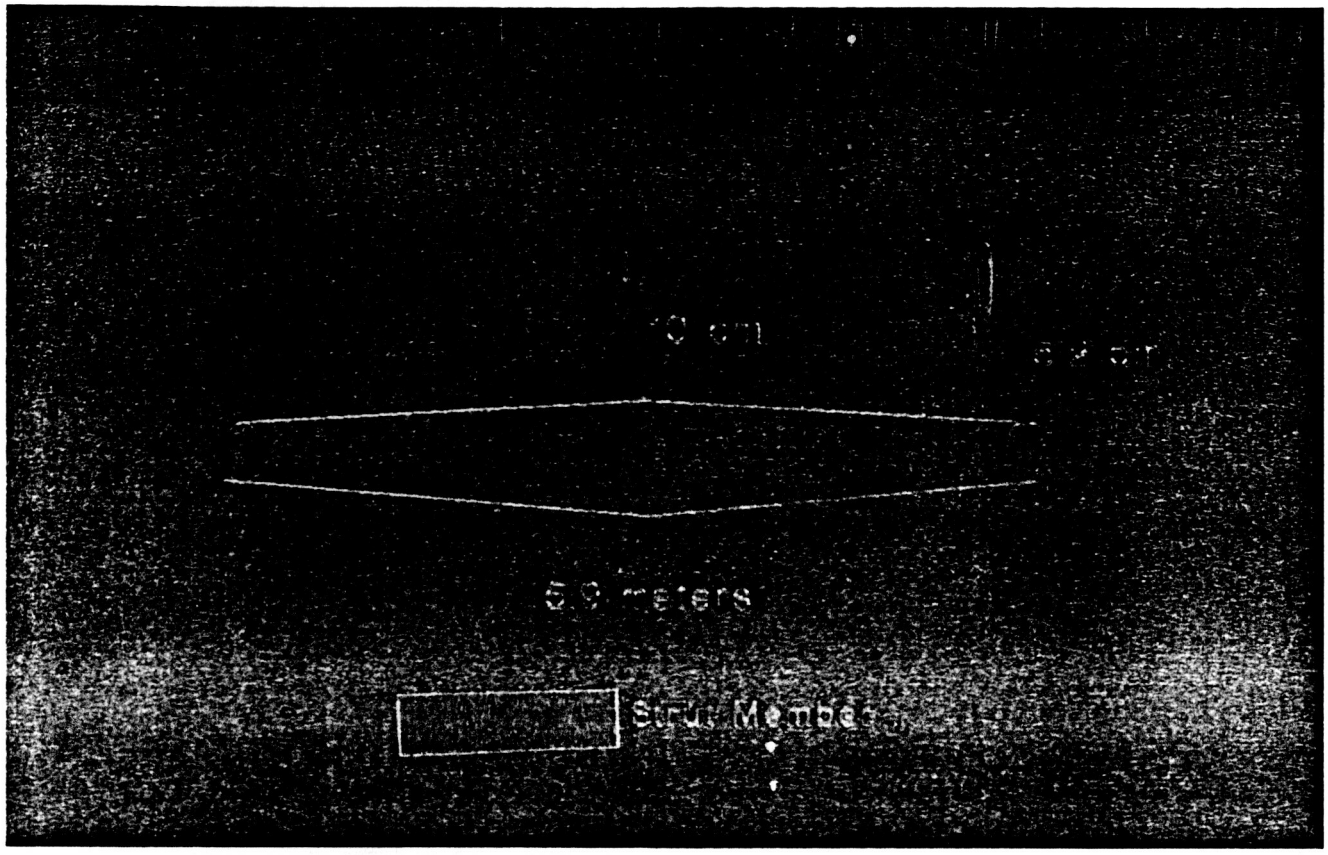

Figure 5.3: Strut Member

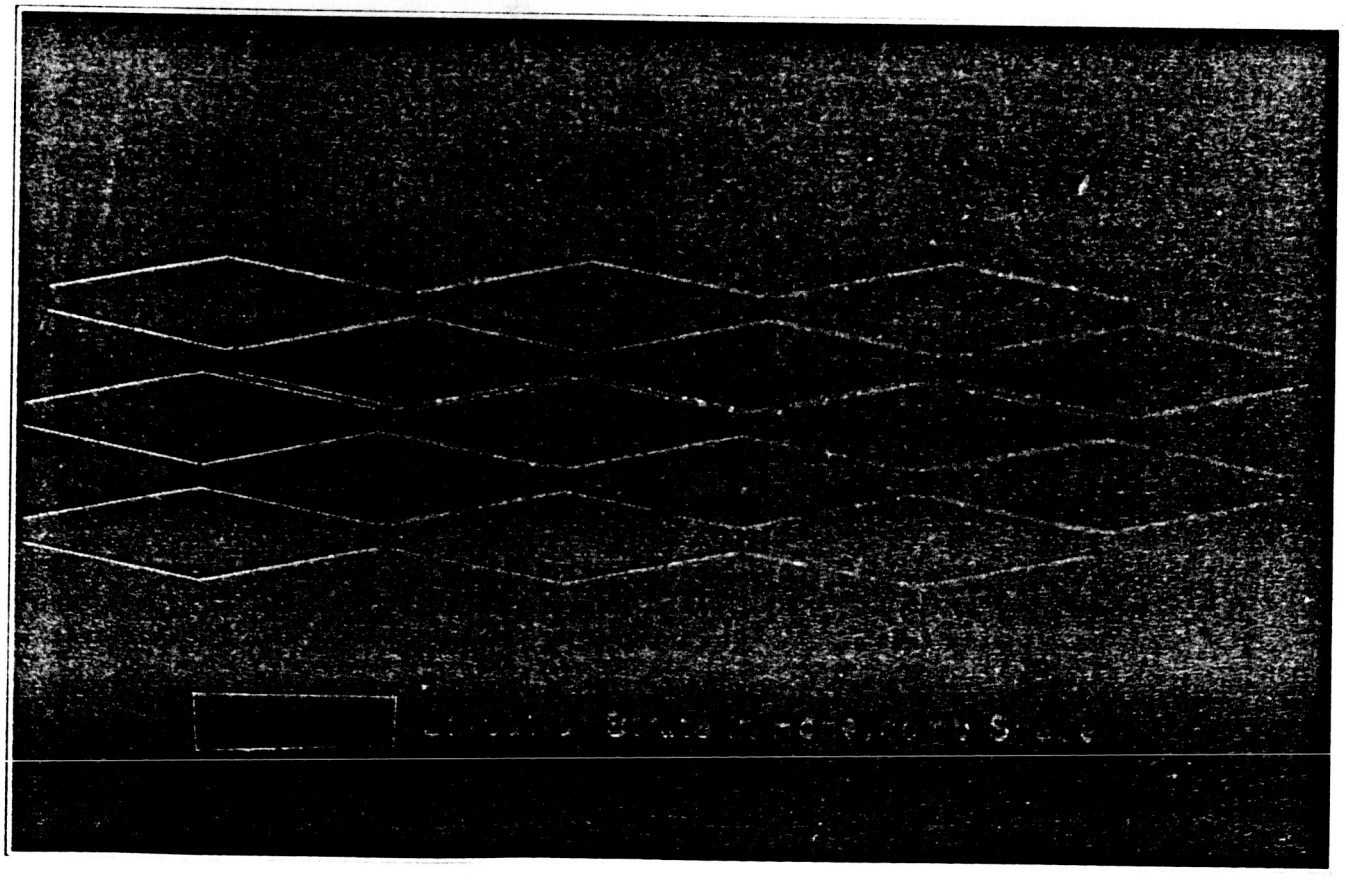

Figure 5.4: Layout of Struts in Honeycomb Shape

placed alongside the larger box. The nodes will be placed in the remaining area next to the support structure package.

Within the additional area on the sides and bottom of the cargo bay surrounding the strut box, the nodes and wiring will be packaged. The spherical nodes will be lined up in a box 5 cm on a side with a length of 4 m. The cylindrical shaped wiring will line the remaining area in the bottom and sides of the cargo area.

After packing the support structure, nodes, and wiring, there remains 5 m of usable height left in the cargo bay for storage of the solar array which is the next priority for assembly in LEO. The solar array will be packed in modules and will be mechanically assembled at SSF.

In packaging the solar array for launch, it is desired to keep the array intact in large segments so that assembly in space is a minimum. The area of the arrays will be split into 105 rhomboid segments which will be 24 m on the long sides and 4.8 m wide. Each segment will be 6.48 cm high and will be separated by 0.02 cm of packaging material so that the glass lenses are not damaged. The remaining area of this first launch will hold 70 of these segments for a mass of 5.5 metric tons.

The six control moment gyros will be split into two sets of three and will be placed in the sides of the cargo pod on either side of the stored solar array. Each gyro is a cylinder 3 m in diameter and approximately 1 m long with a mass of 333 kg each. The total mass of the CMGs and RCS is 2,000 kilograms.

Because of the four g acceleration, which the cargo will have to endure upon takeoff, packing materials will fill any empty spaces in the cargo bay so that the components will remain stationary and rigid.

5.4 Launch Two

The second launch will also be a cargo launch and will consist of the remainder of the solar array and the engine pod structure. In addition, the communications and control systems and additional miscellaneous hardware will be transported in this mission. Figure 5.2b shows a breakdown of launch two.

The remaining 35 segments of the solar array will be packaged in the same cross sectional manner as in launch one and will be 227.5 cm high. The portion of the array to be launched at this time will have a mass of approximately 2.3 metric tons.

The engine pod structure is 5.65 m deep by 4.8 m high and has a mass of 9.14 metric tons. For launch packaging, the pod structure will be placed with its larger dimension (11.2 m) along the length of the cargo bay. The large concentrated mass will be kept in place with springs in order to dampen any large motions it might experience in launching. The engine pod will be attached to the main structure using the robotic arm on SSF.

The communications system will be highly sensitive to jarring and will need careful protection during lifting to LEO. Upon arrival in LEO, the communications will be tested by the SSF crew.

The second launch will carry the power conditioning systems, propellant feed system, guidance, navigation and control systems, and the attachment components for the engines to be fitted to the main ship. This equipment will have a mass of 2 mT. Some of these systems and/or components will be assembled by astronauts.

5.5 Launch Three

The third launch will be a tanker launch and will contain the argon propellant tank. The propellant is launched in this later launch as it is self contained and storage time will be

minimized. The remaining area of the launch can be used to transport other materials to SSF. Figure 5.2c shows a breakdown of launch three.

The propellant tank is a spherical-ended cylinder with a length of 4.16 m and radius of 1.3 m with spherical ends. The tank and propellant have a mass of approximately 26 metric tons. The argon will be launched in a stronger storage tank, hereafter referred to as the "launch tank," as the tank for the mission is not strong enough to withstand the force of the launch from Earth when loaded with the argon. The launch tank will be packaged so as not to move in the cargo bay as this cargo will be sensitive to movement and force. The argon will then be transferred to the ship's tank in LEO, and the launch tank may then be reused. In LEO, the propellant tank will be joined to the ship using robotic assembly.

The remaining space in launch three can be used by NASA to transport equipment needed at Space Station Freedom for this or other projects. In addition, this space may be sold to private industry for transport of experiments or material to Space Station Freedom.

5.6 Launch Four

The fourth and final launch to LEO will consist of the cargo to be transported to Mars as specified. A breakdown of launch four may be seen in Figure 5.2d.

5.7 Repeat Launches from LEO

Upon returning to LEO from the Mars mission, some components which will have to be replaced are:

- Propellant Launch Tank, filled (26 metric tons)
- Engine Pod (if defective) (17.5 metric tons)
- Faulty Segments of Solar Array (if necessary)
- Any faulty components

These components may be launched from Earth using subsequent Shuttle C launches.

Replacement material for each subsequent mission should not require more than one Shuttle "C" launch. Replacement of components will be achieved in LEO using robotic arms and human assemblers.

Table 5.1 Launch to LEO Packaging Scenario

Launch One

Component	Volume Used (m^3)	Estimated Mass (mT)
Struts	75.0	3.2
Nodes	0.0073	0.5
CMG, RCS	7.07	2.5
Solar Array	525.0	5.6
Wiring	0.0016	0.16

Launch Two

Component	Volume Used (m^3)	Estimated Mass (mT)
Communications	50.0	0.8
Thruster System	252.0	9.14
Solar Array	262.0	2.8
Miscellaneous	50.0	1.5

Launch Three

Component	Volume Used (m^3)	Estimated Mass (mT)
Propellant Tank	35.0	0.820
Propellant Launch Tank (filled)	35.0	27.0
Non SEMMII	300.0	40.0
Power Distribution	50.0	1.0

Launch Four

Component	Volume Used (m^3)	Estimated Mass (mT)
Cargo	1225.0	61.0

SECTION 6

Summary

The design of a large, unmanned solar powered electric propulsion cargo vehicle for use in Mars missions presents a number of interesting technical challenges. For each of the areas studied in this report, several solutions were considered. The overall configuration was arrived at through a rough optimization process that attempted to improve the performance of each subsystem, but also considered how each subsystem would fit into the overall mission architecture. The resulting configuration reflects the trade-offs that best suited the mission as a whole.

In the area of trajectory optimization, approximately 400 round trip trajectories were considered using the Quicktop trajectory calculation code. These trajectories were compared on the basis of required propellant, engine thrusting time, loiter time at Mars, refit time at Earth, and overall mission time.

A wide range of possible trajectories were found to consume similar amounts of propellant and require similar thrusting times for a given power input. Because of the relative insensitivity of the trajectory to these two design parameters, the trajectory was optimized primarily with respect to loiter and refit times required. It was desired to minimize the loiter time at Mars and maximize the refit time at Earth for the shortest overall mission (three round trips). The result of this analysis is a trajectory that requires 960 days to reach Mars (including spiral escape and capture), a Mars loiter time of 60 days, a return trip that requires 382 days, and a refit time at Earth of 210 days. Thus an overall mission time for three round trips is just over 12 years.

The electric propulsion system was the next topic considered. In order to achieve a high

payload to mass ratio, electrostatic ion thrusters were selected because of their characteristically high specific impulse. Argon was selected primarily on the recommendation of NASA Langley Research Center.

Mission time parameters lead to a desired initial thrust level at Earth of 60 N. After considering various sizes of thrusters, it was decided that this initial thrust could be achieved using an array of twelve 5 N engines. Five engines will be used near Mars for a maximum thrust of 24 N. Five additional engines were included for redundancy, bringing the total size of the thruster array to 17 engines, each with a projected lifetime of 25,000 hours. The optimum specific impulse was found to be 10,300 seconds.

The solar power collection system was selected after comparing various cell materials in terms of efficiency, radiation resistance, and annealing capabilities; a multistacked cell was chosen to provide 3.5 MW electrical power to our vehicle. To choose an array configuration, design point comparison calculations were carried out for a flat array and for a concentrator system. A Fresnel lens concentrator system was chosen and optimization of the concentrator module size was carried out. The concentrator system was selected with a total area of about 10,800 m^2, divided equally between two hexagonal concentrator arrays.

A wiring scheme was developed so as to minimize both the weight and power loss associated with the solar panel wiring configuration.

The structural support of the Fresnel lens concentrator arrays had to be resistant to out of plane deformations as well as vibrations. The hexagon shaped, three ring truss structure was designed to be light weight, yet resistant to deflections. It consists of 234 half-conical, thin-walled struts with 64 nodes and will be made of aluminum coated graphite epoxy. One of these truss systems was needed to support each of the two solar arrays. Structural analysis with the STAP computer code verified the integrity of the solar array support structure under inertial loads

due to acceleration and rotation.

An orthogonal tetrahedral truss was analyzed for the central supporting structure of the ship. Inertial loads due to engine thrusting with cargo, propellant tank, and solar array attachments were considered. A three cell truss consisting of members 5.4 m and 7.6 m in length resulted in satisfactory stresses and deflections in members.

The control system will be used to a) direct the solar array panels so as to maximize the amount of sunlight captured by the solar cells and b) vary the ship's attitude and orientation during orbital maneuvering and thrusting. The control system will include control moment gyros (CMG) and reaction control system. The CMG system will consist of three double gimballed control moment gyros allowing for 100 percent momentum utilization about three primary axis, as well as 100 percent redundancy of the total control. The selected units will allow the Earth spiral out maneuver to be completed without a need for desaturization.

The transportation of the vehicle components and cargo to LEO will be performed using four Shuttle C missions. The first launch will contain the supporting structure struts and nodes, 70 percent of the solar arrays, and the control moment gyros for a total mass of about 13 metric tons. The second launch will contain the remaining portion of the solar array, the engine pod, the communications package, attachment components, and other miscellaneous items for a total mass of 24.2 metric tons. The third launch will contain the propellant tank at 20 metric tons. The fourth and final launch will carry the cargo at 61 metric tons. The final assembly (both mechanical and human) of the vehicle will take place in LEO.

For each additional LEO-LMO-LEO trip, one shuttle launch will be used to service or replace engines as needed, supply the propellant for the next trip, as well as provide any other miscellaneous components or repair parts.

The vehicle design described in this study represents a feasible, albeit preliminary,

configuration that could fulfill the unmanned cargo support role in a long-term mission architecture for a manned exploration of Mars in the 2010-2020 time frame.

APPENDIX 1

Trajectory Calculations

Nomenclature

a	Orbital parameter
A_t	Constant tangential thrust
E	Orbital energy
e	Eccentricity
EA	Eccentric anomaly
G	Gravitational acceleration of Earth
	Gravitational parameter of a planet
Mp	Dry mass of craft
M_o	initial stage mass (pmefdmai.bas)
ϕ	Flight path angle
p	Curvature radius of orbit
r	Mean orbital radius
r_o	Initial orbital radius
r_a	Radius at apoapse
r_p	Radius at periapse
s	Arc length of an orbit
TOF	Time of flight
v	Orbital velocity
v_o	Initial orbital velocity
v_∞	Hyperbolic excess velocity

A-1.1 Program TIMEOPT.BAS

```
'          Program TIMEOPT.BAS
'
'   This program computes the loiter time at mars and refit time at earth
'   from the QUICKTOP inputs of time and change in true anomaly angle.
'
 OPEN "SYNOD.DAT" FOR INPUT AS #1
 LPRINT"TIMEOUT","TIMEBACK","LOITER","REFIT","MD (years)"
 LPRINT"=======","========","======","=====","==========="
 CLS
 KEY OFF:COLOR 5,0,0
 PI= 3.141593
 WE= .01721
 WM= 9.150999E-03
'
 CLS:    ' User must input times and true anomoly changes below
'
 T1= 152    : '   spiral escape / earth
 T2= 400    : '   hto E - M
 T3= 124    : '   spiral capture / mars
 T4= 0      : '   loiter time (INITIAL GUESS)
 T5= 39     : '   spiral escape / mars
 T6= 300    : '   hto M - E
 T7= 86     : '   spiral capture / earth
'
 A2= 7.85
 A6= 4.25
'
 GOTO 395
'
 INPUT"Earth escape spiral time";T1
 INPUT"HTO Earth to Mars time";T2
 INPUT"True anomoly change, Earth to Mars HTO, deg";AA2:A2=AA2*PI/180
 INPUT"Mars spiral capture time";T3
 INPUT"Mars spiral escape time";T5
 INPUT"HTO Mars to Earth time";T6
 INPUT"True anomoly change, Mars to Earth HTO, deg";AA6:A6=AA6*PI/180
 INPUT"Earth spiral capture time";T7
'
 INPUT#1, T1,T2,T3,T5,T6,T7,AA2,AA6
 A2=AA2*PI/180:A6=AA6*PI/180
 T4=0
 CLS:PRINT"SOLAR-ELECTRIC CARGO FERRY MISSION ARCHITECTURE (ORBITAL MECHANICS
 PRINT
 PRINT"Change in true anomoly, earth to mars =";A2;" rads"
 PRINT"Change in true anomoly, mars to earth =";A6;" rads"
 PRINT"For input phase times, see below ('phasetime' column)":PRINT
 PE0= -WE*T1
 PM0=A2-WM*(T1+T2)
'
 PE1=PE0+WE*T1
 PM1=PM0+WM*T1
'
 PE2=PE1+WE*T2
 PM2=PM1+WM*T2
'
 PE3=PE2+WE*T3
 PM3=PM2+WM*T3
'
'
 T4=T4+10
 PE4=PE3+WE*T4
 PM4=PM3+WM*T4
 PM5=PM4+WM*T5
'
 PE6A=PE5+WE*T6
 PE6B=PM5+A6
 IF PE6A>2*PI THEN PE6A=PE6A-2*PI
 IF PE6B>2*PI THEN PE6B=PE6B-2*PI
 IF PE6A>2*PI OR PE6B>2*PI THEN GOTO 660
 IF ABS(PE6A-PE6B)>.05 THEN GOTO 570
 'PRINT ABS(PE6A-PE6B) : GOTO 190
'
' T4 CORRECT
'
 PE6=PE5+WE*T6
 PM6=PM5+WM*T6
'
 PE7=PE6+WE*T7
 PM7=PM6+WM*T7
'
 PRINT"phase","E pos","M pos","phasetime","missiontime"
 PRINT"=====","=====","=====","=========","==========="
 PRINT "inital  ",PE0,PM0,0,0
 PRINT "E esc SP",PE1,PM1,T1,T1
 PRINT "hto EtoM",PE2,PM2,T2,T1+T2
 PRINT "M cap SP",PE3,PM3,T3,T1+T2+T3
 PRINT "M loiter",PE4,PM4,T4,T1+T2+T3+T4
 PRINT "M esc SP",PE5,PM5,T5,T1+T2+T3+T4+T5
 PRINT "hto MtoE",PE6,PM6,T6,T1+T2+T3+T4+T5+T6
 PRINT "E cap sp",PE7,PM7,T7,T1+T2+T3+T4+T5+T6+T7
'
'
 IF PE7>2*PI THEN PE7=PE7-2*PI
 IF PM7>2*PI THEN PM7=PM7-2*PI
 IF PE7>2*PI OR PM7>2*PI THEN GOTO 920
'
 IF PM7<PE7 THEN PM7=PM7+2*PI
 FZ0=PM0-PE0
 FZ7=PM7-PE7
 IF FZ7<FZ0 THEN FZ7=FZ7+2*PI
 T8=(FZ7-FZ0)/(WE-WM)
'
 PRINT
 PRINT"Refit time (at Earth) until next launch window =";T8;" days"
 PRINT"TOTAL MISSION DURATION =";(3*(T1+T2+T3+T4+T5+T6+T7)+2*T8)/365;" years

 PRINT:PRINT
 LPRINT T1+T2+T3,T5+T6+T7,T4,T8,(3*(T1+T2+T3+T4+T5+T6+T7)+2*T8)/365
 GOTO 395
```

A-1.2 Program SPIRAL

```
      PROGRAM SPIRAL
C     This program calculates the spiral out trajectory, from earth orbit
C     of a solar powered electric propulsion spacecraft.  It assumes a
C     constant acceleration, but takes into account the loss of propellant mass.
      IMPLICIT DOUBLE PRECISION (A-H,M,O,Z)
      FIXMAS = 3.0D4
C     FIXed MASs- mass of ship components that remain essentially remain
C     constant with change in engine number.  In kilograms.
      CARGOM = 6.1D4
C     Cargo mass in kilograms.
      DELTAV = 16800.
C     Delta V for one way mission of craft.
      R0 = 7.118945D6
C     Initial Radius at start of trip in meters.
      V0 = 7.482754247D3
C     Initial velocity in meters/sec.
      FIXP = 1.0D0
C     FIXed Power- power required by systems that do not change in size
C     engine number.  In Kilowatts.
      MU = 3.986012D14
C     Gravitational Parameter of the earth in meters cubed/second squared.
      SAMPKW = 5.0D0
C     Solar Array Mass (in kilograms) Per KiloWatt generated power.
      CELEFF = 0.33
C     Solar cell efficiency.
      RMPKW = 2.50D0
C     Thruster Radiator Mass (in kilograms) Per KiloWatt needed by thruster.
      PPUMPW = 2.0D0
C     Thruster Power Processing Unit Mass (in kilograms) Per kiloWatt needed by
C     thruster.
      ENGMAS = 3.0D1
C     ENGine MASs in kilograms.
      G0 = 9.81D0
C     Gravity at the surface of the earth in N/kg.
      ETAPPU = 0.93D0
C     Thruster Power Processing Unit efficiency.
      CONV = 1.6E-19
C     Conversion from eV to Joules.
      MION = 6.6327D-26
C     Propellant atomic mass in kilograms.
      IONEFF = 0.8
C     Ionization efficiency.
      SDP = 200.0
C     Chamber specific loss level (eV/ion).
      RINF = 1.4959965D11*(MU/1.3271544D20)**4.0D-1
C     Radius of Earth's sphere of influence.
      DO 40 K = 1,5
      ENGT = 1.0*K
C     Thrust per engine (N).
      WRITE(*,5)
    5 FORMAT(1X,'No.',13X,'Propellant',14X,'Total',6X,'Array',6X,
     @ 'Escape',5X,'Escape'/2X,'Of',16X,'Mass',6X,'Total',6X,
     @ 'Craft',6X,'Power',6X,'Radius',6x,'Time'/1X,'Eng',3X,
     @ 'Isp(sec)',3X,'Used(mT)',2X,'Thrust(N)',3X,'Mass(mT)',4X,
     @ '(MWe)',7X,'(DU)',6X,'(Days)')
      ISP = 3000
      DO 30 L = 1,18
      ISP = ISP + 500.0
      C = ISP*G0
C     Exhaust velocity in meters/second.
      MIONF = ENGT/C
C     Found ion mass flow (kg/sec).
      JO = MIONF*CONV/MION
C     Found propellant current.
      VB = MION*ISP*ISP*G0*G0/2.0D0/CONV/IONEFF*1.1D0/1.2D0
C     Found beam voltage.
      JB = IONEFF*JO*1.1/1.2
C     Found beam current.
      PB = JB*VB
C     Found beam power.
      PD = JB*SDP
C     Discharge power.
      PN = 16*(JB + 1.5)
C     Neutralizer power.
      ENGP = (PB + PD + PN)/1.0D3
C     Total power required by thruster in kWe.
      MDOT = (JO + 1.5)/CONV*MION
C     Total mass flow per engine.
      DO 10 NUM = 10, 20, 2
      NUMENG = NUM*5/ENGT
      TENGM = NUMENG*ENGMAS
C     Total ENGine Mass.
      PREQ = (ENGP*NUMENG/ETAPPU + FIXP)
C     Total Required Power. In kilowatts.
      POWM = PREQ*(SAMPKW) + (RMPKW + PPUMPW)*ENGP*NUMENG/ETAPPU
C     Total mas of components whose size are related to generated power
C     & engine numbers.
      SHIPM = FIXMAS + POWM + TENGM
      PROPM = SHIPM*(DEXP(DELTAV/C)-1)
      PROPM = (SHIPM + CARGOM + PROPM)*(DEXP(DELTAV/C)-1)
      TOTM = SHIPM + PROPM + CARGOM
C     Total spacecraft Mass.
      THRUST = ENGT*NUMENG
      ZETA = (MDOT*NUMENG/TOTM)
      AT = THRUST/TOTM
C     Initial acceleration.
      TESC = BISECT(ZETA,C,R0,AT,V0)
      AT = -1.0D0*C*DLOG(1.0D0-ZETA*TESC)/TESC
      SESC = V0*V0*(1-(20.0*AT*AT*R0*R0)**(1/4.))/V0)/2/AT
      RESC = R0*V0/(20*AT*AT*R0*R0)**(1/4.)
      XNESC = V0*V0*(1-(SQRT(20.0)*AT*R0/V0/V0))/8/3.141593/AT/R0
C     Computation of parameters at escape velocity.  TESC = Escape time. AT = Average
C     acceleration during spiral out.  SESC = Distance travelled before escaping.
C     RESC = radius at which craft attains escape velocity.  XNESC = No. of
C     revolutions the craft takes before escaping.
      VESC = DSQRT(2.0D0*MU/RESC)
C     Escape velocity.
      VINF = DSQRT(2.0D0*(VESC*VESC/2.0D0-MU/RESC + MU/RINF))
C     Velocity ship travels when leaving Earth's sphere of influence.
      TOTM = TOTM/1.0D3
      PREQ = (PREQ*1.0D-3)
      RESC = RESC/6.378145D6
      SESC = SESC/6.378145D6
      PROPU = MDOT*TESC*NUMENG/1.0D3
C     Propellent mass used during spiral out.
      TESC = TESC/3600.0/24.0
      DELV = -1.0D0*C*DLOG(1-PROPU/TOTM)
C     Delta V for spiral out.
      WRITE(*,20) NUMENG, ISP, PROPU, THRUST, TOTM, PREQ, RESC,
     @ TESC
   20 FORMAT(1X,I10,2X,I10,2(2X,D9.4))
   10 CONTINUE
      WRITE(*,*)
   40 CONTINUE
      WRITE(*,35)
   35 FORMAT(/)
   30 CONTINUE
      STOP
      END


      DOUBLE PRECISION FUNCTION BISECT (ZETA,C,R0,AT,V0)
C     This program solves a homogenous equation in one variable for a root
C     within the interval [A,B]
      DOUBLE PRECISION EPSILO,A,B,P,E,ZETA,C,R0,AT,TEMP,V0
      DATA EPSILO/1.0D0/
      B = V0*(1.0D0-(20.0D0*AT*AT*R0*R0/V0**4.0D0)**(.125D0))/AT
      A = B/2.0D0
C     The function, interval, and accuracy are entered into the computer using the
C     above two statements.
      I = 1
      N = INT(100*(LOG(B-A)-LOG(EPSILO))/LOG(2.0D0))
   10 P = A + (B-A)/2.0D0
C     The computer makes a guesses the root to be the middle of the current interval.
      E = F(P,ZETA,C,R0,V0)
      IF ((E.LE.EPSILO).AND.(E.GE.-EPSILO)) THEN
      GOTO 20
C     The program has found the root. End.
      ELSE
      I = I + 1
      TEMP = E*F(A,ZETA,C,R0,V0)
      IF (TEMP.GT.0.0) THEN
      A = P
      ELSE
      B = P
      ENDIF
C     The program computes a new interval for the next iteration.
      IF ((A.GE.B).OR.(I.GT.N)) THEN
      WRITE(*,15)
   15 FORMAT(1X,'A root of the equation is probably not in the',
     $ ' given interval.  Try another.')
      STOP
      ENDIF
C     The program checks that its search for the root is not exceding reasonable
C     limits.
      GOTO 10
      ENDIF
   20 BISECT = P
   30 END



      DOUBLE PRECISION FUNCTION F(X,ZETA,C,R0,V0)
C     Evaluates the implicit function that describes TESC.
      DOUBLE PRECISION X,ZETA,C,R0,V0
      F = V0*(1.0D0-(20*C*C*DLOG(1.0D0-ZETA*X)**2*R0*R0/X/X/V0**4)
     @ **0.125D0) + C*DLOG(1.0D0-ZETA*X)
      END
```

A-1.3 Program ORBITB.BAS

Program ORBITB.BAS

```
'
'              EARTH/MARS INTERPLANETARY TRAJECTORY
'              LOW-THRUST SINGLE BURN TO PARABOLIC
'              RELATIVE TO MARS FOR SPIRAL INJECTION
'
'    This model assumes tangential thrust.  Small increments of the
'    independant variable S (arc-length traveled by the ship) are
'    incremented to generate progressive orbits.  A coasting phase
'     is implemented at an RA sufficient to arrive at Mars with
'     parabolic escape speed (i.e. Resc in the Lutze eqns).  At this
'     point, the spiral problem is started in reverse to enter the
'     parking orbit.
'
'
    RDEST=1.524          :'AU
    PI=3.141592654#
    MUMARS=42828!        :'km^3/s^2
    RMARS=3360           :'km
    AU=149599650000#     :'m
    SU=29.784852#        :'km/s
    TU=5022675.7#        :'s
    DU=6378145#          :'m
    ENG=10
    R0=1#:V0=1#          :'au,au/tu
    MASS=137000!         :'kg after spiral out of earth (assumed constant acc)
    MDOT=.000016345#*ENG  :'kg/s
    T0=5#                :'N
    DS=.01               :'AU
'
'
PRINT:PRINT" # OF ENGINES ";ENG;" W/";T0;" NEWTONS THRUST EACH"
PRINT" MASS FLOW RATE (NET) KG/S: ";MDOT
PRINT" IMLEO (AFTER SPIRAL-OUT BURN): ";MASS;" KG":PRINT
'
'
'  Loop to calculate progressive orbits are acceleration increases
'  due to the loss of propellant mass
'
AT=T0*ENG/MASS     :' in m/s^2
AT=AT*TU^2/AU
'
'                    Calculate R and V of new orbit
'
    R=R0/(1#-2#*AT*DS/V0^2)
    V2=2#*DS*AT+(2#/R-1#/R0)
    V=SQR(V2)
    VAVE=(V0+V)/2
    DR=R-R0
    DV=V-V0
    DVTOT=DVTOT+ABS(DV)
'
'         Calculate flight path angle, ang. momentum, energy
'       eccentricity, aphelion, perihelion, and time for increment
'
    X=SQR(DS^2-DR^2)
    GAMMA=PI/2#-ATN(X/DR)
    H=R*V*COS(GAMMA)
    ENERGY=V2/2#-1#/R
    A=-1#/(2#*ENERGY)
    RA=A*(1+E)
    DT=DS/VAVE
    DTTOT=DTTOT+DT
'
'         PRINT ANY DESIRED VALUES FOR THE ORBIT INCREMENTS HERE
'
    DM=MDOT*DT*TU
    MASS=MASS-DM
    DMTOT=DMTOT+DM
    DSTOT=DSTOT+DS
    RAVE=(R+1)/2
'
'         Decision to effect a coast and/or reach Mars orbit
'
IF R>RDEST THEN STOP
IF RA>RDEST THEN 840
'
    R0=R
    V0=V
'
GOTO 400
'
'            Calculate time required for coasting phase
'
'
XR=(1-R/A)/E
YR=SQR(1-XR^2)
ECCR=ATN(YR/XR)
XM=(1-1.524/A)/E
YM=SQR(1-XM^2)
ECCM=ATN(YM/XM)
TAUR=SQR(A^3)*(ECCR-E*SIN(ECCR))
TAUM=SQR(A^3)*(ECCM-E*SIN(ECCM))
DTC=TAUM-TAUR
V=SQR(2*(ENERGY+1/RDEST))
PRINT R,RDEST,A,E,DTTOT,MDOT*DTTOT*TU
'PRINT "RA TO INITIATE COAST ";RA:PRINT" VELOCITY RELATIVE TO MARS ";(V-.810
);" SUN SU'S":PRINT" PROPELLANT REQ'D= ";MDOT*DTTOT*TU:PRINT" TIME TO MARS ENC
NTER ";(DTTOT+DTC)*TU/3600/24:PRINT
    R0=R
    V0=V
GOTO 400
```

APPENDIX 2

Propulsion Calculations

For T = 5 N and Isp = 10,300 s:

$T = m'u_e = m'gIsp$

Mass flow rate per thruster

$m' = T/gIsp = 4.9 \times 10^{-5}$ kg/s

where:

$g = 9.81$ m/s

Propellant current

$J_o = m'e/m_o = 119.4$ A

where:

$e = 1.6 \times 10^{-19}$ C

$m_o = MW \times (1.66 \times 10^{-27}$ kg/1 AU)

and $MW_{argon} = 39.944$ AU

$m_o = 6.63 \times 10^{-26}$ kg

Beam Voltage

$V_b = (m_o Isp^2 g^2)/(2e\eta_i) \times [(1+2\Gamma''/\Gamma')/(1+\Gamma''/\Gamma')]$

$= 2424.2$ V

where:

$\Gamma''/\Gamma' = 0.1$

and $\eta_i \sim 0.8$

Beam Current

$J_b = \eta_i J_o[(1+2\Gamma''/\Gamma')/(1+\Gamma''/\Gamma')] = 104.2$ A

Beam Power

$P_b = J_b V_b = 252.6$ kW

Discharge Power

$P_d = J_b S_{dp} = 20.84$ kW

where:

$S_{dp} = 200$ J/C

Neutralizer Power

$P_n = \xi(J_b + J_n) = 1.69$ kW

where:

$\xi = 16V$

and $J_n = 1.5$ A

Total Power

$$P_{tot} = P_b + P_d + P_n = 275 \text{ kW}$$

Electrical Efficiency

$$\eta_e = P_b/P_{tot} = 0.9185$$

Propellant Efficiency

$$\eta_p = J_b/(J_o+J_n) = 0.8619$$

Total Efficiency

$$\eta_{tot} = \eta_e\eta_p\gamma = 0.714$$

where:

$$\gamma = 0.95$$

Radiator, Titanium

emissivity $\varepsilon = 0.9$

$T = 600$ K

$A = q/(\varepsilon\sigma(T^4-T^4_{space}))$

$= 370{,}000/(0.9*5.67\text{x}10^{-8}(600^4-4^4))$

$= 55.95 \text{ m}^2$

In order to account for (a) the possibility of occasional partial "view - blockage" by the solar array structure and (b) possible degradation of the emissivity, the radiator area is increased to 80 m^2.

APPENDIX 3

Solar Array Calculations

A-3.1 Concentrator/Module Specifications

optical efficiency of module -- $\eta_{opt} = 96\%$
packing efficiency of modules -- $\eta_p = 97\%$
mismatch efficiency of modules -- $\eta_m = 93\%$
solar intensity for AMO -- $I = 1372\ W/m^2$
efficiency of cell at AMO -- $\eta = 27.7\%$ at $T = 115°$
specific area ratio -- $M_{sa} = 1\ kg/m^2$
power required -- $P = 3.5\ MW$

$$D = \eta_{opt} \times \eta_p \times \eta_m = 0.866$$

$$P_{sm} = \frac{\eta_T \times I \times D}{M_{sa}} = \frac{(.27)(1372\ W/m^2)(0.866)}{1\ kg/m^2}$$

$$= 320.8\ W/kg$$

$P_{sa} = 320.8\ W/m^2$ at $115°C$

Area of total array -- $A_a = 3.5\ MW/320\ W/m^2$

Mass of total array -- $M = A_a \times M_{sa} = 10{,}910\ m^2 \times 1\ kg/m^2$

Using the hexagonal design:

$$s = d/(2 \times \cos 30°) = 0.57735 \times d$$
$$b = (d \times \tan 30°)/2 = 0.28868 \times d$$

$$A_a/2 = sd + bd$$
$$= 0.57735d^2 + (0.28868d^2$$
$$A_a = 1.73206d^2$$

Therefore:

$d = 10{,}910/1.73206 = 79.4\ m$
$s = 45.8\ m$
$b = 22.9\ m$

A-3.2 Concentrator Array Wiring Connections

V_{max} = 200 V
V_{oc} = 945 mV
Area of cell -- A_c = 6 cm x 6 cm = 0.0036 m^2
Number of cells per m^2 -- N = 1/0.0036 = 277.8
Max number of cells per series -- $m_s = V_{max}/V_{oc}$ = 211
Max number of resistance per series -- m_R = 210
Design number of modules per series -- n_s = 200
Resistance of Al Gage #7 -- R_s = 2.68 Ω/km

At Earth:

Power per cell -- $P_c = P_{ss}/N$
= 1.155 W

Power per series -- $P_s = n_s \times P_c$
= 231.0 W

Length of series connections -- L = (0.06 m)(200)
= 12 m

Resistance of series -- R = (0.012 km x 2.68 Ω/km)
= 0.032 Ω

Current through each series wire -- I = P_s/V = 231 W/200 V
= 1.155 A

Power loss per series -- $P_{LS} = I^2R = (1.155\ A)^2(0.032\ \Omega)$
= 0.0429 W

Number of series in parallel -- $n_p = P/P_s$ = 15,153

Power loss in series connections -- $P_{TS} = P_{LS} \times n_p$
= 650.10 W

Length of series wire at 0.084 A = 209,538.6 m

Length of parallel wire length at 19.635 A = 76,963.25 m

Using Al Gage #7 at 28.71 kg/km,
Estimated total wiring mass = 8,225 kg

Power loss in series connections -- $P_{TS} = I^2R$
$= (19.64)^2 \times 76.963 \times 2.68$
= 79,520 W

Estimated total power loss -- $P_{TL} = P_{TP} + P_{TS}$

$= 79{,}250 + 650$

$= 80{,}170$ W

A-3.3 Flat Panel Array Specifications

optical efficiency of module -- $\eta_{opt} = 96\%$
packing efficiency of modules -- $\eta_p = 94\%$
mismatch efficiency of modules -- $\eta_m = 95\%$
solar intensity for AMO -- $I = 1372\ W/m^2$
efficiency of cell at AMO -- $\eta = 21.7\%$ at $T = 25 \cdot C$
specific area ratio -- $M_{sa} = 0.85\ kg/m^2$
power required -- $P = 3.5$ MW
temperature dependency factor -- $TD = -0.63\ W/m^2 - \cdot C$

$$D = \eta_{opt} \times \eta_p \times \eta_m = 0.857$$

$$P_{sm} = \frac{\eta_T \times I \times D}{M_{sa}} = \frac{(.217)(1372\ W/m^2)(0.857)}{.85\ kg/m^2}$$

$$= 300.2\ W/kg$$

$$P_{sa} = 255.2\ W/m^2 \text{ at } 25 \cdot C$$

Therefore, at $T = 115 \cdot C$:

$$P_{sa} = 255.2\ W/m^2 + TD \times 25 \cdot C$$
$$= 198.5\ W/m^2$$

Area of total array -- $A_a = 3.5\ MW/198.5\ W/m^2$
$= 17{,}632\ m^2$

Mass of total array -- $M = A_a \times M_{sa} = 17{,}632\ m^2 \times 0.85\ kg/m^2$
$= 14{,}987$ kg

Using the hexagonal design:

$$s = d/(2 \times \cos 30 \cdot) = 0.57735 \times d$$
$$b = (d \times \tan 30 \cdot)/2 = 0.28868 \times d$$

$$A_a/2 = sd + bd$$
$$= 0.57735d^2 + (0.28868d^2$$
$$A_a = 1.73206d^2$$

Therefore:

$d = 10{,}910/1.73206 = 93.0$ m
$s = 53.7$ m
$b = 26.85$ m

A-3.4 Flat Panel Array Wiring Connections

V_{max} = 200 V
V_{oc} = 945 mV
Area of cell -- A_c = 2 cm x 2 cm = 0.0004 m^2
Number of cells per m^2 -- N = 1/0.0004 = 2500
Max number of cells per series -- $n_s = V_{max}/V_{oc}$ = 211
Max number of resistance per series -- n_R = 210

Resistance of Al Gage #7 -- R_s = 2.68 Ω/km

At Earth:

Power per cell -- $P_c = P_{sa}/N$
= 0.079 W

Power per series -- $P_s = n_s \times P_c$
= 16.7 W

Length of series connections -- L = (0.02 m)(210)
= 4.2 m

Resistance of series -- R = (0.0042 km x 2.68 Ω/km)
= 0.0113 Ω

Current through each series wire -- $I = P_s/V$ = 16.7 W/200 V
= 0.0835 A

Power loss per series -- $P_{LS} = I^2R = (0.084\ A)^2(0.0113\ \Omega)$
= 0.00008 W

Number of series in parallel -- $n_p = P/P_s$ = 209,970

Power loss in series connections -- $P_{TS} = P_{LS} \times n_p$
= 16.7 W

Length of series wire at 0.084 A = 654,234 m

Length of parallel wire length at 20 A = 277,830 m

Using Al Gage #7 at 28.71 kg/km:
Estimated total wiring mass = 11,100 kg

Power loss in series connections -- $P_{TS} = I^2R$
= $(20)^2$ x 277.83 x 2.68
= 297,834 W

Estimated total power loss -- $P_{TL} = P_{TP} + P_{TS}$

$= 297,833.3 + 16.7$

$= 297,850$

$= 80,170$ W

APPENDIX 4

Control System

The mechanics of a solar-powered electric propulsion vehicle poses important demands on the vehicle's control system, which stem from two main maneuverability requirements: 1) the solar array panels must be directed so as to maximize the amount of sunlight captured by the solar cells; and 2) attitude adjustments are necessary in order to perform orbital maneuvering.

The most effective spacecraft configuration allows one degree of freedom between the solar arrays and main body of the ship. The extra degrees of freedom needed for attitude control are achieved by roll and yaw of the spacecraft. As the craft spirals out, the longer orbit period permits the angular acceleration of the solar panels to decrease. Therefore, the pitch moments are the most significant orientation maneuvers in the initial orbit.

These conditions allow us to predict that the most drastic moment and attitude adjustments will occur during the low earth orbit height of 400 km.

Three main reaction systems were considered for the attitude controllers: 1) Reaction Wheels, 2) Control Moment Gyros, 3) Engine Thrusters.

Comparison of the Reaction Wheel (RW) with the Control Moment Gyro (CMG), indicated that a cluster of CMG's offers significant advantages over a reaction wheel when dealing with a large vehicle to control. CMG efficiency is better since the CMG wheel operates at one speed for which efficiency can be optimized [1]. Larger maximum moments can be achieved at constant momentum rates. Finally, the reaction wheel's maximum rates tend to become non-linear as it approaches saturation; thus, complex feedback is necessary to control

reactions.

While lighter in weight, thrusters appear to be less suitable for this application because a very slow rate of angular adjustments required (as the ship spirals out or in) call for near-continuous minute thruster impulses, perhaps increasing complexity and demands on reliable and long-life performance.

Therefore, a gyroscopic control system appears to be a preferred solution to our control needs. This system will be supplemented by a system of small thrusters (RCS). Momentum exchange devices can handle cyclic torques on a continuous basis over a limited period of time. Consequently, the external moments applied to the vehicle will cause the controllers to reach maximum capacity; thus becoming saturated. This condition requires the removal of momentum from the device. This may be accomplished at convenient times during the mission. For our case, the optimum desaturization period will be after the spiral-out from Earth, during the geocentric transfer from Earth to Mars. This interval is over a very long orbit period; there will be little solar array rotation involved as well as smaller disturbances from the tangential thrust vector.

As discussed later, our system has been designed so that saturation will not occur during the spiral-out/in phases. When desaturization occurs, it will be accomplished by small electrical thrusters of the RCS system and countering each CMG gimbal controller to a prescribed gimbal angle on a momentum feedback loop (Figure A-4.1a).

From the mass moment of inertia of the solar arrays, I_{xx} = 6.19 x 10^6 kg m^2 (x-x = solar arrays axis of rotation) and the initial angular velocity of the ship in LEO, ϖ_i 1.131 x 10^{-3} sec^{-1}, we can estimate that the total spiral-out angular momentum change required will be about 7,000 kg-m^2/s. A single Sperry M4500 CMG [2] provides an angular momentum capacity of 6,101 kg-m^2/s, thus it would be able to control the solar arrays orientation during most of the spiral out

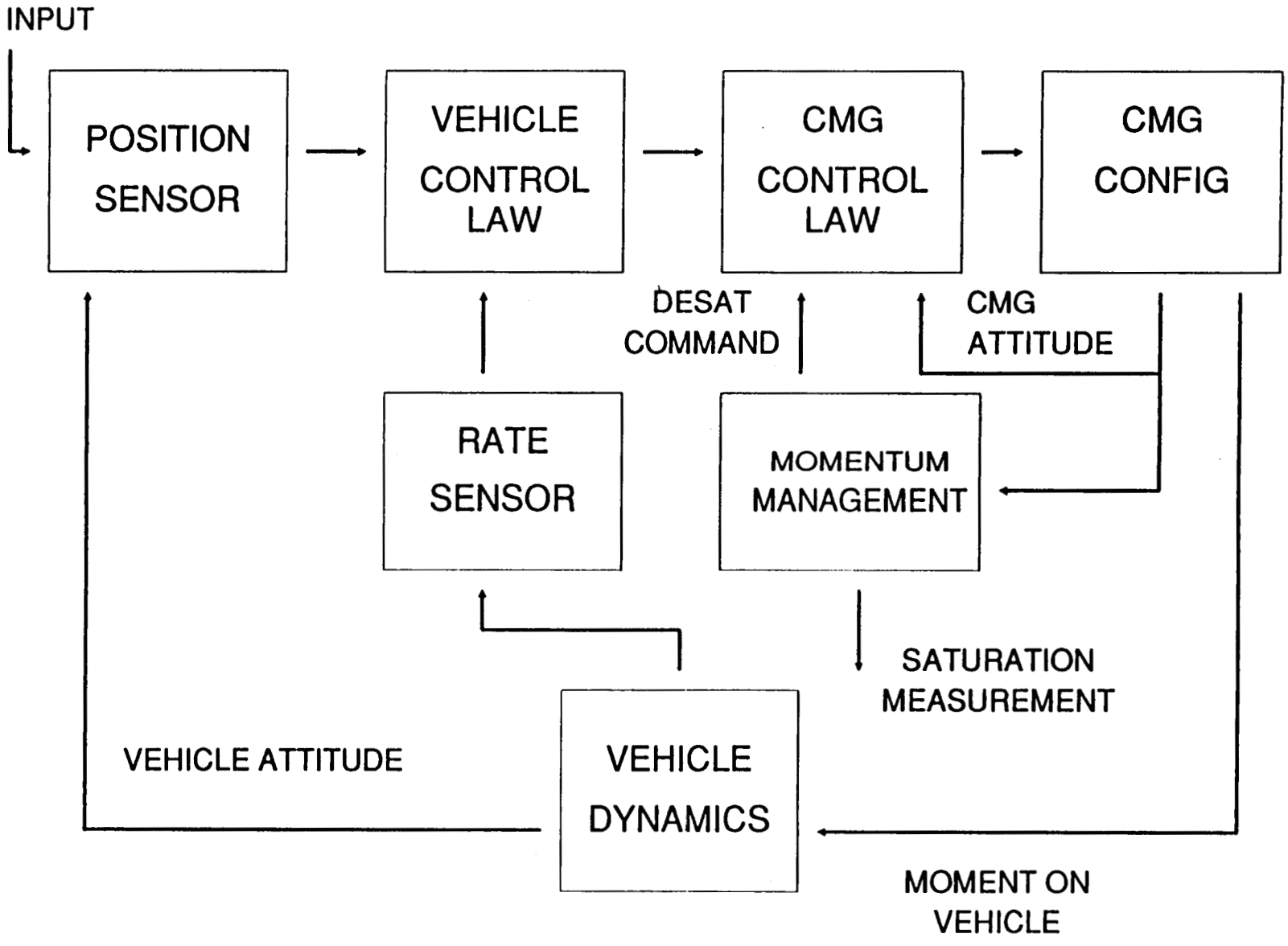

Figure A-4.1: Control Loop Diagram

without becoming saturated.

To provide maximum flexibility and redundancy we selected a system using a "six pac" configuration which consists of three double gimballed control moment gyros. This arrangement will allow for 100 percent momentum utilization about 3 primary axes. Additionally, this configuration provides 100 percent redundancy of total control; two CMG's can be in an active state while the third is not operating.

Navigation software (beyond scope of this study) will convert the steering commands--Vehicle Control Law, CMG Control Law--issued by the ADCOLE Model 20470 V-SLIT sun sensor assembly into drive commands [7]. Each CMG gimbal pivot will be directly coupled with a D.C. motor by a rate generator which drives the individual momentum vectors of each CMG. Thus changing the angular momentum and causing reaction moments on vehicle. Actual control loop functions are as follows:

1) Position Sensor (Star Sensor)[5]
Measures error between actual and desired vehicle attitude

2) Vehicle Control Law
Formulates vehicle moment command

3) CMG Control Law
Processes command moment and provides input commands to the CMG gimbal servos

4) CMG Servos
Drive individual momentum vectors of each CMG, thus changing angular momentum

5) Vehicle Dynamics
Actual change of vehicle attitude

As discussed above, a saturation of the CMG will not occur during the spiral phases. Desaturization, can then be accomplished during the heliocentric transfer phase. At that point, the same D.C. motor that was used to drive the CMG servos can be used to desaturate the

system.

CMG PROJECTED SPECIFICATIONS:

Double Gimbal	
Angular momentum	6,000 kg-m^2/sec
Total system mass	700 kg
Total power required	1 kW

References

1. B.J. O'Conner, L.A. Morine, "A Description of the CMG and its Application to Space Vehicle Control", AIAA 67-589. 1967.

2. Sperry Flight Systems. Honeywell/Sperry Corporation. DOC. 61-1720-08-00, 1982.

3. H.S. Oh, S.R. Vadali, "Feedback Control and Steering Laws for Spacecraft Using Single Gimbal Control Moment Gyros". AIAA 89-3475-CP. 1989.

4. Zondervan,et al,Guidance, "Navigation, and Control Trades for an Electric Orbit Transfer Vehicle." AIAA 90-3458-CP. 1990.

5. Ninomiya, et al,"High Accuracy Sun Sensor Using CCD's." AIAA 88-4180-CP. 1988.

6. Potts, "The Mars Observer Spacecraft." AIAA 89-0255. Jet Propulsions Laboratory, 1989.

7. ADCOLE Aerospace Products, Excerpts from general catalog.

APPENDIX 5
Communications and Navigation Systems

Nomenclature

b/s or bps	bit per second
CD&H	Command, Data, and Handling
dB	Decibel
DSN	Deep Space Network
E_b/N_o	Energy per bit to spectral-noise-density ratio
Hz	Herz
m	meter
SSA	Solid State Amplifier
Sr.	steridian (solid angle)
W	Watt

Specific performance and physical parameters of the communications and navigation systems are tabulated in Tables A-5.1 through A-5.4. The information in these tables incorporate projections of technological accomplishments by 2015 such as fabrication of high temperature superconducting surfaces for antenna dishes and improvements in radiation hardness of the components. All calculations were made assuming that modulation and encoding techniques would be improved such that E_b/N_o could take the following values: 1) 3.0 dB for X-band telemetry, 2) 3.5 dB for Ka-band telemetry, 3) 5.0 dB for X-band commands, and 4) 6.0 dB for Ka-band commands. All calculations also provide a safety margin of at least 2.0. Table A-5.1 summarizes the chosen communications and navigation systems.

A-5.1 The RF Subsystem

The RF subsystem employs six antennas, two 1.5 m high gain antennas and four 0.5 m omnidirectional antennas. Two high gain antennas were chosen for redundancy. They will be placed along the symmetric axis of the ship, between the solar arrays to minimize signal blockage by the arrays. The omnidirectional antennas will be placed as perpendicular pairs on opposite ends of the ship. During normal operations only two of these antennas will be functioning, one

for reception and one for transmission. In the case of an emergency, all four will be functioning, two for transmission and two for reception. The omnidirectional antenna operates at X-band (8400 MHz) frequency with a transmitting power output of 2.5, 5.0, or 40.0 Watts. It delivers telemetry and receives and sends commands during the Earth spiral phase of the mission. Telemetry will be transmitted to the 26 m DSN antenna at 5.0 W and 2 Mb/s. Commands will be transmitted at 10 kb/s and 2.5 W to the 26 m DSN antenna. The omnidirectional antenna will also be used to receive command data during emergency situations. The Command Data and Handling (CD&H) system alerts the spacecraft of an emergency if any of the following criteria are met: 1) Unplanned failure of solar array to properly generate power. This usually occurs when either the attitude control system or the motors on the solar arrays fail, or when some phenomena has caused the ship to tumble, 2) the temperature of the communications system drops below 0•C, or 3) the spacecraft has not received and Earth or Mars transmission in 3 days. (When the spacecraft orbits Mars near Mars/Earth opposition, the spacecraft will be commanded to increase this requirement to 19 days since communications are not possible for 17 days during opposition.) In emergency cases, the omnidirectional antenna is used because its wide beam angle (90•) should allow it a greater chance of contacting an Earth or Mars station than the high gain antenna, with a beam angle of 0.875•. The omnidirectional may also transmit during emergencies. However, the low gain of 0 dB allows the antenna to transmit only 10 bps of commands at 40 W to the 64 m antenna from opposition if one wishes to maintain the standard bit error rate of 1×10^{-5} for commands. If one uses and array of DSN antennas (a 64 m-34 m-34 m-34 m-34 m array, for example) to track the ship in case of an emergency, then the 100 bps transmission can be maintained from as far as 1.8 AU.

One high gain antenna will receive and transmit commands in X-band (8.4 GHz) during the interplanetary phase of the mission. The other will deliver telemetry at Ka-band (32 GHz).

Commands will be carried at 10 kb/s and 5 W of power; telemetry will be sent at 2 Mb/s and 12 W of power. All will be transmitted to a 34 m DSN antenna. Should failure occur in the Ka-band transponder, the X-band transponder will send the telemetry at 10 kb/s and 40 W of power to the 64 m DSN antenna. Both transponders will have connections to both antennas in case an antenna fails, and both antennas are capable of handling four beams of radio signals, two transmitting and two being received. During the near Mars phase of the mission, it will be assumed that the spacecraft will communicated with antenna stations on or circling Mars. It is also assumed that these stations will have an antenna of at least 8 m in diameter and are capable of transmitting only in X-band. These transmissions will begin at around 0.05 AU from Mars using the high gain antennas. Telemetry will be sent at 2 Mb/s and 40 W of output power. Commands will be delivered at 1 kb/s and 2.5 W of power. When the ship begins to spiral in or executes a spiral out from Mars, the high gain antennas will become inactive and the omnidirectional antennas will be used for communication.

In both near Earth and near Mars transmissions, command and telemetry phases of communication are separated. Usually, commands are transmitted and received on a subcarrier along with the telemetry data. However, the use of the subcarrier demands an extra transponder. This adds weight, power drain, and complexity. If separation of the two data streams is not feasible, the Ka-band transponder will transmit command data as a subcarrier through one omnidirectional antenna. The X-band transponder will transmit telemetry through one of the other antennas. The weight will increase by no more than 1 kg, but the power required during transmission will increase by 14.0 Watts to pay for the decrease in transmission time. This system can transmit 2 Mb/s telemetry and 10 kb/s command.

Maximum bit rates were designed for the possible addition of scientific instruments as secondary functions for a mission. The bit rate of 2 Mb/s can handle color video transmission.

The 10 kb/s telemetry rate is meant to be used only in the emergency caused by the failure of the Ka-band transponder; thus only data from ship sensors will be transmitted at this rate. The gimbal pointing assembly has a pointing error of 0.1°. It has the ability to change the direction of the antenna by nearly pi Sr. with respect to the axis of the spacecraft. All gimbal systems are run by 5 W motors. Optionally, the omnidirectional antennas may also have a gimbal system that allows pi Sr. of movement. This will add eight kilograms of weight and the possibility of 10 to 20 Watts of additional power during transmission. All transponders use solid state amplifiers (SSA) for boosting transmission signal power. Both transponders also are fitted with bandpass filters to improve performance.

A-5.2 The CD&H Subsystem

The heart of the command data and handling subsystem is a low power 32 bit processor. This makes multitasking possible and will increasing the speed and efficiency of the CD&H subsystem. In turn, and indirectly, this may increase the efficiency and lifetime of many ship components such as the engines and the arrays. It also decreases the chances of a catastrophic failure because it decreases reaction times to unusual sensor readings. No more than 4 MB of RAM should be required to activate commands and manipulate incoming data. The CD&H system places the data from the ship's sensors onto a read/write laser disk for storage until the ship is in the right position to transmit it. The magnetic disk can hold 1 TB of data which, assuming daily transmission, provides more that adequate storage. All software required by the communications system alone could probably fit in 4 k ROM; however, because of the uncertainty of the complexity of programming required to run other ship systems (particularly the engine array), 128 k ROM has been allocated to contain a copy of all software. The system includes and event sequencer to hold series of delayed commands transmitted from Earth until

activated by a "macro command" transmitted from Earth. The CD&H subsystem uses analog switches for temperature control and requires analog/digital modulators to convert the analog output of certain ship instruments (eg. DRIRU) to digital form for transmission.

A-5.3 Navigation and Batteries

The ship contains three star trackers for precise determination of position over three axes and for purposes of redundancy. These components will lie along the truss structure near the high gain antennas to minimize blockage of their view of surrounding space. The ship also holds three dry inertial measurement units (DRIRU). These systems are self-redundant. One is used for keeping track of the orientation of the spacecraft; the other two are placed one on each solar array structure to monitor the orientation of the arrays. Solar sensors determine the orientation of the solar array to toward the sun. There are eight sensors placed on the array. The other three are placed along the ship's truss structure to aid in calculating the attitude of the spacecraft. The batteries are employed for use during times of peak power drain and during an emergency caused by solar array failure. They are capable of delivering up to 2 kW of power for approximately 1.3 hours. When not in use, the batteries will be charging. Near Earth, where the period in shadow will be longest during the mission and where solar array power is greatest, the batteries will be under full charge. During the interplanetary trajectory, when no shadow should be encountered, the batteries will charge in trickle mode. Around Mars, the high inclination of the orbit keeps the ship within Mars' shadow for a very short period of time, therefore the batteries need only charge at the intermediate level.

A-5.4 Power Requirements

Power required by specific components and the total power for navigation and battery systems is given in Table A-5.2. The various power requirements for typical communications

operations are listed in Table A-5.3.

A-5.5 Mass of System

The masses of the subsystems for communications and navigation are summarized in Table A-5.4.

Table A-5.1 Parameters of the Communications and Navigation Systems

Telemetry System:
X-band transmission frequency: 8.4 GHz
X-band reception frequency: 7.1 GHz
Ka-band transmission frequency: 32 GHz
Ka-band reception frequency: 28 GHz
1.5 m antenna gain (at 8.4 GHz): 39.1 dB
1.5 m antenna gain (at 32.0 GHz): 50.68 dB
1.5 m antenna efficiency: 0.6 (with high temperature superconducting surface.)
Omnidirectional antenna gain: 0 dB
High gain antenna transmission : 2.5/5.0/12.0/15.0/40.0
Omnidirectional antenna output: 2.5 W/5.0 W/40.0 W
Bit error rate for telemetry: 5×10^{-3}
Bit error rate for command: 1×10^{-5}
Bit rates for telemetry transmission: 2 Mb/s (Video/Ship Systems), 4.6 kb/s (Ship systems, Ka-band transponder failure emergency)
Bit rates for command transmission: 10 kb/s, 1000 bps, 100 bps, 10 bps

Command Data and Handling System
16 bit radiation hardened processor
4 MB RAM
1 Terabyte laser disk storage
Software encoded on 128k ROM
Event Sequencer
Analog Switches
Analog/Digital Modulators

Navigation Systems
3 Star Trackers
3 Dry Inertial Reference Units
11 Sun Sensors

Batteries
Capacity: 39.0 Ampere-Hours
Storage: 1316.0 Watt-Hours
Voltage: 27 V
Current: 1 Ampere

Voltage Required for Communications System: 28 7 VDC
Operating Temperature Range for Communications System: 0 to 40•C
Operating Temperature Range for Batteries: 0 to 20•C

2. The different power numbers shown for the DRIRU are the powers required for operation of 1/2/3 gyros respectively.

3. The three normal operation powers for the batteries correspond to trickle/intermediate/full charge rates respectively.

4. The navigation and battery power requirements includes only those values listed under navigation subsystem and batteries. It is assumed that all three gyros in the DRIRU will be working during normal operation. The three different numbers under normal operation refer to different battery charge states (see number three).

Table A-5.3 Communications Power Requirement Totals for Possible Operations

Max power required for near-Earth operation: 360.0 W

Components in use: X-band transponder (transmitting at 40 W), CD&H subsystem.

Nominal power for near-Earth transmission operation: 340.0 W/134.0 W

Components in use: As above. Second value denotes X-band command transmission.

Normal operations power for near-Earth operation: 120.0 W

Components in use: As above, except X-band transponder in receive mode.

Max power for interplanetary operation: 225.0 W

Components in use: X-band transponder transmitting at 5.0 W, Ka-band transponder transmitting at 12.0 W, Gimble pointing system motors running, and CD&H systems running.

Nominal power for interplanetary transmission operations: 195.0 W

Components in use: As above, except gimble system not running.

Normal operations power for interplanetary transmission operation: 145.0 W

Components in use: As above, except X-band and Ka-band transponders in receive mode only.

Max power for Mars orbit operations: 225.0 W

Components in use: Same as for interplanetary operation. Used only if Mars communication systems break down.

Nominal power for Mars orbit transmission: 340.0 W/134.0 W

Components in use: As for "nominal power for near-Earth transmission."

Normal operations power for Mars orbit operations: 120.0 W

Components in use: As above, except the X-band transponder is in receive mode only.

Emergency (solar array failure) operations: 580.0 W

Components in use: X-band transmission at 40 W on two omnidirectional antennas, CD&H subsystem.

NOTE: Max power calculations use the maximum power values for components given in the table. Normal operations and nominal power calculations use numbers listed under "Normal operations power."

Table A-5.4 Communications & Navigation Systems Weight

	Weight (kg.)
Antenna Subsystem	
1.5 m High Gain Antenna (2)	6.5
Gimbal Pointing System (2)	4.0
Antenna Feed Array (2)	4.0
0.5 m Omnidirectional Antenna (4)	2.0
ANTENNA SUBSYSTEM WEIGHT	16.5
Telemetry Subsystem	
X-band Transponder	15.5
Ka-band Transponder	18.0
TELEMETRY SUBSYSTEM WEIGHT	33.7
CD&H Subsystem	
CD&H Subsystem Weight	15.0
TOTAL WEIGHT OF COMMUNICATION SUBSYSTEM:	65.0
Navigation Subsystem	
Star Tracker (3)	24.0
Dry Inertial Reference Unit (3)	48.0
Sun Sensors (11)	1.0
TOTAL WEIGHT OF NAVIGATION SUBSYSTEM:	73.0
Batteries (4)	
Battery Weight	80.0
TOTAL WEIGHT OF NAVIGATION SUBSYSTEM AND BATTERIES:	153.0

References

1. Yuen, Joseph, Ed. Deep Space Telecommunications Engineering. JPL Publication 82-76. July 1982.

2. Morgan, W.L. and Gordon, G.D. Communication Satellite Handbook. John Wiley & Sons. 1989.

3. Lindsey, W.C. and Simon, M.K. Telecommunications Systems Engineering. Prentice Hall, Inc. Englewood Cliffs: 1973.

4. Evans, B.G., Ed. Satellite Communication Systems. Peter Peregrinus Ltd. London: 1987.

5. Ruppe, H.O. Introduction to Astronautics. Academic Press, Inc., New York: 1967.

6. Corliss, W.R. Space Probes and Planetary Exploration. D. Van Nostrand Company, Inc. Toronto: 1965.

7. AIAA Satellite Communications Conferences: 1980-1990.

8. TDRSS User Transponders: The Second Generation. Motorola, Inc. 1983.

9. "Star Tracker Users Guide." Ball Inc.

10. "Sun Sensors." Lockheed Missiles and Space Company Fact Sheet.

11. Farmer, Martin, and Garn. "Conceptual Design of a Communications System for Mars Exploration Missions." AIAA Paper 89-0516. 27th Aerospace Sciences Meeting, Reno, NV. January, 1989.